Master of Science Thesis

Preliminary Design of Composite Wind Turbine Towers

Shreya Ravalappa Kamath

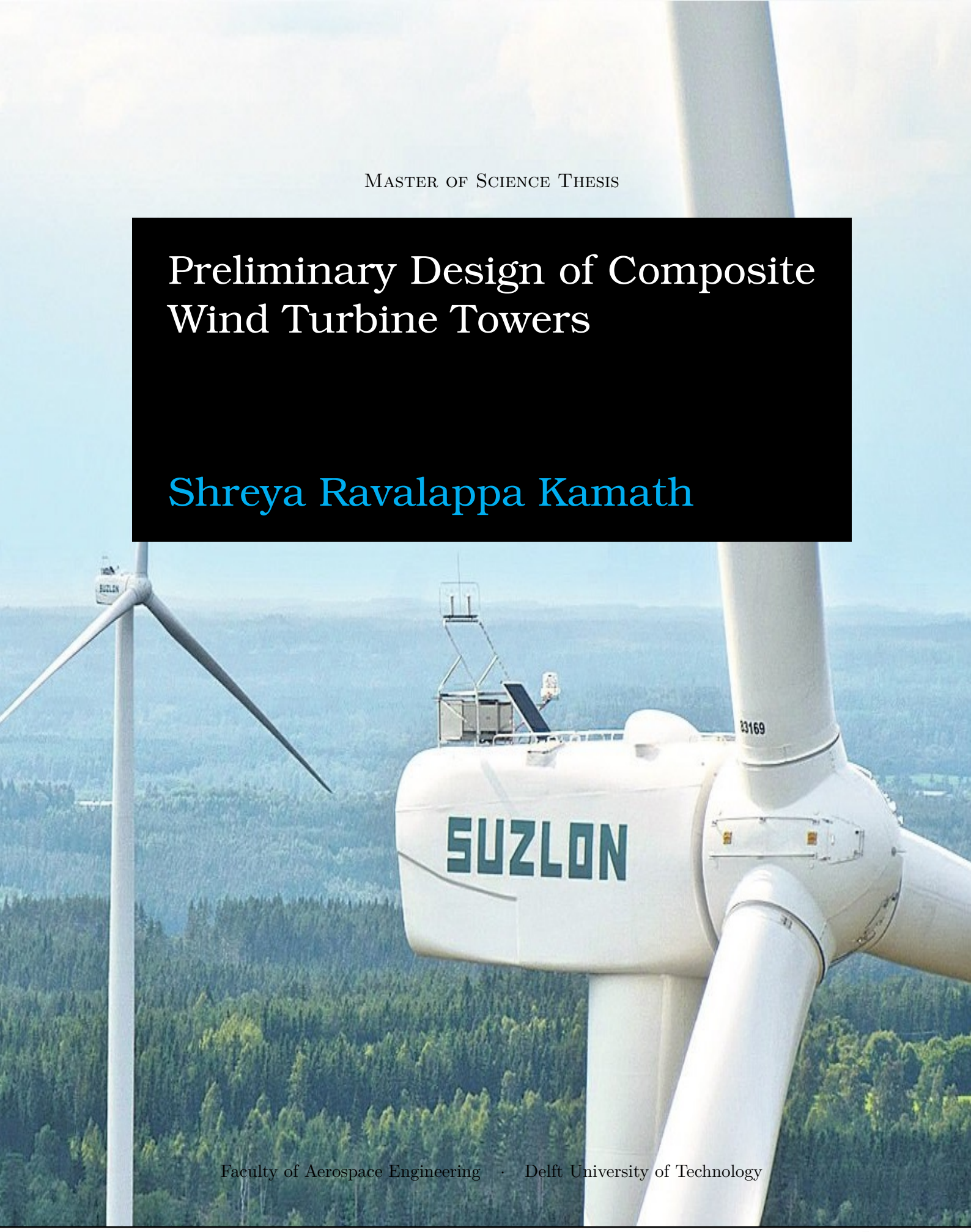

Faculty of Aerospace Engineering · Delft University of Technology

TU Delft Delft University of Technology

Preliminary Design of Composite Wind Turbine Towers

Master of Science Thesis

For obtaining the degree of Master of Science in Aerospace Engineering
at Delft University of Technology

Shreya Ravalappa Kamath

15 Sept 2017

Faculty of Aerospace Engineering · Delft University of Technology

The work in this thesis was supported by Suzlon Energy Ltd. Their cooperation is gratefully acknowledged.

Delft University of Technology
Faculty of Aerospace Engineering
Department of Aerospace Structures and Materials

GRADUATION COMMITTEE

Dated: 15 Sept 2017

Chair holder:

Dr.ir. Roeland de Breuker

Committee members:

Dr. Christos Kassapoglou

Ir. Peter Joosse

Dr.ir. Sonell Shroff

Abstract

Over the past decade, wind turbine towers have grown taller and wider to support high capacity turbines. It may, therefore, be prudent to investigate materials alternative to steel to mitigate an increase in tower mass, cost, and complexities in transportation & manufacturing associated with the steel towers. The current research focuses on the preliminary design of economically feasible composite wind turbine towers.

Some of the project objectives involve setting up the design tool for tubular and lattice tower made up of Glass Fiber Reinforced Plastic (GFRP) and Carbon Fiber Reinforced Plastic (CFRP) material, preliminary design of possible joining techniques, setting up the cost model for various manufacturing approaches and assembly techniques and comparison of composite towers to steel tower design regarding mass and cost. The design tool will incorporate all the essential load cases, structural and geometric constraints and will help to analyze the composite towers with various hub heights and for 2.1 MW and 5 MW turbine capacities.

Loads and constraints are estimated through the literature study. Preliminary design of the tubular tower has been carried out using an analytical approach. For the lattice towers, a Finite Element Method (FEM) approach using Matlab was the suitable method to perform the analysis. A minimum first natural frequency constraint of 0.27Hz and 0.22Hz have been incorporated during the design for 2.1MW and 5MW turbine capacity towers respectively. For the joint design, bolted and adhesive joints are considered and the failure modes associated with these joints have been incorporated into the design to get an estimate of the joint mass and cost. The cost modeling of composite structures was done using the parametric equations that fit the Process Cost Analysis Database (PCAD) cost model in the region of interest. These parametric equations are usually functions of the surface area of the structure, perimeter, number of plies and the complexityof the part. The final part involves comparison of the GFRP and CFRP towers with steel towers and comments on the feasibility of the composite towers.

CFRP tubular and lattice towers show a mass reduction of up to 60% for lower hub height towers (<=100m), but this advantage decreases with height. Due to the high material cost, the CFRP towers are at least 3-4 times costlier than steel towers. For the GFRP material system, up to 35% mass reduction was found in the tubular design with lower hub height (<=100m). 5MW-100m hub height GFRP tubular tower showed the highest mass advantage (35%) and was the closest in cost to the steel design with the GFRP tower being 4% costlier. The GFRP lattice towers showed a similar trend with up to 35% but were at least 27% costlier than steel tower due to the high material and joint costs.

The only region where composite currently show any promises of mass and cost feasibility is for smaller hub heights (<=100m) and on tubular towers. The major existing difficulties with steel towers are for heights in the range of 125-150m, and in this region, the composite tower design does not show mass or cost advantages. Based on the results of the various trade studies and optimized designs, it was concluded that the composites do not hold a definitive promise as an alternative material for wind turbine towers over steel. With the current technology and understanding of the tower designs, the mass advantage promised by composite towers is not enough for composites to be deemed a viable option that can thrive in a competitive market for renewable energy. Thus a few scopes for future research are provided that can help in strengthening the understanding of the composite tower design.

Table of Contents

List of Figures

List of Tables

List of Acronyms

FRP	Fiber Reinforced Plastic
GFRP	Glass Fiber Reinforced Plastic
CFRP	Carbon Fiber Reinforced Plastic
TST	Tubular Steel Tower
TSTR	Tubular Steel Tower sectioned Radially
TCT	Tubular Concrete Tower
LT	Lattice Tower
TTT	Tubular Timber Tower
HT	Hybrid Tower
IEC	International Electrotechnical Commission
ASCE	American Society of Civil Engineers
NWS	Normal Wind Speed
EWM	Extreme Wind Model
EWM1	Extreme Wind Model- 1 year occurrence period
EWM50	Extreme Wind Model- 50 year occurrence period
ETM	Extreme Turbulence Model
NTM	Normal Turbulence Model
DNV-GL	Det Norske Veritas-Germanischer Lloyd
GL	Germanischer Lloyd
CLT	Classical Laminate Theory

UD	Uni-Directional
OEF	One Edge Free
NEF	No Edge Free
LCC	Life Cycle Cost
VI	Vacuum Infusion
LT	Lattice Topology
RAND	Research and development
CER	Cost Estimation Relationships
ACCEM	Advanced Composite Cost Estimating Manual
PCAD	Process Cost Analysis Database
NREL	National Renewable Energy Ltd.
FEM	Finite Element Method
SQP	Sequential Quadratic Programmer
ATP	Automated Tape Placement

List of Symbols

δ	Tower deflection	$[m]$
δ_{top}	Tower deflection at the top	$[m]$
γ	Load factors	$[-]$
μ_{xy}	Possoin's ratio when laminate is loaded in X direction	$[-]$
μ_{yx}	Possoin's ratio when laminate is loaded in Y direction	$[-]$
ω_t	Natural frequency of the tower	$[Hz]$
ρ_{mat}	Density of the material	$[Kg.m^{-3}]$
σ	Total axial stress in the laminate	$[N.m^-2]$
σ_b	Stress in the laminate X-direction due to bending	$[N.m^-2]$
σ_c	Compressive stress in the laminate due to dead loads	$[N.m^-2]$
σ_x	Stress in the laminate/link X-direction	$[N.m^-2]$
σ_y	Stress in the laminate/link Y-direction	$[N.m^-2]$
$\sigma_{bear,flange}$	Bearing strength of the flange,	$[N.m^{-2}]$
$\sigma_{cr,crip}$	Critical crippling stress	$[N.m^-2]$
$\sigma_{cr,ebuck}$	Critical Euler buckling stress	$[N.m^-2]$
$\sigma_{cr,lbuck'}$	Critical buckling stress before knock-down factor	$[N.m^{-2}]$
σ_V	Standard deviation in velocity due to turbulence	$[-]$
$\sigma_{x,ut,C}$	Ultimate longitudanal strength in compression of the laminate/link	$[N.m^-2]$
$\sigma_{x,ut,T}$	Ultimate longitudanal strength in tension of the laminate/link	$[N.m^-2]$
$\sigma_{y,ut,C}$	Ultimate transverse strength in compression of the laminate/link	$[N.m^-2]$
$\sigma_{y,ut,T}$	Ultimate transverse strength in tension of the laminate/link	$[N.m^-2]$
τ	Inplane shear stress in the laminate	$[N.m^-2]$
$\tau_{cr,lbuck'}$	Critical buckling shear stress under torsional loading	$[N/m^{-2}]$
$\tau_{torsion}$	In-plane shear stress in the laminate due to torsion	$[N.m^-2]$
$\tau_{ut,adhesive}$	Ultimate shear strength of the adhesive	$[N.m^-2]$
$\tau_{ut,bolt}$	Ultimate shear strength of bolt	$[N.m^{-2}]$
τ_{ut}	Ultimate inplane shear strength of the laminate/link	$[N.m^-2]$
θ_{Cone}	Cone angle of the nacelle	$[^\circ]$

θ_{Shaft}	Shaft tilt of the nacelle	$[^\circ]$
ζ	Damping factor	$[-]$
$\underline{S}$	Cumulative stiffness of laminate	$[N.m^{-2}]$
A	Area of the tower cross section	$[m^2]$
a	Overlap length in a joint	$[m]$
A_L	Cross section area of the link	$[m^2]$
A_{surf}	Surface area of the tubular section	$[m^2]$
b_L	Breadth/width of the lattice tower links	$[m]$
b_{found}	Breadth of the foundation	$[m]$
b_{leg}	Base leg distance in lattice tower	$[m]$
b_{top}	Width of the lattice tower on top	$[m]$
C_θ	Cos of the ply angle	$[^\circ]$
C_b	Buckling factor for column buckling	$[-]$
D	Diameter of the tubular tower	$[m]$
$d\theta_{x,y,z}$	Rotation in the X,Y,Z axis	$[rad]$
D_b	Diameter of the base of the tubular tower	$[m]$
D_t	Diameter of the top of the tubular tower	$[m]$
D_{bolt}	Bolt diameter	$[m]$
$d_{x,y,z}$	Displacement in the X,Y,Z direction	$[m]$
DA	Dynamic amplification factor	$[-]$
DF	Damage factor in fatigue	$[-]$
E_x	Modulus in X direction	$[N.m^{-2}]$
E_x	Modulus of tower laminate in X direction	$[N.m^{-2}]$
E_y	Modulus in Y direction	$[N.m^{-2}]$
E_{bolt}	Bolt young's modulus	$[N.m^{-2}]$
F	Shear load acting on an arbitrary section of the tower	$[N]$
$F_{L,x,y,z}$	Forces apperaing on link in the X,Y,Z axis	$[N.m]$
F_p	Bolt preload	$[N]$
F_{top}	Tower top shear load	$[N]$
$F_{Z,top}$	Tower top axial load	$[N]$
FC	Final blade clearance	$[m]$
G	Gust factor	$[-]$
G_{xy}	Shear modulus of the tower laminate	$[N.m^{-2}]$
h	Total height of the tower	$[m]$
h'	Height of an arbitrary section in the tower	$[m]$
h_2	Height of the lattice tower section 5	$[m]$
h_{found}	Height of the foundation	$[m]$
I	Area moment of inertia in tubular section	$[m^4]$
I_{ref}	Turbulence intensity	$[-]$
$I_{y,L}$	Area moment of inertia the link cross section in Y-axis	$[m^4]$

$I_{z,L}$	Area moment of inertia the link cross section in Z-axis	$[m^4]$
IC	Initial blade clearance	$[m]$
J_L	Polar moment of inertia the link cross section in Y-axis	$[m^4]$
K_e	Element stiffness matrix	$[N.m^{-2}]$
K_t	Thickness coefficient	$[-]$
L	Length of the tower section	$[m]$
L_e	Element length after discretization	$[m]$
L_{blade}	Max deflection of the blade	$[m]$
M	Moment acting on an arbitrary cross section of the tower	$[N.m]$
M_e	Element mass matrix	$[Kg]$
M_z	Torsion acting on an arbitrary cross section of the tower	$[N.m]$
M_{sec}	Secondary Moment acting on a cross section	$[N.m]$
$M_{L,x,y,z}$	Moment apperaing on link in the X,Y,Z axis	$[N.m]$
M_{ply}	Rotation matrix for a ply	$[-]$
M_{top}	Tower top moment	$[N.m]$
$M_{Z,top}$	Tower top torsion	$[N.m]$
$Mass_{top}$	Mass on the tower top	$[Kg]$
$Mass_{tower}$	Mass of the tower	$[Kg]$
n_b	Number of bolts	$[-]$
$n_{section}$	Number of sections in tapered part of lattice tower	$[-]$
P	Rotor frequency	$[Hz]$
p_{bolt}	Pitch of the bolt	$[-]$
P_{surf}	Perimeter of the tubular section	$[m]$
Q	Velocity pressure	$[m^{-1}.s^{-1}]$
Q_{ply}	Ply stiffness at 0 degree	$[N.m^{-2}]$
R_i	Inner radius of tubular tower	$[m]$
R_L	Radius of the lattice tower links	$[m]$
R_o	Outer radius of tubular tower	$[m]$
$R_{curvature}$	Radius of curvature	$[m]$
S_i	Stiffness of the lamina	$[N.m^{-2}]$
S_θ	Sine of the ply angle	$[^\circ]$
$SF_{l,buck}$	Safety factor in local buckling	$[-]$
SF_{mat}	Material safety factor using Tsai-Hill criterion	$[-]$
t	Thickness of the tower laminate	$[m]$
t_b	Thickness of the base of the tubular tower	$[m]$
t_i	Thickness of the i th lamina	$[m]$
t_L	Thickness of the lattice tower links	$[m]$
t_t	Thickness of the top of the tubular tower	$[m]$
t_f	Thickness of the flange	$[m]$
V_{hub}	Velocity of the wind at hub height	$[m.s^{-1}]$

V_{ref}	Reference wind speed over 10 min	$[m.s^{-1}]$
W_a	Width of the Adhesive joint	$[m]$
w_{found}	Width of the foundation	$[m]$

Acknowledgments

Numerous people have played an instrumental role in helping me with my master's thesis and to get me where I am today.

I would like to thank Dr.ir. Sonell Shroff, for helping me find this wonderful thesis opportunity at Suzlon Energy Ltd., for mentoring me throughout the master's course and for the kind words, support and feedback when I needed it the most.

I would like to thank Dr. Christos Kassapoglou and Ir. Peter Joosse, my daily supervisors from TU Delft and Suzlon for inspiring me to put in my 100% on this project and for being the best mentors one could ask for.

Thank you, Amma, Aanu and Sharath for being my support pillars and for pampering me with your love and care. Special thanks to mom for the many calls reminding me to be happy & healthy and for **not** assuming I am gravely injured every time I missed a call.

Finally, thank you Athul and Varun for being my best buddies. Your witty comments and exhilarating conversations have always helped me pop out of my fear bubble.

Delft, University of Technology
15 Sept 2017

Shreya Ravalappa Kamath

Chapter 1

Introduction

Wind turbines harness kinetic energy from the wind and convert it into electricity. Though wind energy currently accounts for only 1-1.5% of the world energy production, it is one of the most efficient and promising forms of renewable energy and is projected to account for up to 7% of the global power supply by 2040 [1]. It is required to have high capacity turbines to meet this demand which implies larger rotors at higher hub heights. The rotor area and hub height determine the magnitude and strength of available wind flow. Wind speed increases with height enabling wind turbines to work at full capacity.

1.1 Background

A wind turbine consists of the rotor, nacelle and the tower. The rotor includes blades, the hub, and the mechanisms for the control of the blades as shown in Figure 1.1. The nacelle houses the gear box, generator, brakes, etc. The tower carries the nacelle and the rotor and transfers the loads appearing on the yaw bearing to the foundation. It is one of the costliest components of the turbine. It accounts for 20-25% of the turbine cost and around 13-15% of the overall cost [2].

The likely specifications and points of concern with a typically tall and wide tubular tower made of steel used for 3MW and a 5MW turbine are given in Table 1.1. Companies in the wind industry like Vestas, GE, Suzlon are on a constant lookout to improve the design focusing on these points of concern. Some of the attempts include sectioning the tower radially to avoid transportation issues, use of timber or concrete as an alternative material or even adopt hybrid tower designs usually consisting of lattice design for the bottom half and steel tubular design for the tower top. Increase in the tower mass and cost with the increase in height and turbine capacity, among others, are issues that remain unsolved.

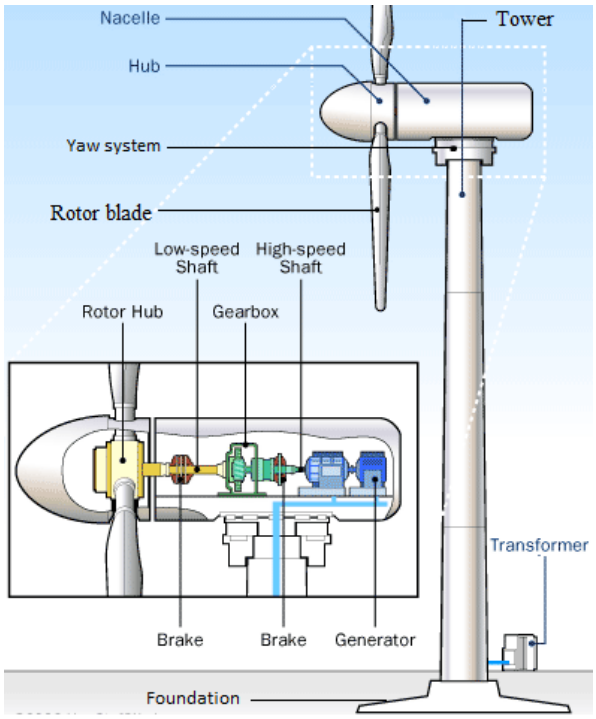

Figure 1.1: Wind turbine parts and tower system

	3MW	5MW	Points of concern
Height (m)	125	150	Transportation issues, needs special trailer
Base diameter (m)	5.8	7.6	Road transportation limit in many countries is 4.5m in width
Thickness (cm)	3.8	4.5	Steel sheet metal rolling process thickness limit is 4cm
Natural frequency (Hz)	0.26	0.22	Resonance effects as tower frequency decreases and nears rotor frequency
Mass (tons)	368	777	Difficulties in assembling on-site

Table 1.1: Points of concern with increasing turbine height and capacity [2]

Composite structures could help in mitigating these problems with their high stiffness/mass ratio and manufacturing flexibility. Also, they possess other advantages in the long run like superior corrosion resistance and better fatigue performance. Until now, there have been very few attempts to use composites in wind turbine towers. Lim et al. [3] and Han et al. [4] have made such efforts, but their design lacks study of economic feasibility in detail, which is a major factor since composites are costlier than steel.

Hence this project involves developing a preliminary design of a Fiber Reinforced Plastic (FRP) composite tower taking into account economics of the structure to eventually help mitigate some if not all of the above problems existing in the current design.

1.2 Requirements from Suzlon and research objective

The advantages of composite structures over metallic structures are well documented, but the feasibility of composite structures especially for high load carrying structures like wind turbine tower is still a gray area. Hence the main expectations of this project by Suzlon is outlined below.

1. Survey the available knowledge on composite wind turbine towers and build a design tool for the preliminary analysis of composite tower for tubular and lattice designs using Matlab. This tool should include all the necessary loading conditions, failure modes and an inbuilt cost model to provide a reasonably optimized tower design for a predefined hub height and turbine capacity.

2. Identify the possible hub heights and turbine capacities where composite towers show potential promise over steel towers. This task intends to subsequently help Suzlon identify the gap in the existing knowledge of composite tower and focus future research on developing an economically sustainable alternative to the contemporary steel tower design.

The research objective is "To investigate the economic and structural feasibility of composite wind turbine towers by developing and analyzing a preliminary design of a composite wind turbine tower."

1.3 Thesis workflow

Initially, a literature study was carried out to find out the existing designs, loads & constraints and cost parameters needed to set up the design tool. Then a set of research questions were proposed based on literature survey and the shortcomings of the steel tower. After the literature review, the tubular tower and the lattice tower model were set up using the analytical method and the numerical method respectively. The model provided with design outputs like deflection, stresses, and the natural frequency. To come up with the final tower design, it was required to perform trade studies to see how the geometric parameters will affect the mass of the structure. A cost model was developed subsequently, and the likely values of cost contributors were decided through the literature survey and Suzlon in-house knowledge. The final tower designs for various hub height were found either using brute force method (in the case of the tubular towers) or a robust optimizer inbuilt in Matlab like Sequential Quadratic Programmer (SQP) (in the case of the lattice towers) depending on the number of design parameters.

Since the lattice structure was developed using a Finite Element Method (FEM) framework in Matlab, a verification of the mathematical operations conducted in Matlab was done using Ansys. For a similar geometry and input, the model must behave similarly on both the platforms. In the final task, the final tower designs of 2.1MW and 5MW towers were compared with existing steel towers. The comparison was made quantitatively concerning mass and cost. The mass included the approximate joint mass and the cost included major cost contributors like material, transport and installation cost.

1.4 Reader's guide

Chapter 2 provides with the literature on existing tower designs, the loads, constraints and cost contributors needed to setup the tool and the research questions relevant to the study. Chapter 3 outlines the methodology used to setup the preliminary design of the tubular tower structure. This also includes the description of the joint design adopted for tubular structure. Further, this chapter addresses the methodology to set up the lattice tower structure. Chapter 4 describes the cost modeling technique selected to evaluate the likely costs involved in composite tower structures. Finally, Chapter 5 discusses the results, comparison and findings of the study. Chapter 6 concludes the study with recommendations for future research.

Chapter 2

Literature Review

This chapter reviews the background needed to carry out the research objective of the master's thesis. In the following sections, the currently existing tower types followed by the study done on composite wind turbine towers is presented. The background needed to setup the structural and cost model for a wind turbine tower is discussed. Finally, the economic impact and relevance of the project are discussed, and the research questions are formulated.

2.1 Wind tower design types

Some of the wind turbine tower designs that have been tried and tested in the past are the lattice, tubular, Danish tripod design, space truss structure and the tall, slender towers with guy wires. But, the industry has narrowed it down to either free standing tubular tower or the lattice tower as shown in Figure 2.1.

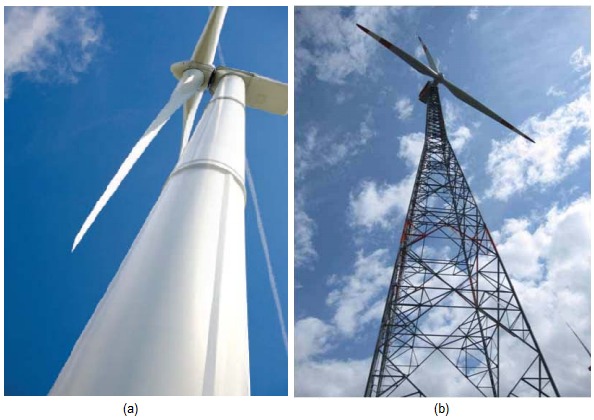

Figure 2.1: Common wind turbine tower designs (a) Tubular structure (b) Lattice structure [2]

Another categorization of towers would be based on the stiffness of the tower. They are categorized as soft-soft, soft-stiff, stiff-stiff depending on the relative position of the natural

frequency of the tower ω_t w.r.t. rotor frequency (P) and the blade passing frequency (3P in the case of three blade rotor system) as shown in Figure 2.2.

With increasing tower height the mass of a stiff-stiff tower will be commensurately high since it will need a large amount of material to attain such high stiffness/mass ratio. In a soft-soft tower, the rotor frequency will interfere with the natural frequency of the tower during the start and shutdown phases leading to unnecessary vibration. This can be avoided by the soft-stiff design which is adopted for large wind turbines since its natural frequency lies beyond rotor frequency and below blade passing frequency. But, here a point of concern is the allowable bandwidth for the natural frequency of the tower, which could be narrow due to the low rpm of large rotor turbines.

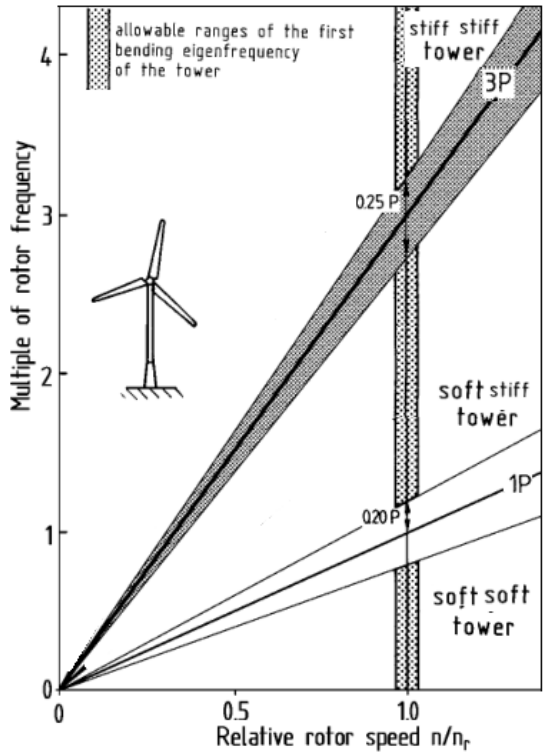

Figure 2.2: Tower based on stiffness properties [5]

2.1.1 Comparison of existing wind turbine towers

Table 2.1 shows the comparison between Tubular Steel Tower (TST), Tubular Steel Tower sectioned Radially (TSTR), Tubular Concrete Tower (TCT), Lattice Topology (LT) made out of steel, Tubular Timber Tower (TTT), Hybrid Tower (HT) with bottom half of the tower made from concrete and top half from steel for a 125m, 3MW turbine tower.

Most of the modern turbine towers are made of steel. For a taller tower, if the base radius is limited, the thickness of the tower increases (TST) and rolling of steel metal plates becomes progressively difficult with the increase in the thickness. Sectioning it radially (TSTR) makes manufacturing and transportation easier, but assembly and maintenance can be a problem. A solution to this would be to use concrete as an alternative material since it can be cast on

	TST	TSTR	TCT	LT	TTT	HT
Base diameter(m)	4.5	5.8	9.25	25	10	9.25
Base thickness (mm)	59	38	-	-	450	-
Tower mass (t)	425	368	1155	307	594	902
Tower cost (1000 €)	978	920	1016	706	712	905

Table 2.1: Mass, cost and geometric properties of various tower for 3MW capacity and 125m height [2]

site (TCT). But, concrete towers are very heavy, need a large foundation and have low tensile strength. Lattice structures (LT) have lower cost and weight, but assembly, maintenance, and ice accumulation can be a point of concern. Legal constraints in some countries prevent the use of lattice structures as they are aesthetically less pleasing than tubular structures. Though timber towers have a higher mass when compared to other towers, their cost is comparable to lattice towers. But, these towers are susceptible to degradation due to the environment. Hybrid towers (HT) have the edge over concrete towers regarding mass and cost, but many of the shortcomings of concrete towers are still applicable to hybrid towers.

2.1.2 Tubular composite towers

Research in composite tower includes the work carried out on static and dynamic characteristics of multi cell glass fiber reinforced composite tower structures by Polyzois et.al. [6]. Lim et al. [3] conducted trade studies to come up with an optimal design for an 80m tall, 2MW capacity wind turbine tower using the composite sandwich panel with glass polyester face sheet and sand-polyester sandwich core. Their study has shown a great improvement in the mass of composite tower (270t) against steel tower (480t). They used filament winding for manufacturing, and no study was done regarding the economic feasibility. Filament winding can be a costly manufacturing process, especially in places like India where labor is cheap, and such automated processes may lead to a higher cost than the current cost. Han et al. [4] have done some investigation on a hybrid material involving double skinned composite shells made of reinforced plastic and filled with concrete. Aspects like manufacturing feasibility and cost estimations have not been fully incorporated in any of the above designs.

2.1.3 Lattice composite towers

Though there has been no application of composites in lattice wind turbine towers, there has been some research in the field of application of composites in lattice cooling structures and power transmission. Here composites have shown great promise owing to low susceptibility to degradation by the environment. But, composites have rarely been used for high load carrying structures, like wind turbine towers.

No criterion dictates when tubular tower design should be chosen over lattice design or vice versa, as it is mainly dependent on the climatic conditions and laws of the country it is installed. For a fair comparison, it is wise that both the designs are pursued at this preliminary stage and compared with the steel counterparts.

2.2 Design loads on a wind turbine tower

2.2.1 Dead Loads or gravity Loads

Dead loads comprise of tower top weight which includes the weight of all the components in the nacelle-rotor assembly and self-weight of the tower. The turbine manufacturer usually provides the tower top mass in the design load matrix, and in the absence of such data, parametric relations which are a function of the turbine rated power is given by Griffin [7] and can be used to calculate the dead loads and the wind loads.

2.2.2 Wind Loads

The wind loads acting on the tower are contributed to by the wind turbine loads and the direct wind pressure on the tower as shown in Figure 2.3.

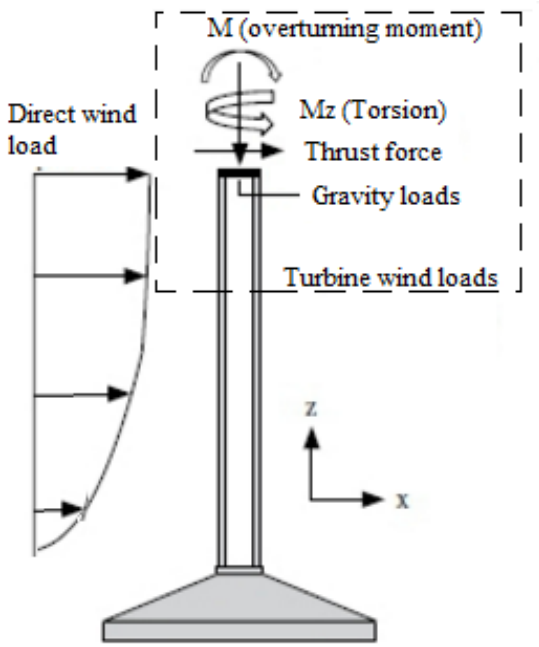

Figure 2.3: Wind load and dead loads acting on the tower

Turbine wind loads

These loads include the aerodynamic loads on the turbine which are transferred to tower via the yaw bearing. The thrust force is the most influential load. The other moments and forces acting on tower top can be a result of the nonuniform velocity field of the wind and the random loads because of wind turbulence and are provided in the design load matrix given by the turbine manufacturer. In the absence of such design load matrix, the known turbine loads on an existing tower can be scaled using scaling relationships presented by Griffin [7]. These scaling relationships take into account the diameter of the rotor and power rating of the turbine and predict the forces and moments on the tower top.

Direct wind load on the tower

The wind exerts a force on the cross section of the tower due to its viscous drag and change in the direction of wind streamline while going around the tower. This force is a function of the wind velocity profile, shape of the tower and the geographical contributors.

Wind loading cases

Wind turbine tower should be designed to withstand normal wind conditions occurring during operation and extreme wind conditions. International Electrotechnical Commission (IEC) 61400 [8] defines 21 load cases for conditions such as start up, shut down, normal operation, extreme condition, parked condition, maintenance condition, etc. Most of the civil engineering structures and preliminary design for towers are based on non-operating extreme wind model with a recurrence period of 50 years. But, LaNier [9] has considered a variety of wind loading cases and observed that depending on factors like dynamic amplification factor, even load cases in operating condition can be critical.

The wind turbines are categorized into class I, II or III as shown in Table 2.2, based on the wind conditions at the site they are installed at [8]. V_{ref} is the reference wind speed at the location over a duration of 10 mins, I_{ref} is the expected turbulence intensity at the site and A, B, C corresponds to high, medium and low turbulence conditions, respectively. Some of

Wind turbine class		I	II	III
V_{ref}	$[m.s^{-}1]$	50	42.5	37.5
A	I_{ref}	0.16		
B	I_{ref}	0.14		
C	I_{ref}	0.12		

Table 2.2: Turbine classes and corresponding reference velocity & turbulence intensity parameters [8]

the important load cases as prescribed by IEC are outlined below:

1. Normal Wind Speed (NWS): This is the loading case to be considered during the operational condition between the cut in and the cutoff velocity.
2. Extreme Wind Model (EWM): Extreme wind speed model is used to simulate scenarios like storms and hurricanes. It is classified either as Extreme Wind Model- 50 year occurrence period (EWM50), which is extreme wind model with a recurring period of 50 years or Extreme Wind Model- 1 year occurrence period (EWM1), with a recurrence period of 1 year.
3. Extreme Turbulence Model (ETM): This load case is similar to NWS except for a standard deviation in the velocity caused by turbulence that is included (σ_V), given by Equation 2.1. Here I_{ref} is the intensity of turbulence, given in Table 2.2.

$$\begin{gathered}\sigma_V = I_{ref}\left(0.144\left(\frac{V_{ave}}{2}+3\right)\left(\frac{V_{hub}}{2}-4\right)+20\right) \\ V_{ave} = 0.2V_{ref}\end{gathered} \tag{2.1}$$

where V_{hub} is the velocity of the wind at hub height.

4. Normal Turbulence Model (NTM): This is an operating condition load case with a wind profile similar to NWS but standard deviation as given by (σ_V), Equation 2.2 is included in the wind velocity.

$$\sigma_V = I_{ref}.0.75V_{hub} + 5.6 \tag{2.2}$$

A sample set of loads for different loading cases for a 5MW turbine with a hub height of 100m is given in Table 2.3. Here, F_{top} is the shear force acting on the tower top. $F_{Z,top}$ is the tower top axial load, which also includes the tower top mass (turbine mass). M_{top} is the tower top moment and $M_{Z,top}$ is the tower top torsion. It is seen that though ETM load case occurs at a wind velocity of $14.22m/s$, it has an F_{top} almost 2-4 times higher than the F_{top} occurring during non operating loading cases (EWM1 and EWM50). Thus ETM load case may still prove to be critical in combination with load factors.

	NTM	ETM	EWM1	EWM50
F_{top} (KN)	6.15E+02	1.44E+03	5.82E+02	3.69E+02
$F_{Z,top}$ (KN)	-4.71E+03	-4.71E+03	-3.49E+03	-3.18E+03
$M_{Z,top}$ (KN.m)	5.87E+03	1.41E+03	2.48E+03	9.32E+03
M_{top} (KN.m)	7.08E+03	6.60E+03	1.33E+04	4.22E+03
V_{hub} (m/s)	9.78	14.22	54.02	70.37

Table 2.3: Tower top loads for 5MW, 90m tower for different wind loading case [10]

2.2.3 Fatigue loads

A tower is supposed to have a service life of at least 20 years. Fatigue loading is often critical during the design phase of a tower. For steel design, using the damage equivalent load method provides a good model for fatigue in preliminary design. Germanischer Lloyd (GL) guidelines recommends a series of steps for modelling fatigue in composite laminates for which S-N curve is not available [11].

2.2.4 Load factors

Since the loading on a tower is a function of wind velocity, some deviations from the mean can be expected due to turbulence and are captured by load factors (γ). The load factors suggested by various standards like American Society of Civil Engineers (ASCE) [12], IEC [8] and GL [11] are tabulated in Table 2.4. ASCE recommendations are conservative compared to IEC or GL standard. During operating condition, an additional load factor to be considered is the Dynamic Amplification factor (DA) which captures the interaction between the tower natural frequency and the rotor & the blade passing frequency (P & 3P). The importance of this term in magnifying the loads to create a quasi-static design load is explained by Erich Hau [5] and given by Equation 2.3:

$$DA = \frac{1}{\sqrt{\left(1 - \frac{P^2}{\omega^2_t}\right)^2 + \left(2\zeta\frac{P}{\omega_t}\right)^2}} \tag{2.3}$$

	IEC	ASCE	GL
Gravity Load (γ_{GL})	1.1	1.2	1.1
Turbine Load (γ_{TL})	1.35	1.6	1.2
Wind Load (γ_{WL})	1.35	1.35	1.35

Table 2.4: Load factors according to various standards

where ζ is Damping factor (structural + soil + aerodynamic). Damping factor depends on the material, type of joint, rotor rpm, soil conditions, etc, and can vary between 2-10%. The likely breakdown of damping factor for a Glass Fiber Reinforced Plastic (GFRP) material with bolted joints, as obtained from the literature, [13], [14], [15], is presented in Table 2.5. The effect of dynamic amplification factor can be reduced either by making sure the tower's natural frequency does not coincide with P or 3P frequency or by increasing the damping factor. The former of the two options is more practical because controlling the damping factor is quite convoluted.

Factor	ζ
Aerodynamic damping during operating condition	1-6 %
GFRP material damping	0.8 %
Soil damping	0.44-1%
Bolted structures	0.8-1.5%

Table 2.5: Likely damping ratio values [13], [14], [15]

2.3 Design Requirements

2.3.1 Frequency requirement

It is discussed in Section 2.1 that based on the natural frequency of the towers, they are classified as soft-soft, soft-stiff and stiff-stiff towers. According to GL guidelines in all cases it is to be ensured that the margins of safety between the tower natural frequency and P & 3P frequencies should be greater than 10% of P and 3P frequencies respectively [11]. A suitable dynamic amplification load factor as given in Equation 2.3 should be included if it is near P or 3P frequency. Lanier [9] has calculated that for a frequency ratio of 0.9 and 1.1 with 10% damping, the dynamic magnification factor DA is equal to 3.82 and 3.29 respectively, which is high but manageable during design.

2.3.2 Geometric requirements

Tower height

Nicholson [16], in his preliminary design for steel tower, has considered constraints regarding tower height and has recommended it to be at least 1.4 times the rotor radius. As suggested by

IEC-61400 guidelines, the lowest point in the rotor diameter should clear the highest nearby wind obstacle by 30 feet and is another constraint on height [8]. There is no upper limit for height. The taller the tower, higher is the probability that it will function at its rated speed consistently.

Tower radius

In many countries the maximum allowable width of the structure for road transportation is 4.5m [16]. To circumvent this constraint, towers with large base diameter are often radially sectioned.

Blade tip deflection

The maximum tip deflection of the blade can be important especially if we are aiming for a tower with large base diameter. Turbine manufacturer usually provides the maximum tip deflection for a blade along with details like shaft tilt and precone angle, which is shown in Figure 2.4. This information can be converted into constraint equation to calculate maximum possible tip deflection, as given by Jonkman et.al. [17] in Equation 2.4. IEC standards recommend keeping a clearance of 30% of the initial clearance between blade tip and tower at all points of time during operation. This gives an upper limit to the tower radius or the tower leg distance near blade tip as shown in Figure 2.4.

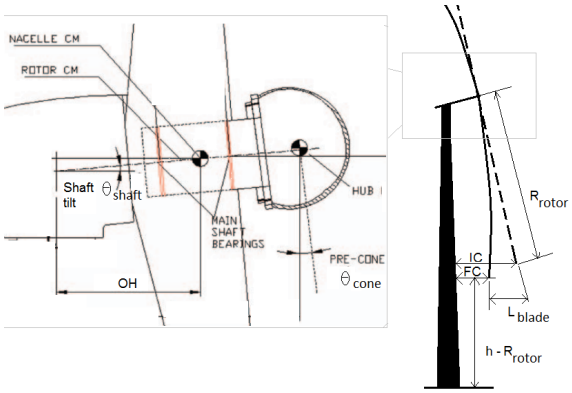

Figure 2.4: Blade tip deflection of a turbine

$$IC = (OH + R_{rotor}\sin(\theta_{Cone}))\cos(\theta_{Shaft}) - \frac{D_{tower}}{2}(h - R_{rotor}) - (L_{blade})$$
$$FC = 0.3(IC) \tag{2.4}$$

h - Total hub height of the tower
IC - Initial clearance
FC - Final clearance
OH - Overhang length of the nacelle shaft from tower midpoint
L_{blade} - Max tip deflection of the blade
$D(h - R_{rotor})$ - Radius of the tower at height near blade tip

θ_{Cone} - Angle made by blade with vertical axis
θ_{Shaft} - Angle made by shaft with horizontal axis

Tower top deflection

Nicholson in his thesis has assumed that the allowable tower tip deflection is 1.25% of the height of the tower [16]. But, there is no strict constraint imposed on tower top deflection as long as other structural and design constraints are respected.

In addition to the external loads, the tower top deflection produces an overturning moment on the tower also called the P-delta effect, shown in Figure 2.5. This additional load appears to oppose the restoring forces by the structural stiffness and gives rise to nonlinear behavior in the tower [18]. If the tower top deflection is not controlled this nonlinearity can exacerbate under turbulent wind conditions and may cause premature failure of the tower. If the allowed tower

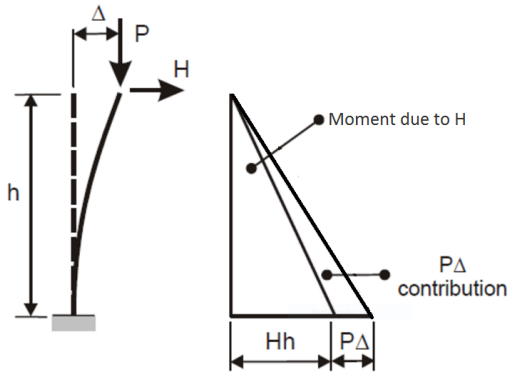

Figure 2.5: P-delta effect on a simple cantilever beam [18]

deflection is too conservative, then the stiffness of the tower needed to satisfy this requirement also increases. The tower stiffness can be favorably manipulated by increasing the effective moment of inertia of the cross-section of the tower. Any modification in favor of the moment of inertia increases the mass and makes the manufacturing of the tower progressively more complex.

It can be concluded that both, a substantial tower top deflection and a highly restricted tower top deflection can produce unfavorable designs. Thus the tower top deflection is usually limited to a rationally and arbitrarily selected value while making sure the mass and manufacturing complexity of the tower remain realistic.

2.3.3 Stiffness calculations & structural requirements

Stiffness calculation

The stiffness of the laminate can be determined either by thin Classical Laminate Theory (CLT) or thick CLT. If the laminate experiences predominantly in-plane loading, the relative position of the layers becomes, irrelevant and thin laminate theory can be used to calculate

the stiffness of the laminate. In a tower, the most prominent forces are axial compression due to dead loads and moments induced due to wind force which causes axial tension-compression stresses in the laminate. Hence, the laminate is assumed to be predominantly Uni-Directional (UD) plies with the position of the individual plies having little or no relevance. The stiffness matrix (Q_{ply})of a 0° ply, as given by thin CLT, is given in Equation 2.5.

$$Q_{ply} = \begin{bmatrix} \frac{E_x}{1-\mu_{xy}\mu_{yx}} & \frac{\mu_{xy}E_x}{1-\mu_{xy}\mu_{yx}} & 0 \\ & \frac{E_y}{1-\mu_{xy}\mu_{yx}} & 0 \\ sym & & G_{xy} \end{bmatrix} \tag{2.5}$$

Here E_x is the modulus of tower laminate in X direction, E_y is the modulus of tower laminate in Y direction, G_{xy} is the shear modulus, μ_{xy} possoin's ratio when laminate is loaded in X direction and μ_{yx} possoin's ratio when laminate is loaded in Y direction.

For any other angle, the stiffness matrix can be rotated using the rotation matrix (M_{ply}) and the stiffness matrix of an angle-ply (S_i) can be found in Equation 2.6. The cumulative stiffness matrix ($\underline{S}$) of the entire laminate can be found by simply superimposing the stiffness matrices scaled by their thickness fraction and is given by Equation 2.6.

$$\begin{gathered} M_{ply} = \begin{bmatrix} {C_\theta}^2 & {S_\theta}^2 & 2.C_\theta.S_\theta \\ {S_\theta}^2 & {C_\theta}^2 & -2.C_\theta.S_\theta \\ -C_\theta.S_\theta & C_\theta.S_\theta & {C_\theta}^2 - {S_\theta}^2 \end{bmatrix} \\ S_i = M_{ply}(\theta_i).Q.M'_{ply}(\theta_i) \\ \underline{S} = \frac{1}{t}\sum_{i=1}^{n} S_i t_i \end{gathered} \tag{2.6}$$

C_θ, S_θ - Cosine and sine of angle made by fibers in the ply
t - Total thickness of the laminate
S_i - Stiffness matrix of i^{th} lamina
t_i - Thickness of the i^{th} lamina

Material failure

Material failure occurs if the loads surpass the strength of the laminate. If the laminate undergoes uniaxial loading, then a simple non-interactive maximum stress based failure criterion can be used to check for material failure. If there is loading in multiple directions, a failure criterion with stress interaction, like Tsai-Hill [19] [20], Tsai-Wu [21], can be used to predict the first ply failure. Material failure given by Tsai-Hill failure criterion is analogous to Von Mises criterion for isotropic materials and is given in Equation 2.7 [22]. When the left-hand side of the equation 2.7 becomes equal to or exceeds, one failure is predicted. Tsai-Hill criterion provides a good prediction of failure when the laminate is under a combination of stress, except for biaxial compression [22]. The original Tsai-Hill theory does not distinguish between tensile and compressive strength and underestimates the failure stress. The modified Tsai-Hill criterion uses conditions given in Equation 2.8 to take into account this drawback [23].

$$\frac{{\sigma_x}^2}{X^2} - \frac{\sigma_x\sigma_y}{W^2} + \frac{{\sigma_y}^2}{Y^2} + \frac{\tau^2}{S^2} = \frac{1}{(SF_{mat})^2} < 1 \tag{2.7}$$

SF_{mat} - Material safety factor in the laminate
σ_x, σ_y , τ - Applied stress in x, y, and shear

$$X = \begin{cases} \sigma_{x,ut,T} : \sigma_x \geq 0 \\ \sigma_{x,ut,C} : \sigma_x < 0 \end{cases} \quad Y = \begin{cases} \sigma_{y,ut,T} : \sigma_y \geq 0 \\ \sigma_{y,ut,C} : \sigma_y < 0 \end{cases}$$
$$W = \begin{cases} \sigma_{x,ut,T} : \sigma_x \sigma_y \geq 0 \\ \sigma_{x,ut,C} : \sigma_x \sigma_y < 0 \end{cases} \quad S = \tau_{ut} \tag{2.8}$$

$\sigma_{x,ut,T}$, $\sigma_{x,ut,C}$, $\sigma_{y,ut,T}$, $\sigma_{y,ut,C}$, τ_{ut} - the failure strength in X, Y and shear direction and in tension and compression respectively.

Buckling failure in tubular tower

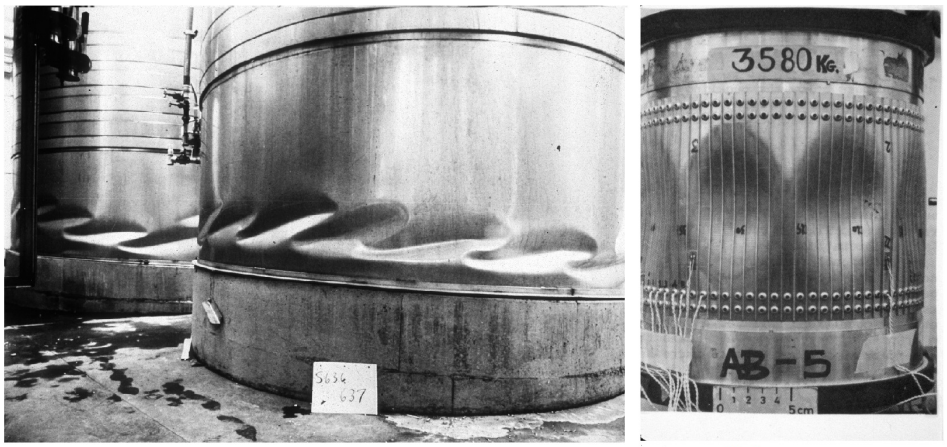

Figure 2.6: Buckling of shells (a)Tosional loading (b) Axial loading [24]

Wind turbine towers have high aspect ratio which makes them susceptible to buckling. Global buckling, like column buckling (Euler buckling), can be expected in case of tubular tower. Further, a part of the composite shell structure can undergo local buckling due to axial, bending or torsional loading as shown in Figure 2.6. Since the loading in the tower laminate is predominantly axial, the laminate is expected to be made up of mostly UD plies making it orthotropic. Nemeth et.al. [25] have given simplified equations for orthotropic shells under axial loading. Seide & Weingarten [26] have demonstrated in their research that under pure bending or bending coupled with axial load the buckling occurs when the peak stress along the circumference reaches classical buckling stress under pure axial compression. Manevich et.al. [27] has presented with analytical equations to calculate the critical buckling stress of orthotropic shells under torsional loading.

Buckling failure in links of a lattice tower

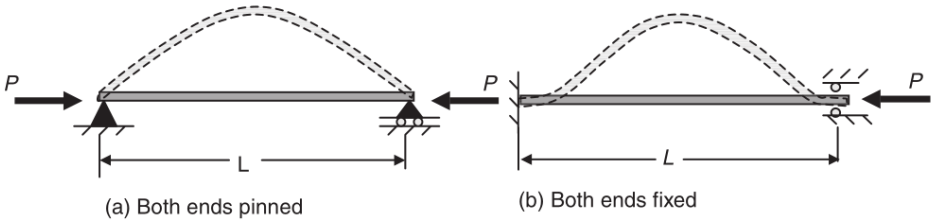

Figure 2.7: Euler buckling of slender beams/shells with (a) pinned and (b) fixed boundary conditions [22]

Euler buckling can be expected in the case of the tubular tower or in links used in lattice tower, as shown in figure 2.7. The Euler buckling critical stress for links differs with the boundary condition, with fixed boundary condition having a higher critical buckling stress than simply supported boundary condition. Crippling is a local failure of the links/beams used in the lattice structure, in which usually a flange collapses as shown in Figure 2.8, leading to a redistribution of loads. The link might catastrophically fail if it does not have appropriate post buckling strength. Failure by crippling of flanges is more common than column buckling in slender structures with open cross sections. [22]. The crippling strength of flanges and web in a beam can be found using the semi empirical relationship given by Kassapoglou [22] or the buckling equation for an infinitely long flange.

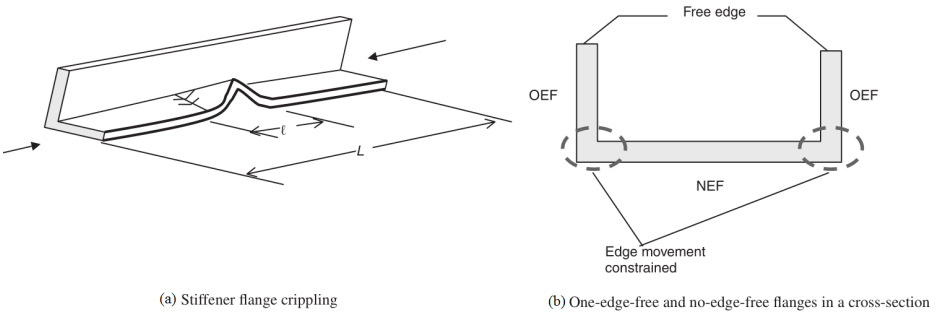

Figure 2.8: Crippling of links with OEF,NEF [22]

2.3.4 Joint requirements

Joining in composites is still a gray area, and in many cases, joint failure may be more critical than material failure or structural failure. Depending on the joining technique adopted some additional constraints may apply due to the failure modes in the joints.

Bolted joint and failure modes

A bolted joint is the most popular joining technique and failures in composite bolted joint are similar to failures in other bolted joints. The following failures of bolted joints in the laminate can be expected.

1. Net section failure
2. Shear-out failure
3. Bearing failure

Figure 2.9 depicts the modes of failure and their corresponding failure plane. Also, there may

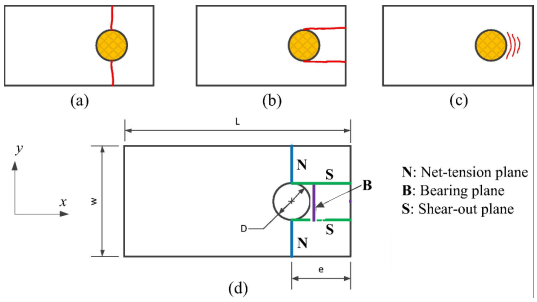

Figure 2.9: (a)Net section failure (b) Shear out (c) Bearing failure (d) Failure planes [28]

be the separation of joint, if it's loaded in tension and the applied pretension is inadequate. Bolt pull through or push through can be a failure mode. Also, Kassapoglou [22] has suggested some good design practices, where a few thumb rules are provided for the distance between bolts, the distance between bolt and flange edge, etc. These can be included as a part of design constraints to come up with a feasible joint design.

Adhesive joint

The adhesive joint is a popular joining method for composite structures due to its lower weight and low-stress concentration, relative to bolted joints. In adhesive joints, force is transferred by shear in the adhesive. At the edges where the loads are introduced into the adhesive, there will be stress concentrations. To account for this, an appropriate knock-down factor must be applied to the strength of the adhesive. The failure is expected to occur when the average stress in the adhesive joint exceeds the knocked down strength of the adhesive.

2.4 Cost modeling in composites

The wind industry is highly profit-driven, unlike the aerospace industry where customers are ready to pay for enhanced performance. Hence, the cost is one of the main drivers when looking into alternative materials. It is important to note that raw material cost is just one of the factors contributing to the overall cost. Development of cost estimation models during

preliminary stage can encourage the use of composites as it is estimated that 70% of the final product cost is determined during design stage [29]. It is essential for designers to have at least some cost modeling technique that helps them predict the cost and adapt to it in early stages of design.

Most of the cost advantage of composites is spread out in the Life Cycle Cost (LCC), and it is quite tricky to formulate a model that gives a complete evaluation of all the factors influencing LCC. Some of the cost contributors gathered from the literature ([30], [31], [32]) are presented in Figure 2.10 and explained in detail below.

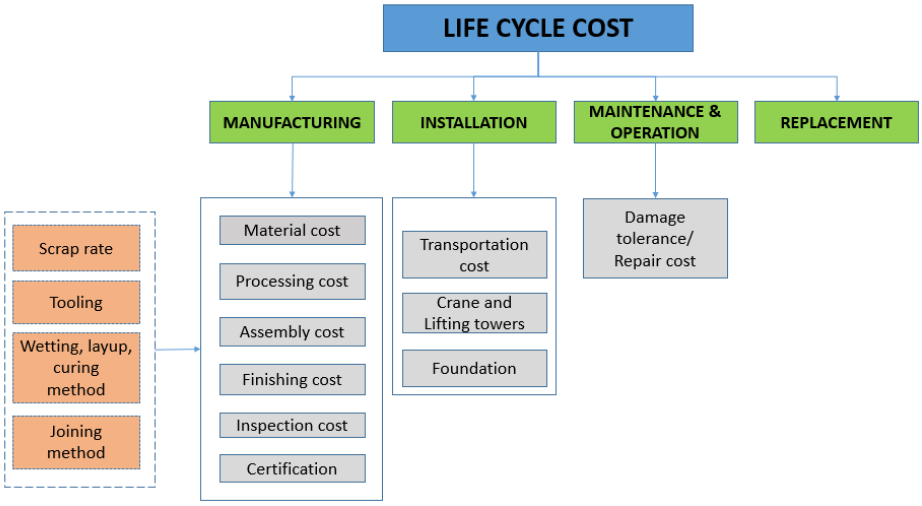

Figure 2.10: Cost contributors in a composite structure

1. Material cost: Composite materials usually consist of glass or carbon fiber reinforcement in a polymer matrix. These fibers can either be dry or pre-impregnated with resin, also known as pre-pregs. Most commonly used resins are epoxy and vinyl ester. The raw material cost of the constituent materials can be added to get the final material cost. Also, there are aiding materials that depend on the manufacturing process, that contribute to the raw material cost. Another important factor is scrap rate, which is also dependent on manufacturing process and varies commonly between 10-20% of the volume of raw materials used, as estimated by Kassapoglou [22].

2. Process cost: The processing cost includes labor costs and machine costs involved in manufacturing. Other contributors to process cost will be tooling like molds, mandrels, hydraulic presses, etc. Two popular approaches to calculating process time are by parametric cost modeling and process-based cost modeling. In parametric cost modeling, the time involved is calculated by observing manufacturing of a sample part of an arbitrary size and scaled proportionally to fit the size or volume of the part in focus. In process-based cost modeling, the time needed for each step in a process is calculated, and then the step times are summed to produce the final time taken by the entire process. An example of parametric cost modeling is the Cost Estimation Relationships (CER) developed by Research and development (RAND) [33]. This method is based on a historical database and may be too dangerous to be used outside the focus of the database or in a different company

environment, without extensive testing. Examples of the process-based technique include Advanced Composite Cost Estimating Manual (ACCEM) cost model by Northrop Corporation [34] and Process Cost Analysis Database (PCAD) model by Gutowski [29]. The total manufacturing time can be multiplied by labor rate and machine rate to get the total labor and machine costs involved in the process.

3. Assembly: Joining is a major step in composite structures and can add significant mass and cost to the overall structure. The assembly cost can be incorporated in preliminary design steps. One such example for including the joint cost in early stages of design for secondary aircraft structures is given by Choi et al. [35], who has used the PCAD model to estimate the likely cost/bond length for adhesives and cost/bolt for mechanical fasteners.

4. Finishing & inspection: According to Suzlon internal data, an estimated 30-40% of the overall manufacturing time is taken up by finishing & inspection which involves applying primer, coating, painting, visual inspection, C-scan, etc. These are labor intensive.

5. Installation: Transportation cost usually depends on the volume and mass of the tower sections. An additional trailer may be needed for transportation for long tubular sections, which will add to the cost. For installation of the smaller capacity tower up to a height of 100-120m, mobile cranes are used which take lesser time for installation, hence lowering cost for hiring the equipment. However, tower cranes are used for larger capacity and taller towers, which have a 5% additional cost over mobile cranes. A study by Engstrom et al. [2] shows that installation can amount up to 20% of overall tower cost, including foundation costs.

6. Maintenance, operation, and repair: Composites need less maintenance than metal structures, and not much research is carried out in this field. There has been a study done by Nystrom et al. [36] regarding Fiber Reinforced Plastic (FRP) bridge structures where a rate of 6.51\$/m^2 is identified for repairs every two years and an inspection cost of 0.0097\$/m^2.

2.5 Economic impact and relevance of the study

The mass and cost distributions of tubular and lattice towers for a 3MW turbine are given in Figure 2.11. The work of this project will directly impact the mass of the tower which currently accounts for nearly 70% of the total mass of the tower and turbine assembly. The tower accounts for only 18% of the overall mass of the structure overshadowed by the massive foundation. But, reduction in the mass of the tower will also lead to a reduction in mass of the foundation which will cause an enhanced reduction in the overall mass. Viewed from the cost point of view, the tower has more contribution towards overall cost because of costlier materials used in its fabrication. Changes in design and material of the tower will affect the cost contribution directly from the tower and indirectly from the foundation, lifting, and transportation, as shown in Figure 2.12. This accounts for 23-25% of the overall cost.

Effects of cost improvement in the tower will be more pronounced in the tubular design as the tower is a larger contributor to the cost of tubular design as compared to lattice design. The final cost of a wind turbine for a 3MW tower will vary from 3.5 million €to 5.7 million €depending on height. The weight can range anywhere from 2000t to 4500t according to Engstrom [2]. Even a 1% savings in the tower cost amplified by the installation of a few

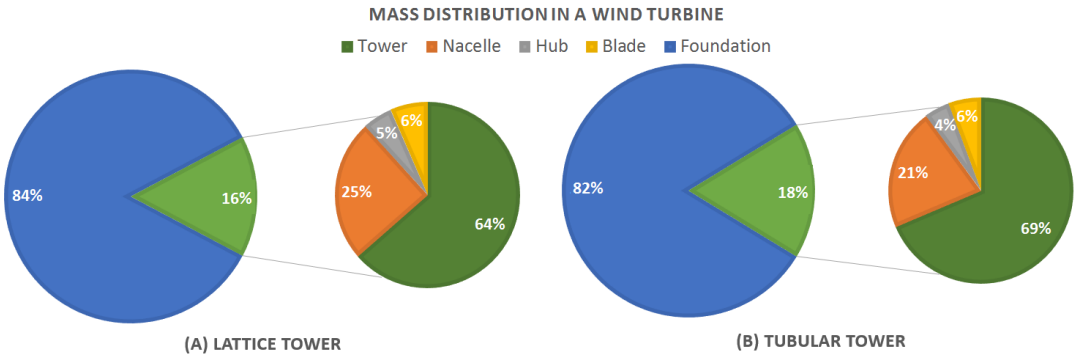

Figure 2.11: Mass distribution of 3MW turbine tower [2]

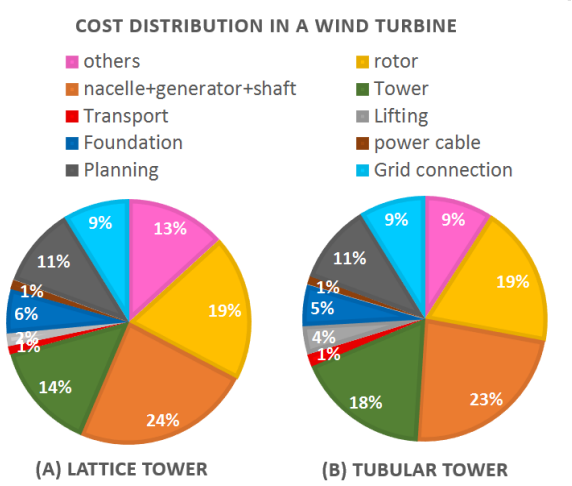

Figure 2.12: Total cost distribution of 3MW turbine tower [2], [37]

thousand towers will amount to a considerable value making this project highly worthwhile. Keeping this in view, composites hold a large potential for being an alternative material candidate for the fabrication of the wind turbine tower, and this project aims to investigate further into this potential and either validate and improve or refute the promise shown by composites.

2.6 Research questions

The project will be an attempt at outlining the preliminary design for composite wind turbine tower based on the most optimum topology, materials, and geometry from a superset of multiple feasible designs. It will require knowledge about the defining structural characteristics of the tower. Detailed knowledge of cost contributors will aid in drawing up a sound preliminary design which incorporates the economic aspects.

The questions will help in setting up the composite tower design tool. These questions will assist in identifying the right geometry, loads, constraints, joining techniques and cost

contributors to set up structural and cost modeling part of the design tool. Once the tool is ready, it is important to find the best solution via trade studies and design iterations to come up with a final design for a specific height 2.1 MW and 5MW turbine tower. Once the final design is set, it is necessary to know if it's a feasible option when compared to the steel-based reference design. Based on these end objectives research questions can now be framed.

1. What is the defining geometrical parameters for the tubular and lattice tower?
2. What type of composite material should be chosen?
3. What are the most critical loading conditions acting on a wind turbine tower throughout its service life?
4. What are the most critical structural constraints when designing the wind turbine tower?
5. Which is the best joining technique to join tubular tower sections and lattice tower links made up of composites?
6. What are the major cost contributors for a wind turbine tower?
7. What are the geometric parameters of a tubular structure and a lattice structure that can be iterated to get the best mass and cost in a wind turbine tower?
8. What is the best method to obtain the most optimized design for mass and cost
9. Does composite hold a potential promise over steel as an alternative material for wind tower?

Question 1-6 will assist in setting up the tool. Question 7-8 will focus on setting up the optimization framework. Answering question 9 will conclude the thesis.

2.7 Chapter summary

Based on literature survey, there is no hard and fast rule to state why or when tubular tower design should be chosen over lattice structure or vice versa. Hence, both the designs will be pursued in this project.

Some of the ways to incorporate wind turbine loads and geometry & structural constraints by various researchers have been discussed. It is important to note that they have been applied to metal structures and care must be taken when applying the constraints to composite structures. Also, it is necessary to identify all the additional structural constraints that can apply due to change in material type.

Different cost factors and prominent cost estimation techniques have been reviewed. Finally, the research questions are formulated based on the literature review and the requirements of the project.

Chapter 3

Structural Modeling of the Tower

This chapter discusses the methodology to design and perform trade studies on a tubular and a lattice Fiber Reinforced Plastic (FRP) tower structure. The optimization framework and the flowchart used in setting up the preliminary design tool is also presented.

3.1 Loads on the tower

For this study, the tower top load appearing on a 90m hub height tower is considered. It is assumed that this tower top load is constant irrespective of the hub height and only the direct wind loading and self-weight changes accordingly. For operating condition, the Extreme Turbulence Model (ETM) given by International Electrotechnical Commission (IEC) is considered as the extreme case. For a 5MW National Renewable Energy Ltd. (NREL) reference turbine, the extreme non-operating load case was the Extreme Wind Model- 50 year occurrence period (EWM50). For the Suzlon 2.1MW turbine, Extreme Wind Model- 1 year occurrence period (EWM1) is the driving tower top load. This decision was made after applying the loads and moments given in the design load matrix and calculating the tower top deflection. For the 2.1MW turbine, the design load table was provided by Suzlon Energy Ltd., and for the 5MW NREL reference turbine this table was obtained from the study by K. Dykes et al. [10] and given in Appendix B. The tower top loads at these loading conditions with load factors included are given in Appendix B. For calculating the direct wind load, the design steps given by American Society of Civil Engineers (ASCE) have been followed, and the steps outlined in the ASCE7 manual and detailed calculation of direct wind loads considered in this study have been included in Appendix B, Section B.2.

3.2 Material system

The properties of Glass Fiber Reinforced Plastic (GFRP) and Carbon Fiber Reinforced Plastic (CFRP) with Epoxy matrix is given in Appendix A. CFRP has around three times the

stiffness and around twice the strength of GFRP UD ply in the X direction. But, according to Suzlon data, CFRP raw material costs is approximately 16€/Kg which is around four times than GFRP material cost which cost around 3.5€/Kg. The trade studies for geometric parameters are conducted using the GFRP material, and the effect is assumed to be similar for CFRP towers as well. However, both the GFRP and CFRP designs are presented for various hub heights to get a complete picture on the feasibility of composites over steel in the manufacturing of the wind turbine towers.

3.3 Geometry of the tubular tower and methodology

The geometry of a tubular tower structure and the loads and geometric parameters associated with the tower are given in Figure 3.1.

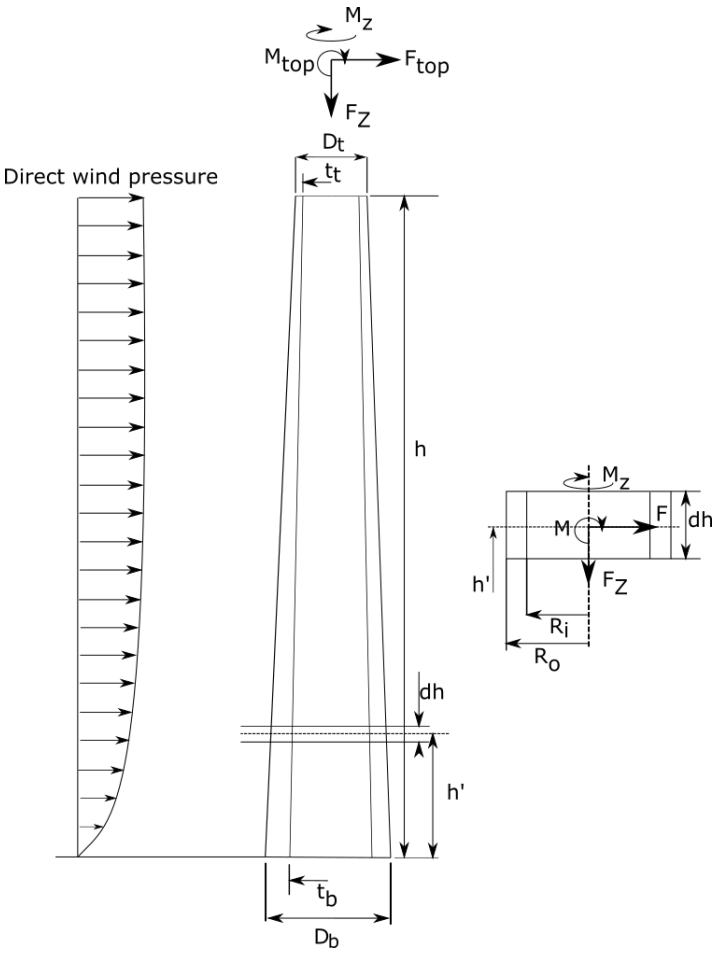

Figure 3.1: Tubular tower structure geometric parameters and loads

In Figure 3.1, D is the outer diameter of the tower and D_b and D_t represents the bottom and top diameter of the tower respectively. Similarly, t is the thickness of the tubular tower and t_b and t_t is the bottom and top thickness of the tubular tower respectively. h is the overall height of the tower and h' is an arbitrary height from the ground.

3.3.1 Beam model analysis

For a tubular tower, due to the high aspect ratio, Euler beam theory is used for the analysis. The tower is assumed to be a cantilever beam. The applied loads are shown in Figure 3.1. M_{top}, M_z, F_z and F_{top} constitute of the tower top wind loads given in Table B.1 of Appendix B. The direct wind pressure is a continuous load appearing on the tower as shown in Figure 3.1. The calculation of this load is detailed in Appendix B, Section B.2.

Using Euler beam theory, it is possible to calculate the global deflection and stresses in the tower. To calculate the natural frequency of the tower, a Finite Element Method (FEM) approach is adopted. For buckling analysis analytical equations for Euler buckling and column buckling are used. Fatigue analysis is carried out on the tubular tower to make sure that the service life is at least 20 years.

The shear force (F) and the overturning moment (M) acting at any cross section h' distance from the base are given by Equation 3.1 and Equation 3.2 respectively and are represented in Figure 3.1.

$$\begin{aligned} F(z) &= F_{top} + \int_{h'}^{h} 0.7.Q(z).G.D(z).dz \\ M(z) &= \int_{h'}^{h} F(z)dz + M_{top} + M_{sec} \end{aligned} \tag{3.1}$$

Here, M_{sec} is the secondary moment acting on the tower section due to the deflection of the tower. Q is the wind velocity pressure, G is the gust factor for flexible structures, $D(z)$ is the outer diameter of the tower at a height h'. The equations to calculate $Q(z)$ and G is given in Appendix B, Section B.2.

The loads acting on the tower will cause the tower to bend and deform producing a radius of curvature at each point along the height of the tower. The radius of curvature ($R_{curvature}$) for an Euler beam along the height is given by Equation 3.2.

$$\begin{aligned} R_{curvature}(z) &= \frac{E_x.I(z)}{M(z)} \\ I(z) &= \frac{\pi}{4}\left(R_o(z)^4 - R_i(z)^4\right) \\ A(z) &= \pi\left(R_o(z)^2 - R_i(z)^2\right) \\ R_i(z) &= R_o(z) - t(z) \end{aligned} \tag{3.2}$$

Here, R_i, R_o are the inner and outer radius of the tower respectively. A is the area of the tower cross section, I is the moment of inertia of the cross section area and E_x is the modulus of tower laminate in its X direction.

Global deflection

Integrating the curvature in the tower twice will give the global deflection (δ) at any point along the height as shown in Equation 3.3.

$$\delta''(z) = \frac{1}{R_{curvature}(z)} \tag{3.3}$$

The secondary moment (M_{sec}) at any height can be calculated using Equation 3.4. The secondary moment is a combined effect of the tower top load and its self weight.

$$M_{\text{sec}}(z) = F_{z,top}(\delta_{top} - \delta(z)) + \int_{h'}^{h} \rho_{mat}\pi(R_o(z)^2 - R_i(z)^2)(\delta\left(\frac{h'+h}{2}\right) - \delta(z)).dz$$
$$Mass_{tower} = \int_{h'}^{h} \rho_{mat}\pi(R_o(z)^2 - R_i(z)^2) \tag{3.4}$$

Here, ρ_{mat} is the density of the material considered, δ_{top} is the tower top deflection and $Mass_{tower}$ is the total mass of the tower.

To include the effect of secondary moments on the deflection, the total moment is updated after the first iteration, and the calculations for curvature and deflection are iterated until the tower deflection converges.

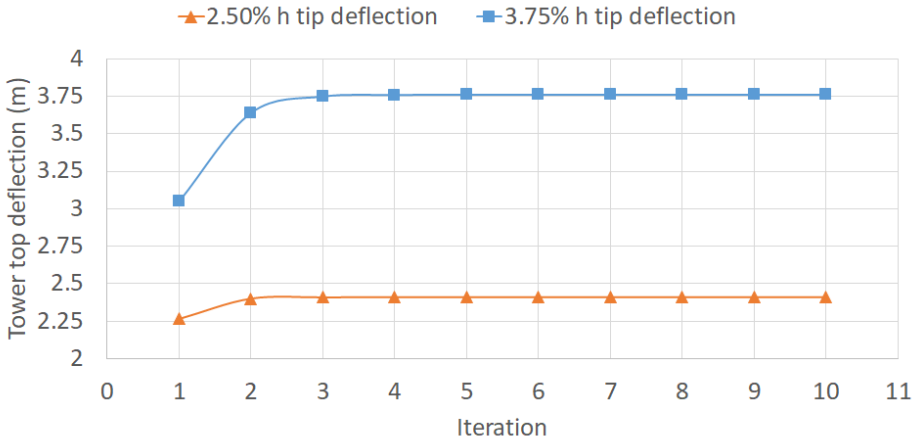

Figure 3.2: Effect of secondary moment on a 100m hub height, 2.1MW turbine capacity tower

The effect of the secondary moment on a 100m tall, 5MW Suzlon tower is shown in Figure 3.2. When the deflection is constrained to 2.5% of the height of the tower, the inclusion of the secondary moment increases the tower top deflection by only 6%. When the deflection is relaxed to 3.75% of the hub height an increase of 23% in tower top deflection is observed due to the secondary moment. Hence, it is recommended to constraint the tower top deflection to 2.5% of the height of the tower to avoid excessive deflection due to secondary moments.

Axial and shear stress in tubular sections

The different stresses in any given section of the tubular tower is shown in Figure 3.3.

The axial stress is a summation of the compressive stress due to dead loads and the bending stress due to the overturning moments caused by wind loading and secondary moments. The Equations to find these stresses are given by Equation 3.5. The maximum bending stress

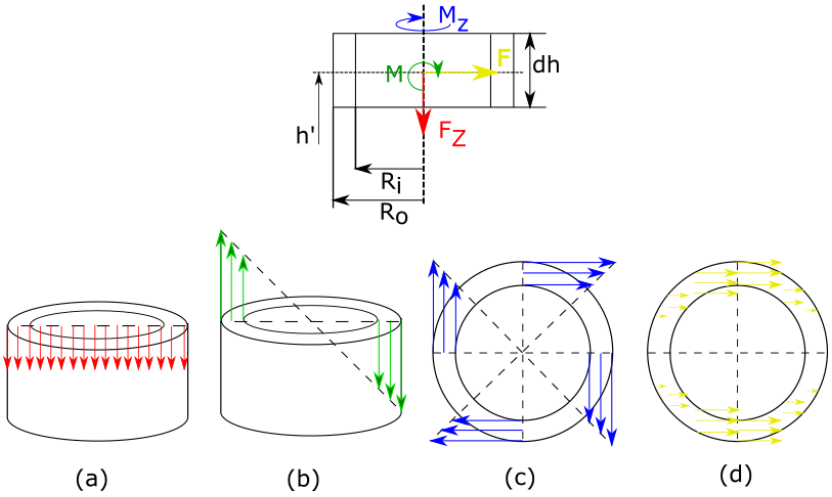

Figure 3.3: (a) Compressive stress (b) Bending stress (c)Torsional stress (d) Shear stress

occurs at the outer radius of the tubular tower, which is the critical bending stress considered in a section.

$$\begin{aligned} \sigma_c(z) &= \frac{F_{z,top} + \int_{h'}^{h} 9.81 \rho_{mat} \pi ({R_o}^2(z) - {R_i}^2(z)) dz}{\pi ({R_o}^2(z) - {R_i}^2(z))} \\ \sigma_{b,\max}(z) &= \frac{R_o(z)}{R_{curvature}(z)}.E_x \\ \sigma(z) &= \sigma_c(z) + \sigma_{b,\max}(z) \end{aligned} \tag{3.5}$$

Here, σ_c is the compressive stress due to dead loads, $\sigma_{b,max}(z)$ axial stress due to moments and σ is the maximum compressive stress.

The maximum shear stress is a combination of stress due to the torsional load on the tower top and the shear forces appearing on the tower section due to the wind loading(F_{top} + Direct wind load). The shear stress occurring at any given height in the tower section is given by the Equation 3.6.

$$\begin{aligned} \tau_{torsion,\max} &= \frac{M_z.R_o(z)}{\frac{\pi}{2}\left({R_o}^4(z) - {R_i}^4(z)\right)} \\ \tau_{shear,\max} &= \frac{2.F(z)}{\pi ({R_o}^2(z) - {R_i}^2(z))} \\ \tau &= \tau_{shear,\max} + \tau_{torsion,\max} \end{aligned} \tag{3.6}$$

Here, M_z is torsion acting on an arbitrary cross section of the tower and equal to $M_{z,top}$, τ_{shear} is the shear stress due to wind loads, $\tau_{torsion}$ in-plane shear stress in the laminate due to torsion and τ is the maximum shear stress on any cross-section.

Though the location of the maximum axial stress and shear stress is different in the representation in Figure 3.3. The direction of the wind loading is not fixed. Hence, it is assumed that the maximum compressive and shear stress occurs at the same location. The Tsai-Hill failure criterion as described in Section 2.3.3 is evaluated by considering the maximum axial

and shear stress and making sure that at every section along the height the material safety factor (SF_{mat})>1.

3.3.2 Buckling analysis in tubular tower

It is discussed in the literature study chapter, Section 2.3.3 that column buckling, as well as local buckling due to axial, bending and shear forces, can occur in a tubular tower section. Due to transportation issues, the tower is usually divided into sections of 15-25 m in length (L). Hence this reduced length (L) is considered while evaluating the critical Euler buckling stress ($\sigma_{cr,ebuck}$) and local buckling stresses ($\sigma_{cr,lbuck'}$, $\tau_{cr,lbuck'}$) as it is assumed that the joints act as simply supported boundary conditions. The Euler buckling critical stress/force for an orthotropic tubular shell structure is given in Appendix C and it is to be made sure that the safety factor in Euler buckling (SF_{ebuck}) >1.

The critical buckling stress for buckling under axial load ($\sigma_{cr,lbuck'}$) can be calculated using analytical equations in Appendix C. Same critical stress is considered for a structure under bending. Similarly, the critical buckling stress under torsion and shear load ($\tau_{cr,lbuck'}$) is given by Equation C.4. The critical buckling stresses in real life will be much lower than that predicted by analytical equations because of imperfections present in the structure. Hence, the critical buckling stresses obtained by analytical equations have to be multiplied by its corresponding knock-down factors given by Det Norske Veritas-Germanischer Lloyd (DNV-GL) guidelines. These knock-down factors have been developed for metal structures, but in this study, these factors are adopted to the composite structure without any change and are given in Table 3.1.

$$Z_t = \frac{L^2}{R_o t}\sqrt{1-\mu_{xy}^2} \tag{3.7}$$

Loading	Critical buckling stress	Factors for calculating knock down				Knock-down factor
		φ_b	Z_e	ρ_b	C_b	
Axial load	$\sigma_{cr,lbuck'}$	1	$0.702Z_t$	$\frac{1}{2}\left(1+\frac{R_o}{150t}\right)^{-0.5}$	$\varphi_b\sqrt{1+\left(\frac{\rho_b Z_e}{\varphi_b}\right)^2}$	$K_a = \frac{C_b}{Z_e}$
Bending load	$\sigma_{cr,lbuck'}$	1	$0.702Z_t$	$\frac{1}{2}\left(1+\frac{R_o}{150t}\right)^{-0.5}$	$\varphi_b\sqrt{1+\left(\frac{\rho_b Z_e}{\varphi_b}\right)^2}$	$K_b = \frac{C_b}{Z_e}$
Shear load	$\tau_{cr,lbuck'}$	5.34	$0.856Z_t^{\frac{3}{4}}$	0.6	$\varphi_b\sqrt{1+\left(\frac{\rho_b Z_e}{\varphi_b}\right)^2}$	$K_\tau = \frac{C_b}{Z_e}$

Table 3.1: Variables to calculate knock-down factors [38]

Here, R_o and t are the average dimensions of the tubular section over the section length (L) and μ_{xy} is the Poisson's ratio when the laminate is loaded in its X axis. The intermediate variables used to calculate the knock-down factors are given in Table 3.1. The final knock-down factor in axial, bending and shear loading is given by K_a, K_b and K_τ respectively.

Once the knock down factors are calculated, it is made sure that the stresses appearing in the tower laminate is less than the critical stress. It is necessary to check if the buckling occurs during combined loading. To calculate this failure, the interaction formula given in

DNV-Germanischer Lloyd (GL) guidelines has been adopted. This interaction formula is for metallic structures. In this study, the formula have been adopted for composite structures without any change. The final interaction formula and the safety factor for local buckling ($SF_{l,buck}$) can be obtained by following the operations given in Equation 3.8.

$$\begin{gathered}
\sigma_t = \sqrt{(\sigma_c + \sigma_b)^2 + \tau^2} \\
\lambda_b = \frac{\sigma_{ut,x}}{\sigma_t}\left(\frac{\sigma_c}{K_a \sigma_{cr,lbuck'}} + \frac{\sigma_b}{K_b \sigma_{cr,lbuck'}} + \frac{\tau}{K_\tau \tau_{cr,lbuck'}}\right) \\
f_b = \frac{\sigma_t}{\sqrt{1 + {\lambda_b}^2}} \\
SF_{lbuck} = \frac{f_b}{K_m} \\
\text{where} \\
K_m = \begin{cases} 1.15 & \sqrt{\lambda_b} < 0.5 \\ 1.45 & 5 \leq \sqrt{\lambda_b} < 1 \\ 0.85 + 0.6\sqrt{\lambda_b} & \sqrt{\lambda_b} \geq 1 \end{cases}
\end{gathered} \tag{3.8}$$

Here, σ_t is the total stress appearing in the tower section. λ_b and f_b are factors representing how close the applied stress is to the critical stress and SF_{lbuck} is the safety factor in local buckling.

3.3.3 Fatigue analysis in tubular structure

Fatigue calculations are important in any wind turbine component due to the periodic loading it undergoes. The fatigue calculations have been briefly described in literature study section 2.2.3. Only the thrust and dead loads are considered as these are the major loads. The tower top moments and the direct wind load on the tower are neglected. The dynamic amplification factor (DA) is taken into consideration and used to amplify the loads depending on the rpm of the rotor. The fatigue analysis consists of obtaining the max/min stress at each velocity between the cut in and cut off velocity of the wind and obtaining the tolerable number of cycles. Further knowing the distribution of loading cycles corresponding to each velocity the damage factor (DF) is calculated and made sure it is lesser than 1 for the given service time of the tower. The steps to perform the fatigue analysis on a composite wind turbine tower are given in Appendix E.

3.3.4 Natural frequency

It is to be made sure that the natural frequency of the tower lies at least 10% away from P and 3P frequencies to avoid resonance. The bending frequency is calculated using FEM approach. The tubular structure is converted into a lumped mass system as shown in Figure 3.4.

The element type used is a 2D beam element. The element stiffness matrix (K_e) and the

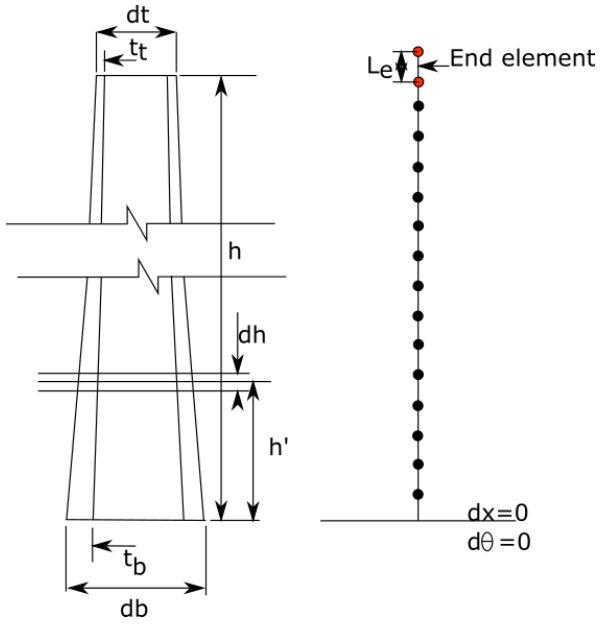

Figure 3.4: Lumped mass system of tubular structure

element mass matrix (M_e) for this element type is given in Equation 3.9.

$$K_e = \frac{E_x.I(z)}{L_e^3}\begin{bmatrix} 12 & 6L_e & -12 & 6L_e \\ 6L_e & 4L_e^2 & -6L_e & 2L_e^2 \\ -12 & -6L_e & 12 & -6L_e \\ 6L_e & 2L_e^2 & -6L_e & 4L_e^2 \end{bmatrix} \quad M_e = \frac{\rho_{mat}A(z)L_e}{420}\begin{bmatrix} 156 & 22L_e & 54 & -13L_e \\ 22L_e & 4L_e^2 & 13L_e & -3L_e^2 \\ 54 & 13L_e & 156 & -22L_e \\ -13L_e & -3L_e^2 & -22L_e & 4L_e^2 \end{bmatrix} \tag{3.9}$$

Here, L_e is the element length after discretization. The mass element at the end should account for the tower top mass ($Mass_{top}$) which is given in Appendix B. This modified mass matrix is given by Equation 3.10.

$$M_e(h) = \frac{\rho_{mat}A(h)L_e + Mass_{top}}{420}\begin{bmatrix} 156 & 22L_e & 54 & -13L_e \\ 22L_e & 4L_e^2 & 13L_e & -3L_e^2 \\ 54 & 13L_e & 156 & -22L_e \\ -13L_e & -3L_e^2 & -22L_e & 4L_e^2 \end{bmatrix} \tag{3.10}$$

The frequency can be found by applying the necessary boundary conditions ($dx = 0$; $d\theta = 0$) at the bottom node and performing Eigen value analysis to extract the first few frequencies. A.C.Way [39] has indicated that the foundation stiffness can affect the frequency of the system by as much as 20%. For the study a foundation of dimension, breadth (b_{found}), width (w_{found}) and height (h_{found}), is considered as 20m, 20m & 3.m respectively and made of concrete. This foundation dimension is considered to find the effect of foundation on a tower frequency. The properties of the soil and the equations used to model the horizontal & rotational stiffness, and the virtual mass of the soil are given in Equation A.1. Once the foundation stiffness and virtual soil mass are evaluated, the fixed boundary condition at the bottom most node is replaced with the foundation stiffness ($K_{e,soil}$), and mass ($M_{e,soil}$) and the Eigen value analysis is performed to extract the necessary frequencies.

The natural frequency of the tower with fixed boundary condition and with foundation stiffness considered for a 100m tall 2.1MW tower is given in Figure 3.5. It is observed that the foundation stiffness boundary condition does not alter the natural frequency of the tower much in the range we are concerned, since, for a soft-stiff design with composite material $\omega_t < 0.4$ Hz and it is very difficult to attain higher stiffness due to the low material stiffness and geometry.

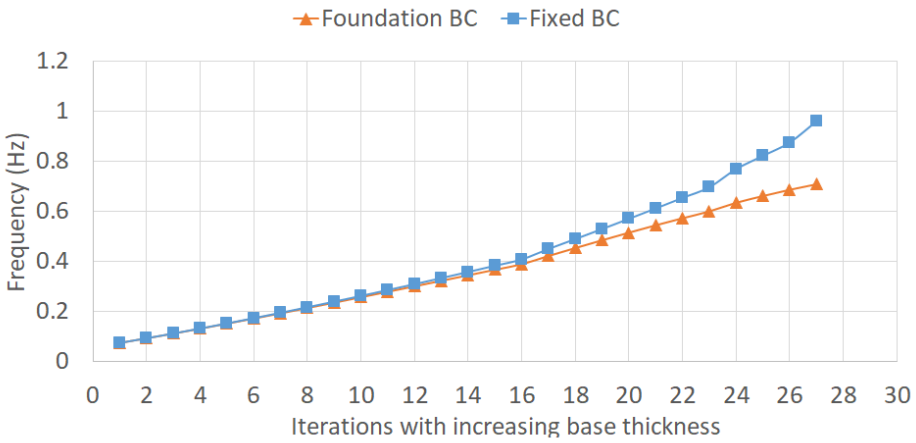

Figure 3.5: Effect of foundation stiffness on the tower natural frequency

3.3.5 Trade studies of the tubular tower

There are a few parameters that define the geometry of the tubular tower as given below.

1. The diameter and thickness at the base of the tower
2. The variation of the thickness of the tower along the height. The tower can either have constant cross section thickness at all points along the height or the thickness can vary with height.
3. The taper or transition in the tower diameter from the base diameter to top diameter.

Effect of base diameter and thickness on the tower properties

It is seen from Equation 3.2, that the moment of inertia (I) is one of the main geometric properties that can affect the tower deflection as well as the bending stresses appearing on the tower. An increase in moment of inertia can reduce the deflection of the tower as well as the bending stresses. In a tubular cross section, I can be increased by increasing the radius of the cross section or by increasing the thickness. For studying the effect of diameter on the moment of inertia, a tubular cross section with thickness 0.1m is considered, and the diameter is varied from 5 to 10m. To study the effect of thickness on the moment of inertia, the diameter was kept at 6m, and the thickness was varied from 0.01m to 0.5m. Both these changes cause an increase in mass, but it is seen from Figure 3.6 that I/A ratio increases with increasing base diameter, but, this ratio increases as we increase the thickness. This implies

that it is better to increase the diameter of the tower rather than increasing the thickness to increase I without adding much mass to the tower.

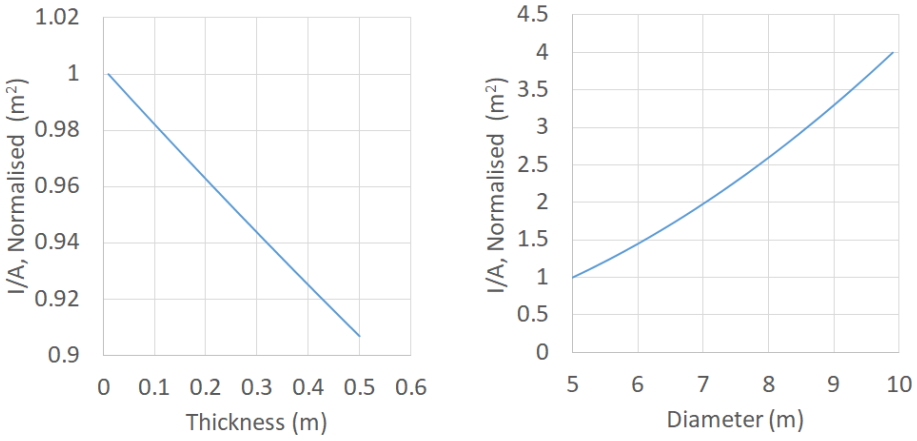

Figure 3.6: Effect of diameter and thickness on I/A in a tubular cross section

This statement is further justified by Figure 3.7 which shows that for the same tower top deflection, it is possible to have other combinations of the tower with increased tower base diameter and reduced thickness and altogether a reduced mass of the tower when compared to the base model. For the 125m tall 2.1MW turbine capacity tower, the base diameter is increased from 5.7m to 8m while reducing the thickness of the tower gradually from 0.15m to 0.07m in the study while keeping the deflection constant. Here the deflection is considered because this is one of the critical constraints in a tubular tower.

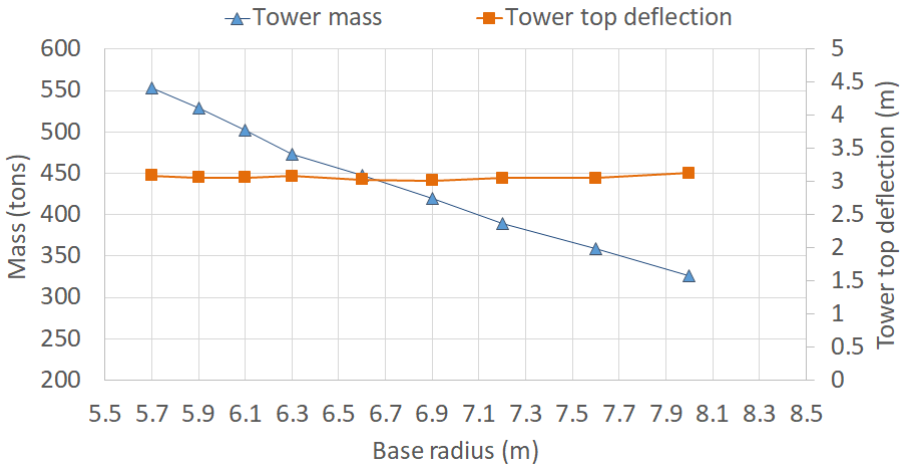

Figure 3.7: Effect of base diameter and thickness on the deflection and mass of a 125m, 2.1MW tower

Effect of variation of the thickness of the tower on the tower properties

Usually, in a tubular wind turbine tower structure, the base thickness is more than the top thickness. This is because of the material needed to take up the large compressive and shear

loads appearing at the base. If a constant thickness is provided, the stiffness at the top of the tower is high and may be over designed. Some degree of stiffness is needed at the top since direct wind loads are maximum at the tower top and low stiffness will lead to large tower deflection. To study the effect of constant thickness tower and variable thickness tower on the mass of the tower, a 100m tall 2.1MW tower was chosen. In variable thickness tower, the thickness is assumed to be a function of radius as shown in Equation 3.11.

$$t(z) = (1 - K_t)\frac{D(z)}{2} \tag{3.11}$$

Where K_t is a constant usually considered between 0.9 and 0.99. E.g. if a tubular tower has a base diameter of 6m and a top diameter of 3m and K_t is chosen as 0.99, then the bottom thickness is 0.06m, and the top thickness is 0.03m and both the diameter and thickness decrease linearly with height.

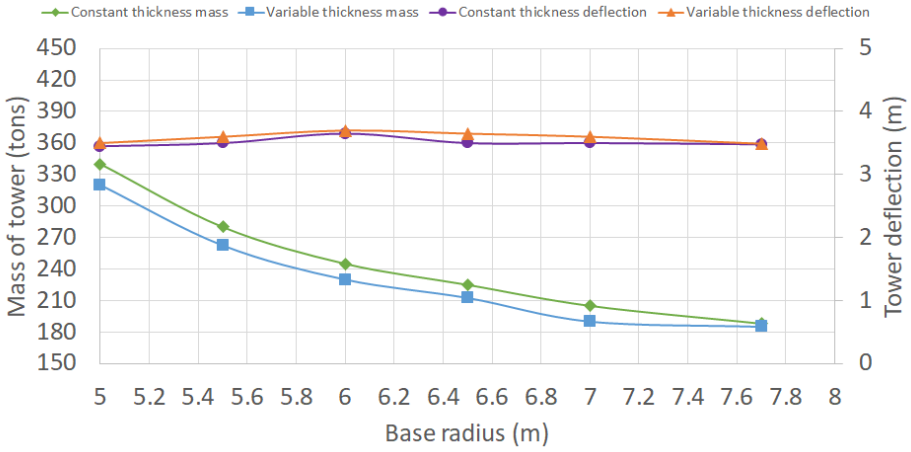

Figure 3.8: Effect of constant and variable thickness on the deflection and mass of a 100m, 2.1MW tower

It is seen from Figure 3.8 that a variable thickness tower has lower or equal mass to that of a constant thickness tower for the same tower top deflection. This may be because of the higher moment of inertia at the tower base in a variable thickness tower is high when compared to constant thickness tower. The higher inertia reduces the curvature at the base and since deflection is the double integration along the height of the curvature, the moment of inertia at every point on the tower affects the tower deflection. The difference in mass between variable thickness and constant thickness tower is reducing with increasing base diameter because with increasing tower base diameter the thickness is reducing as well. Hence the influence of variable or constant thickness on the tower mass is diminishing.

Effect of taper on mass and deflection

In this study, different ways of interpolating the tower top and base diameters (taper) are studied. The linear taper is the most common type of tapering. A limitation is that the maximum base diameter will be constrained depending on the maximum blade deflection. In a stepped taper, the diameter and thickness are averaged over each section. This helps in

the easy manufacturing of the tower. In a straight-taper, the geometry has a straight section until 30% of the height from the top followed by the taper. An exponential taper can be helpful to increase the base of the tower, but the manufacturing can be complex because of the double curvature in the tower section. To study their influence on the mass of the tower a 90m tall 2.1MW turbine capacity tower is chosen. The rotor radius at the height of 54m is 3.25m to comply with IEC blade tip clearance, and the tower top diameter is kept at 3m. The study is presented in Figure 3.9.

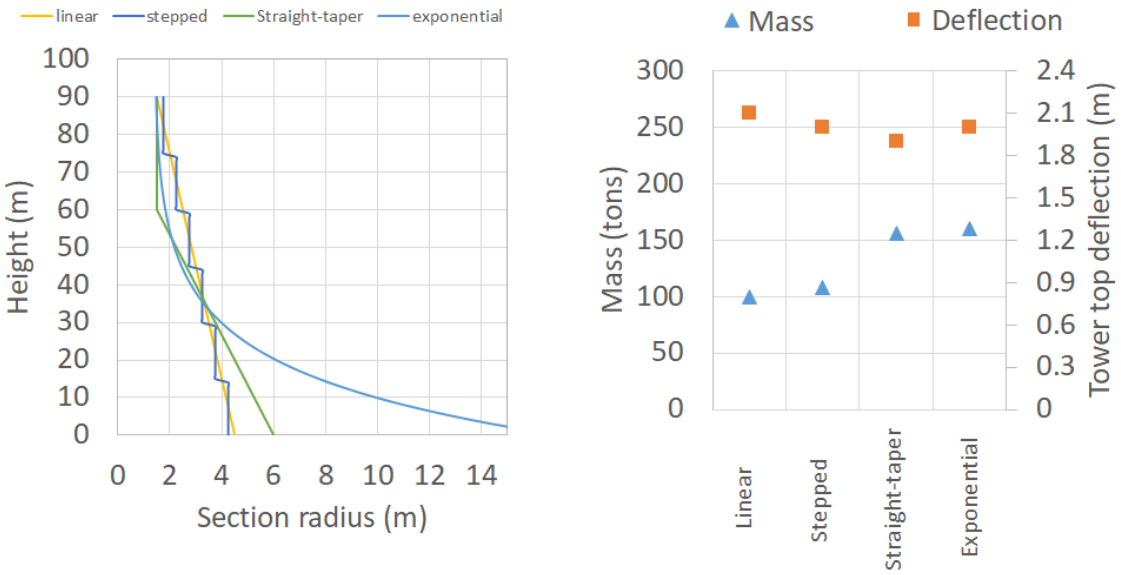

Figure 3.9: Effect of taper on the deflection and mass of a 90m, 2.1MW tower

It is seen that in exponential taper and straight-taper the mass of the tower has increased to maintain the necessary tip deflection. This is because of the low stiffness on the top half of the tower, the tower becomes quite flexible and has a large deflection. Since tower top deflection is one of the main constraints in this study, using these tapers may be a disadvantage. On the other hand, it is seen that there is no significant increase in mass of the tower for the same tower deflection in case of a stepped tower.

3.3.6 Joining in tubular tower structures

For ease of transportation, the tubular structure is usually divided into sections along the height. These sections usually vary from 15-25m depending on the transportation limit of the country and also on the total height of the tower. In this study, each section is considered to be of 25m in height and joined using Joint-1. Joint-2 is necessary if each section is further divided radially to satisfy the constraint of 4.5m road transportation limit on width. In the event of base diameter having to exceed 4.5m, it is necessary to radially divide the tower into two or more parts. In this study, the maximum number of such sections is assumed to be 2. Hence a maximum base diameter constraint of 9m has to be imposed in all tower designs. The joints are further represented in Figure 3.10. Conceptual design and a quick estimation of the mass and cost of the joint on the overall tower mass and cost yields a realistic comparison with equivalent steel towers.

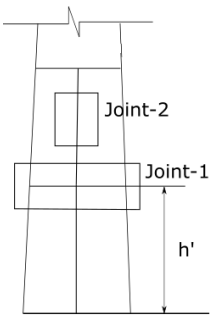

Figure 3.10: The joints involved in tubular structure

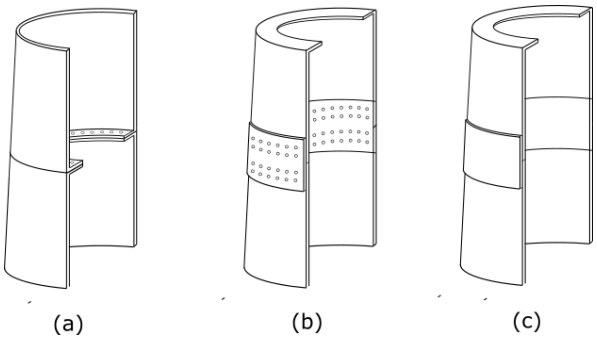

Figure 3.11: (a) Bolted flange joint (b) Bolted Vertical lap joint(c) Vertical adhesive joint

For Joint-1, three joining methods are considered for trade studies. The bolted flange joint is the most common joint in steel tubular towers. This joint may not be the best design for a composite structure due to the thick flanges and high prying effect on the bolts. Hence, the vertical bolt joint and the vertical adhesive joint are also considered for the study. The joining methods considered are shown in Figure 3.11. The failure modes for these joints are presented in Table 3.2.

Bolted flange	Bolted vertical lap	Vertical adhesive lap
Joint separation	Shear failure in bolts	Adhesive failure
Shear failure in bolts	Bearing failure in laminate and plate	Material failure in plate
Bearing failure in laminate	Bolt shear out in laminate and plate	
Bolt shear out	Net section failure of laminate and plate	
Bolt pull through		

Table 3.2: Failure modes due to different joining techniques adopted for Joint-1

Detailed calculation of these failure modes for this project is included in Appendix D. In the case of the bolted flange joint, the protruding flange acts as a circular stiffener that will prevent ovalization of the tubular tower. This joint will prevent radial displacement at the point, and the rotation will be restricted to a certain degree. In the case of bolted and adhesive vertical lap joints, it's assumed that circular stiffeners of 20cm $\times$ 2cm are placed at intervals of 25m. This is an arbitrary number and detail designing of such stiffeners and placement is out of scope. It is expected these stiffeners will prevent ovalization as well as constrain the radial displacement and rotation. This type of constraint is intermediate between the simple support and the clamped condition. In this study simply supported boundary condition is assumed for conservative design.

The mass and cost comparison of various joining techniques for Joint-1 for the 2.1MW capacity turbine towers of various hub height are plotted in Figure 3.12. The cost of the joint includes only the raw material cost, and the detailed methodology of cost estimation is outlined in

Chapter 4. It is seen from Figure 3.12 that the adhesive joint is less expensive as well as

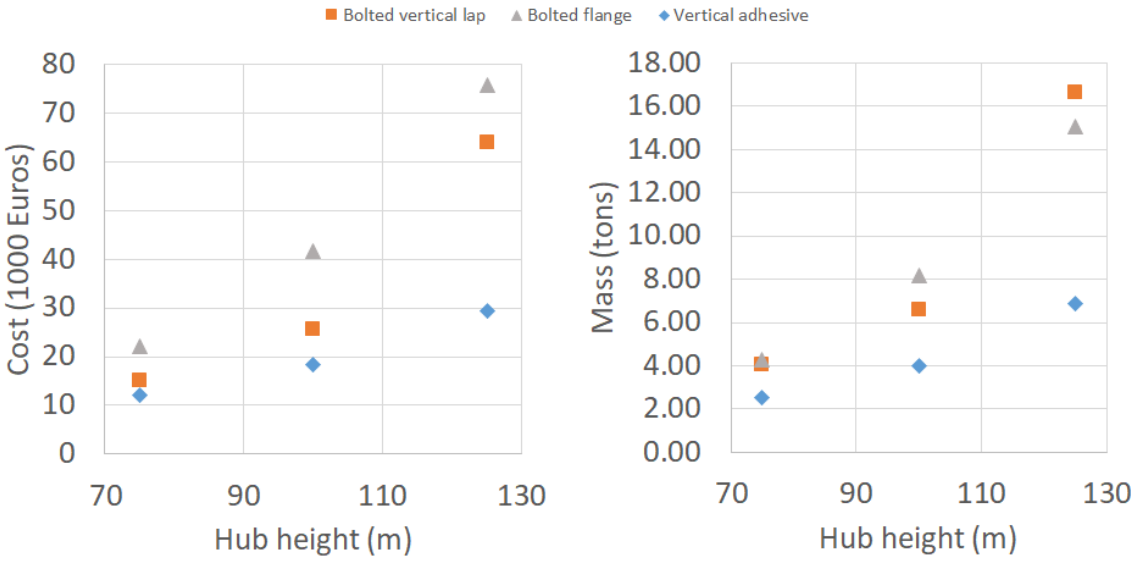

Figure 3.12: Joint mass and cost for joint -1, 2.1 MW turbine

lighter than the bolted joints. This behavior is because the tower laminate is the more critical component in both the types of bolted joints. To prevent bearing failure, a large number of bolts have to be used, and additional biaxial plies have to be added to provide enough bearing strength to the laminate. Hence in this study for the tubular tower Joint-1, adhesive joining method has been adopted.

For the Joint-2, adhesive joining is considered because of the long joint length available. The adhesive joint transfers the load via shear through the adhesive. The ultimate adhesive shear strength ($\tau_{ut,adhesive}$) considered is 3.14Mpa according to GL guidelines. This shear strength includes the safety factor and a stress concentration factor of up to 3. The details of the adhesive joint for Joint-2 is given in Figure D.5.

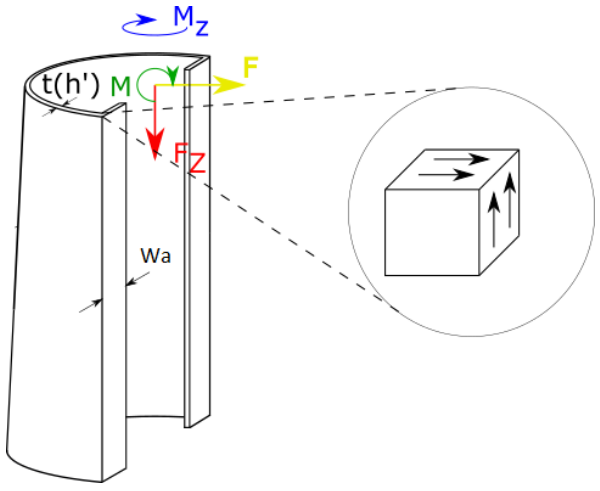

Figure 3.13: Adhesive joint sfor Joint-2

The minimum width of the overlap (W_a) to avoid the adhesive failure can be found using Equation 3.12.

$$\frac{2F + M_z/R_o}{\pi D(h')t(h')} \frac{t(h')}{W_a} < \tau_{ut,adhesive} \tag{3.12}$$

3.3.7 Conclusion on tubular tower and flow chart

The Euler beam model of the tower used to find the stresses and deflection in the tubular tower, and the FEM model used to find the tower natural frequency have been verified using Ansys. The comparison between the results obtained using Ansys, and the analytical methodology is discussed in Appendix F. In the Ansys, shell elements are used to model the tubular tower. The difference between the stresses and deflection given by the Euler beam model and the Ansys model was less than 5%. The difference in the natural frequency between the Matlab FEM model using 2D beam elements and Ansys FEM model using shell elements was less than 2%. This verification ensures that the Euler beam model and the FEM model used in the Matlab tool for the tubular tower is in agreement with the more established model in Ansys.

From the above methodology and trade study the following conclusions are drawn:

1. Secondary moments need to be considered especially when the tower top deflection is large.

2. Material safety factor will be evaluated at each location along the height assuming the maximum axial and shear stress occurs at the same location. This is a conservative approach.

3. For local buckling under combined loading the equations given by DNV-GL for metallic structures will be used without any modification.

4. The effect of foundation stiffness can be neglected in this study as it has little or no impact in the working frequency region we are interested in.

5. Try to maximize the diameter of the tower instead of the thickness of the tower if tower tip deflection is the critical constraint, but care must be taken such that all the other constraints like safety factors in different loading condition, buckling, blade tip clearance condition, etc. are satisfied.

6. Variable thickness towers will be adopted.

7. A linear taper will be assumed, but while doing buckling and joint analysis, the diameter and thickness will be averaged along the section so that it emulates stepped taper.

8. For joint-1, three different joining techniques are considered, but the adhesive joint is presented in the results based on the trade studies conducted. For the joint-2 only the adhesive joining is considered.

3.3.8 Optimization framework and flowchart of the tool

Through trade studies, it is decided that variable thickness and linear taper will be adopted. This leaves out only two parameters that can be modified to obtain the design with least mass among the possible combination of these parameters. Hence, a brute-force approach is adopted rather than using a dedicated optimizer which is time and memory intensive.

The range of the base diameter and thickness have to be decided and input in the Matlab tool. The tool iterates the base diameter in steps of 0.1m and the base thickness in steps of 10mm. All the designs are analyzed. But, only the designs which pass the constraints listed below will be recorded.

$$\text{Clearance between blade and tower} > 30\ \%\ \text{initial clearance}$$
$$\mathrm{P} < \omega_t < 3\mathrm{P}$$
$$\text{Tower top deflection} < 2.5\ \%\ \text{height}$$
$$\text{Material and buckling safety factor} > 1$$
$$\text{Fatigue damage factor} < 1$$

Once the tool evaluates all possible combination of input parameters, the design with the least mass is identified from the Output mass array. The corresponding parameters and analysis results are extracted, and the tool further proceeds to evaluate the cost and joint design for the design with least mass.

The methodology followed along with the constraints and inputs is represented in the flow chart given in Figure 3.14. The flow diagram is translated to Matlab to create a tool which will perform the preliminary analysis of the tubular tower.

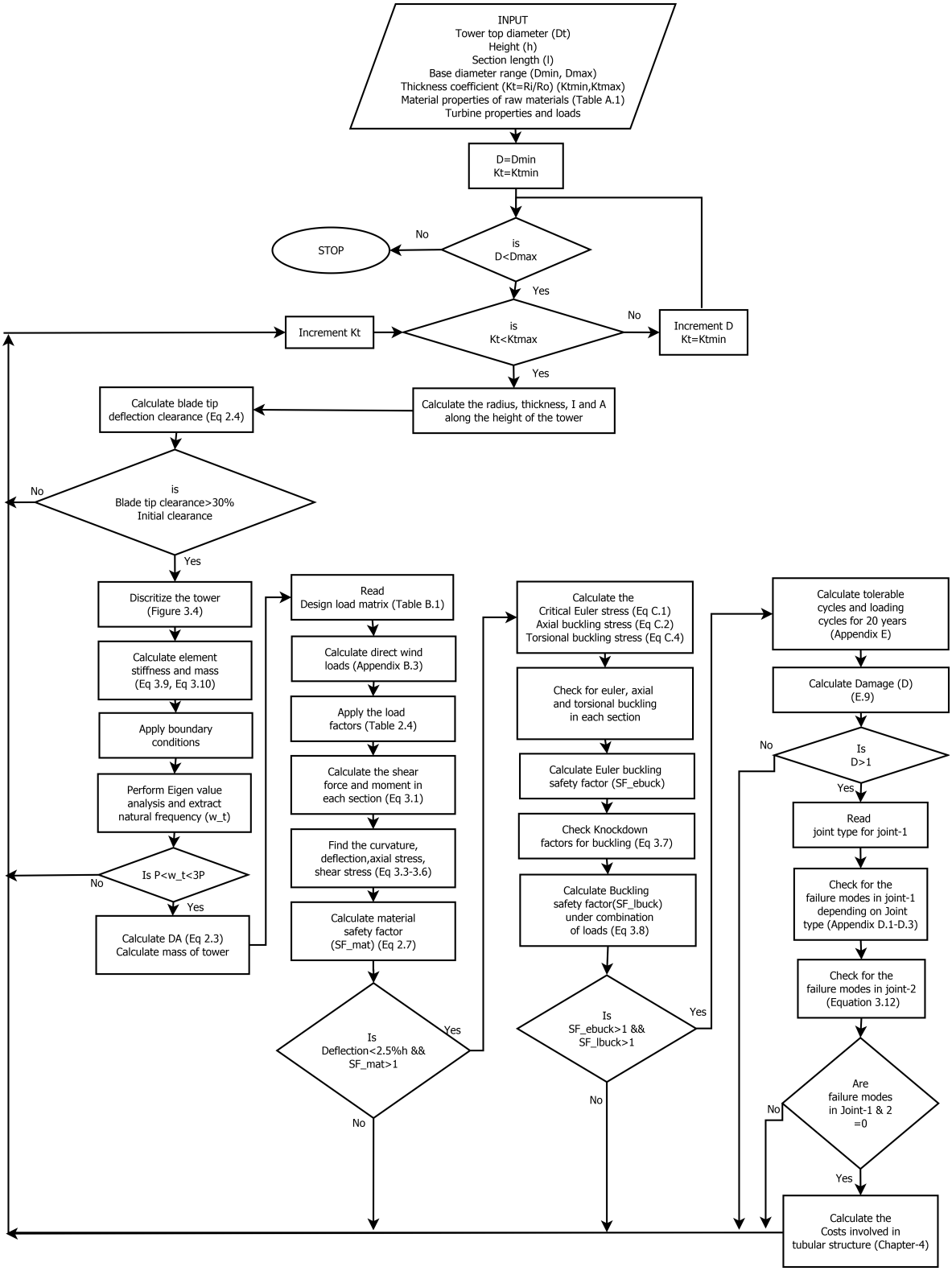

Figure 3.14: Flow chart for the design of tubular tower

3.4 Geometry of the lattice tower and methodology

The preliminary design is based on FEM approach due to the complex geometry of the lattice. Two baseline geometries are chosen from literature. The first Lattice Topology (LT)-1 has been adopted from the study by Long et al. [40] for a 90m offshore wind turbine tower. The second topology LT-2 has been adopted by Gencturk [41] in his study for the optimal design of the lattice tower. Both the topologies are shown in Figure 3.15. LT-1 has no web members and may be susceptible to buckling at tall hub heights. LT-2 has web members and has better buckling resistance. The tapering is given to help prevent blade interference with tower and given only to the bottom part of the tower; this is because the lattice tower has a wide base to overcome the large overturning moment and this constraint can be critical if a continuous taper is given throughout its height.

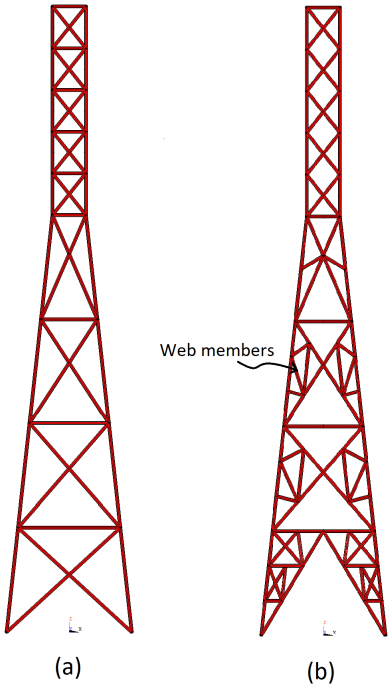

Figure 3.15: Topology of the lattice structure towers (a) LT-1 (b) LT-2

3.4.1 Details of parameters in a lattice structure

Details of the parameters in a lattice structure are given in Figure 3.16. Only the detail design of LT-2 truss structure is shown as it is almost identical to LT-1 but with additional web members. Further for the study, the links are grouped into five main categories listed below and as shown in Figure 3.16. This categorization is important so that each category can be assigned link cross section properties independently instead of same cross section throughout, to prevent over-design of the lattice. The categories are:

1. Main links from section 1 to section 4 (M-1)

2. Main links in section 5 (M-2)

3. Diagonal and horizontal bracing in section 1 to 4 (D-1)

4. Diagonal and horizontal bracing in section 5 (D-2)

5. Web members (W-1)

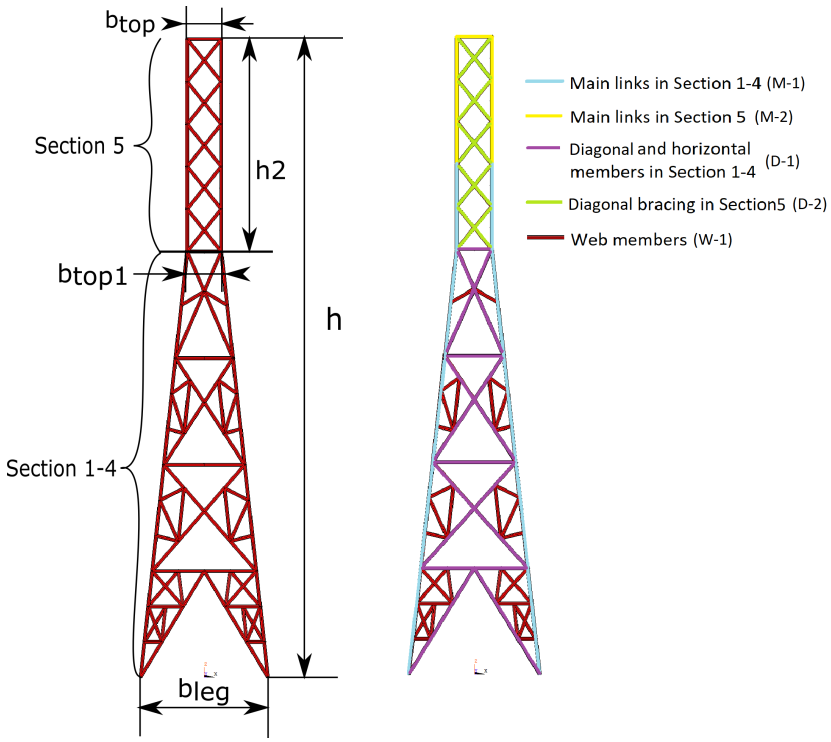

Figure 3.16: (a) Dimensions of the lattice structure LT-2 (b) Categorization of lattice structure

In the above figure, h is the total height of the tower. b_{leg} is the base leg distance in lattice tower, b_{top} is the width of the lattice tower on top and b_{top1} is the width of the lattice tower before the start of straight section (section 5). h is the height of the lattice tower and h_2 is the height of the lattice tower section 5. $n_{section}$ indicates the number of sections in the tapered part of lattice tower and it is 4 for the topology presented in Figure 3.16.

The cross section of the links initially considered for the lattice structure is given in Figure 3.17. R_L is the radius of the lattice links, t_L is the thickness of the lattice links in case of O, C, I and box sections. C, I and box sections are assumed to have an aspect ratio of 1:1, and the width/height of the cross section is given by b_L.

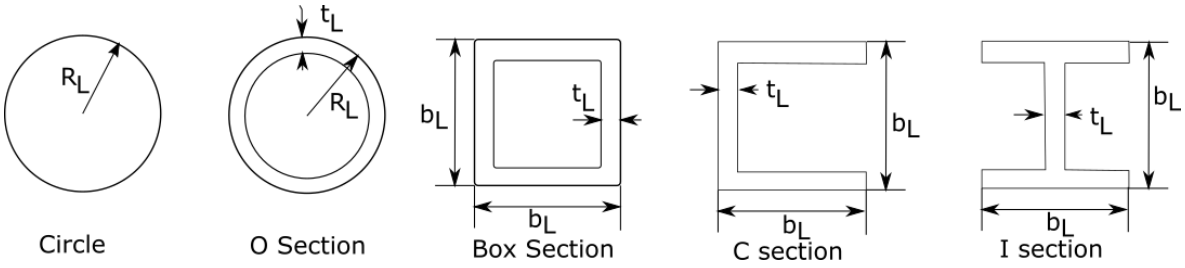

Figure 3.17: Types of cross sections and dimensions of links

3.4.2 FEM framework

Due to the complex geometry of the lattice structure, a FEM approach is followed for the design and analysis of a lattice structure. For the two topologies chosen, based on the input the coordinates of the nodes will be calculated accordingly. For LT-1 topology, there are 77 nodes. For LT-2 topology, the number of nodes is 170. Once the coordinates are decided, the links have to be setup. For LT-1 the number of links is 220. For LT-2 the number of links is 436. Each link and the nodes it connects is predefined by the topology chosen. The properties like the link length depend on geometric properties like base leg distance, the height of the tower. The nodes the links connect are also critical while assembling the local stiffness and mass matrix into the corresponding global matrix. Other geometric & material properties that are important in calculating the local stiffness and mass matrix are the area moment of inertia, area of the cross section of the links, material density, Modulus of elasticity in longitudinal and shear direction. The element type chosen to model the lattice structure is 3D beam elements. This element type was chosen over truss element type because it can take bending loads as well.

3.4.3 Design steps to set up the FEM framework

The following design steps are adopted to get to the final design of the lattice composite tower structure.

1. Input tower details: The list of input details is given in Table 3.3. The Geometric properties and loading conditions have already been explained previously. The turbine and material properties considered in this study are given in Appendix A.

2. Set up the topology by calculating the coordinates of the nodes and creating the links. The database of the links and the corresponding nodes are pre-decided and can be imported to the matlab code from an excel file.

3. Group the links based on the different type of links and given in Section 3.4.1.

4. Choose an initial point for the optimizer, such that the tower is highly over designed. In this case, the starting point was chosen such that all the links had the same b_L and t_L and the design has a frequency just below 3P frequency.

	Properties
Geometric properties of tower	Height (h), Base leg distance (B_{leg}) Top width (B_{top}) Top width-1 (B_{top1}) Height of section 2 (h2)
Loading condition	Operating load case, Non operating load case Fatigue load for 20 years
Turbine properties	Rated power, Rotor radius, Rotor rpm, Nacelle and rotor mass, Max deflection of blades Tip speed ratio of blades
Material properties	Material density, Material cost Modulus and possoin ratio, Ultimate strength

Table 3.3: Input properties fr the lattice tower

5. Calculate the cross-section properties (A_L, $I_{z,L}$, $I_{y,L}$, J_L) of each group of links and calculate the stiffness (K_e) and mass matrices (M_e) of the links. The links are modeled as beam elements hence the stiffness and mass matrix of a 3D beam element will be used.

6. Rotate the local stiffness and mass matrix depending on the orientation of the beam and assemble the global stiffness and mass matrix.

7. Apply the boundary condition on the bottom four nodes of the lattice structure. In the study of the lattice structure, no foundation stiffness has been considered since it was studied in Section 3.3.4 and seen that foundation stiffness doesn't have considerable effect on the natural frequency of the tower in the region of interest. Fixed boundary condition on the displacement ($d_{x,y,z}$) and rotation ($d\theta_{x,y,z}$) on the last node is applied as shown in Equation 3.13.
$$d_{x,y,z} = 0; d\theta_{x,y,z} = 0 \tag{3.13}$$

8. Perform Eigen value analysis and extract the first few natural frequencies. If the first natural frequency is in the allowable working frequency range, then proceed with static calculations.

9. For each load case, calculate the necessary load factors, tower top loads, direct wind loads. For operating and non-operating cases, the tower top loads are given in the Appendix B. These loads can be applied to the last node 170 on the top for LT-2 and node 77 for LT-1. For operating load case, in addition to the load factors mentioned by GL and ASCE guidelines, the dynamic amplification factor needs to be multiplied. The direct wind loads can be calculated for each section using steps from ASCE-7 and have been outlined in Appendix B.2. Instead of applying the direct wind loads on the whole frame facing the wind, equivalent loads are applied to only the four corner nodes as shown in Figure 3.18. The self-weight of each section is applied on the four corner nodes.

10. Apply the necessary loads and find the global displacement of all the nodes. The displacement of the tower top nodes can be extracted to check if the maximum deflection criterion is met.

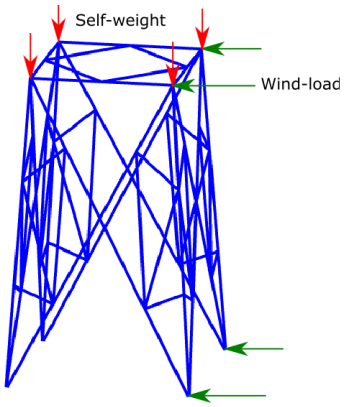

Figure 3.18: Wind force and self weight applied on nodes of each section

11. The global displacement of each node can be rotated into the local coordinate system of the links. Using this local displacement and the inverse of stiffness matrix the forces in the links in its local coordinates can be obtained. This, in turn, will give the stresses due to the forces and moments acting in the links.

12. Calculate the safety factor in each link. In each of the lattice links, there are three forces and three moments acting in its local coordinates. The net axial stress and shear stress due to the influence of these forces can be found using Equation 3.14 and represented in Figure 3.19. If the SF_{mat} of all the links >1, then buckling analysis can be carried out.

$$
\begin{aligned}
M_r &= \sqrt{{M_{L,y}}^2 + {M_{L,z}}^2} \\
F_r &= \sqrt{{F_{L,y}}^2 + {F_{L,z}}^2} \\
\sigma_b &= \frac{M_r.R_L}{I_L} \rightarrow \text{Circular cross-section} \\
\sigma_b &= \frac{M_{L,y}b}{2I_{L,y}} + \frac{M_{L,z}b}{2I_{L,z}} \rightarrow \text{Other cross-sections} \\
\sigma &= \frac{F_{x,y}}{A_L} + \sigma_b\,;\ \tau = \frac{F_r}{A_L} \\
SF_{mat}(\sigma,\tau) &< 1
\end{aligned}
\tag{3.14}
$$

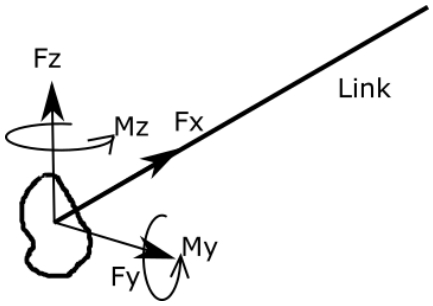

Figure 3.19: Link local coordinate axis

Here $F_{L,x,y,z}$ and $M_{L,x,y,z}$ are the forces and moments acting on the links in the local coordinate system of each link.

13. The equations to check for Euler buckling are given in Appendix C. Further, the crippling failure in the links has to be checked for One Edge Free (OEF) in case of I and C cross-sections and No Edge Free (NEF) crippling in case of box, hollow,I and C cross-sections. The crippling critical stress ($\sigma_{cr,crip}$) can be obtained using equations found in Appendix C.

14. Calculate the damage factor (DF) for a service life of 20 years in each link using steps outlined in Appendix E.

3.4.4 Trade studies

There are a lot of parameters that define the shape of the lattice structure. Important geometric parameters necessary to set up the lattice are:

1. Type of cross-section of the links
2. Base leg distance (b_{leg})
3. Number of sections
4. Ratio in section 5 (b_{top}/b_{top1})
5. Height of the straight section (Section-5) with respect to tapered section (Section 1-4) ($h2/h$)
6. Effect of web members (LT-1 vs. LT-2 truss)

In the next subsections, trade studies are performed to check the effect of these parameters on the mass of the tower. During this trade study, only the non-operational wind loading is considered, since the operational and fatigue loading is affected by the natural frequency of the tower.

Type of link cross section

In this study, five different types of link profiles are chosen and studied. They are circular, hollow, box, C and I section. The effect of the different cross-section on the mass of the tower for a 100m and 125m tall, 2.1MW capacity turbine tower on the mass is shown in Figure 3.20. It is seen from the study, that while using circular cross-section the mass of the tower is highest. This is because the circular cross-section is highly susceptible to buckling. Further, the closed cross-section like O and box section have the highest mass advantage because of the high moment of inertia of these cross sections which provides a good buckling resistance. The disadvantage with closed sections is the difficulty in joining. The C section may have a better moment of inertia, but the shear center of the C section lies outside the body leading to unfavorable torsion in the links. The I section has a slightly higher mass, but joining is relatively simple for I sections when compared to C section. For these reasons the I section is preferred over other cross sections and the remaining trade studies are performed by considering I section for the links.

Base leg distance

To check the effect of the leg distance, a 125m tall, 2.1MW capacity turbine tower is chosen, and the base leg distance is varied from 8-25m. The result of this study is shown in Figure 3.21.

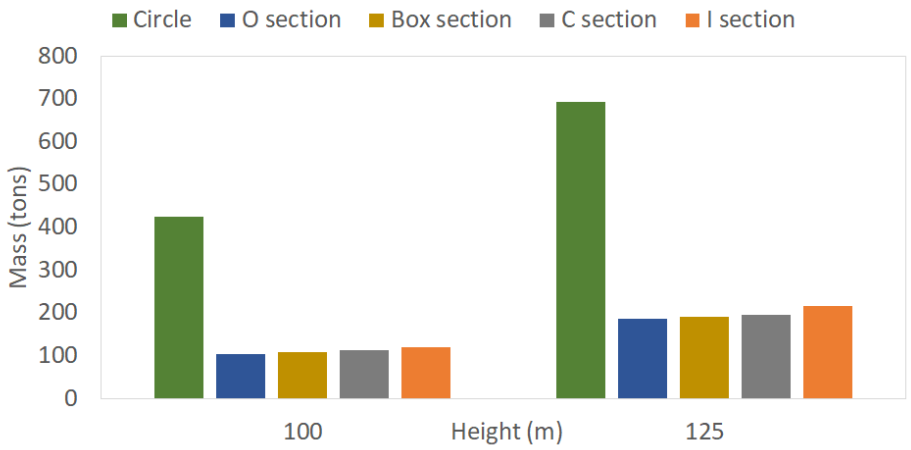

Figure 3.20: Effect of different cross-section on the mass of the tower

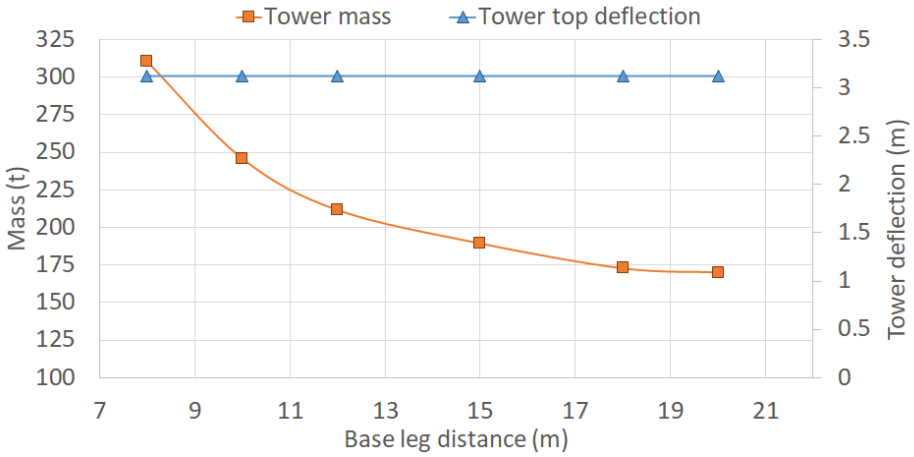

Figure 3.21: Effect of base leg distance on the deflection of the tower

It is seen from Figure 3.21 that for a constant tower top deflection there is a reduction in mass while increasing the base leg distance. This is because with lower base leg distance, the overall stiffness of the tower reduces and this has to be compensated by the increase in link dimension, leading to an overall increase in mass of the tower. As the base leg distance increases, the stiffness of the tower increases. Hence, smaller cross section area of the links is required. The cross section reduces to a point when the tower tip deflection is not the only critical constraint, but the material safety factor becomes a governing constraint too. Hence the mass of the tower saturates, and we no longer see the mass advantage with a further increase in base leg distance. One of the constraints that restrict the base leg distance is the blade tip deflection. Hence the maximum base leg distance that can be attained is fixed in a tower with a given hub height.

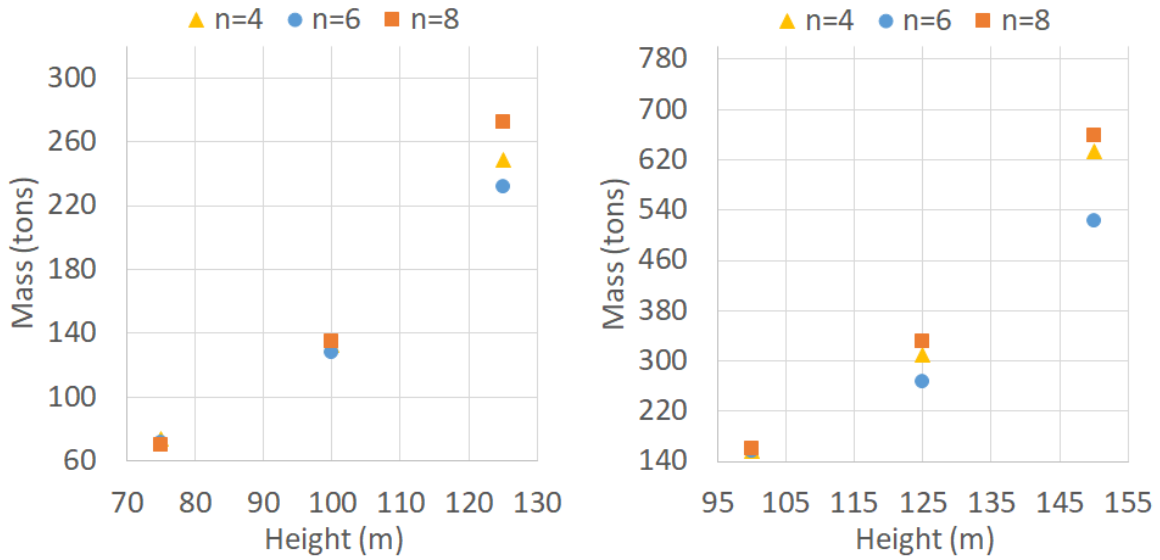

Figure 3.22: Influence of the number of section on tower mass

Number of sections

The influence of the number of sections is shown in Figure 3.22. The study was conducted on 2.1MW and 5MW towers with hub height 75, 100 and 125m and 100, 125, 150m respectively. The number of section were varied from 4 to 8 in steps of 2. For higher height, the difference is more prominent since buckling is one of the critical failure criteria for tall towers. Increasing number of sections from 4 to 6 switched the critical criterion from buckling to tower deflection. On further increasing the number of sections to 8 there was no advantage as buckling was not a critical criterion anymore and increasing number of sections just increased the number of links and thus the overall mass of the tower. The advantage observed when increasing number of sections from 4 to 6 might be negligible because the number of nodes increases from 170 to 242 and this may, in turn, increase the joint mass. But, in the case of 150m tall, 5MW tower there is a significant mass improvement when the number of sections is increased from 4 to 6. Hence, for this hub height, it is advantageous to consider six sections.

Ratio in section 5

To study the effect of introducing taper in Section 5, the breadth of the lattice structure at the top (b_{top}) was kept constant, and the breadth 1 (b_{top1}) was changed accordingly to give the necessary linear taper. b_{top}/b_{top1} was changed from 0.5 to 1 for a 125m tall, 2.1MW turbine capacity tower and the influence of this change on the overall mass of the structure was noted. It was seen that for the same tip deflection by giving a taper in section 5, the stiffness of the structure is increased due to geometry, and hence for the same tip deflection, the structure has a lower mass when no taper is given. This change in mass is not advantageous. One disadvantage of giving taper in section 5 is that the blade tip deflection can be an important constraint and thus the base leg distance may have to be decreased leading to a higher mass of the tower.

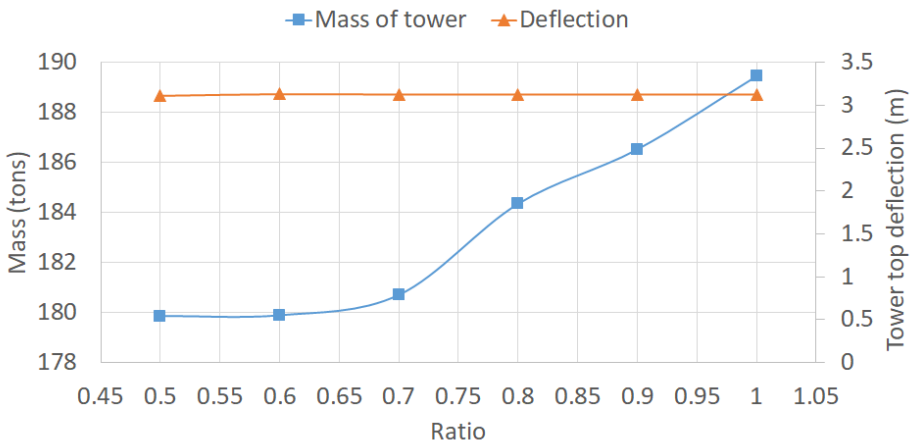

Figure 3.23: Ratio in section 5

Height of section 5/ Height of the tower

To study the effect of increasing the proportion of the section 5 vs section 1-4, the height h2/h was varied and the effects on mass and safety factor while keeping a constant tip displacement is shown in Figure 3.16. This ratio was changed from 0.1 to 0.6 for a 125m tall, 2.1MW capacity tower and the influence of this parameter on the deflection, material safety factor and mass was noted and given in Figure 3.24. It is seen from Figure 3.24 that when we increase the ratio of the height of section 2 to the height of section 1, we encounter minima. This is because initially, the safety factor is the governing factor as seen from the Figure 3.24. As we increase the ratio, the tower top becomes more and more flexible allowing for larger tower tip deflection, to maintain this constraint the dimensions of the links increase thus causing an increase in the safety factor of the links. Hence, it is seen that a minimum occurs when both the safety factor and the tower tip deflection constraint are critical in the design, leading to an optimum design.

Effect of web members LT-1 vs LT-2

To study the two topologies chosen, a variety of towers of different capacities and heights are evaluated. For both the topologies the base leg distance, height, ratio of section 5/section 1-4 and other shape parameters were kept constant. Only the link dimensions were iterated until the optimum design in each case was found. The results are shown in Figure 3.25.

Comparison between the simple and complex lattice structure is shown in Figure 3.25. It is seen that for a lower height, and lower capacity turbine simple lattice has a better mass over the complex structure. Safety factor was the most critical constraint in this region. With the increase in height, buckling is more critical due to the way the geometry of the lattice structure is defined and absence of web members. Hence, the complex lattice structure has a mass advantage when compared to the simple lattice structure.

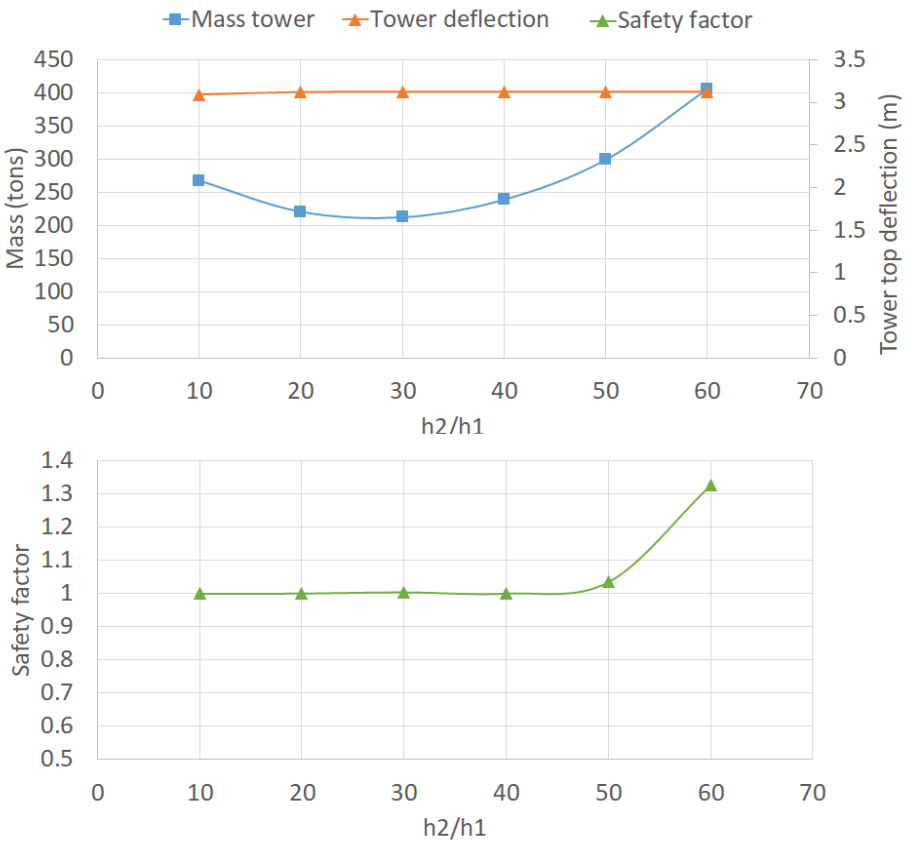

Figure 3.24: Height of Section 2/ height of section 1 vs. mass, deflection and safety factor

3.4.5 Joining in lattice structures

Joining of lattice links is a time-consuming process due to a large number of connections involved. The main links are assumed to be made up of a single pultruded element with the diagonal & horizontal bracing and web members attached to the main links. The following steps and approximations are made to obtain the approximate joint mass using adhesive joining technique and bolted technique.

1. Only the axial force is considered since this is the most prominent force appearing on the links. The axial force and the dimensions of all the links minus the main links coincident at a node are stored.

2. Extract the maximum axial (F_x) force and min dimension of the links (B, T) from the links at a given node.

$$\begin{aligned} F_x &= max(F_1, F_2 ... F_n) \\ B &= min(B_{L,1}, B_{L,2} ... B_{L,n}) \\ T &= min(T_{L,1}, T_{L,2} ... T_{L,n}) \end{aligned} \tag{3.15}$$

3. For the adhesive joint, the overlap length(a)for the maximum axial force and minimum

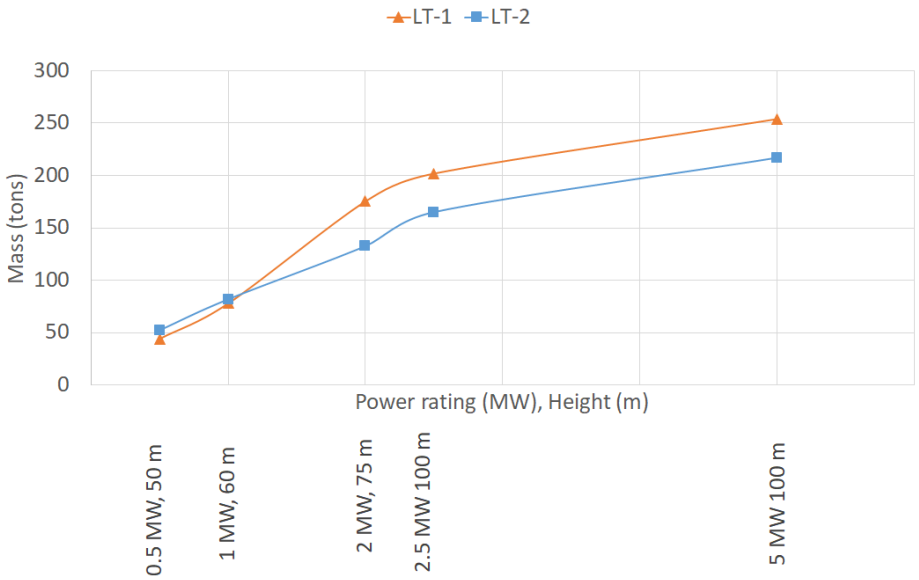

Figure 3.25: Comparison of the two topologies in lattice tower

link dimension. This gives the worst case scenario. The Equation to find the overlap length (a_1)while using adhesive is given by Equation 3.16. The thickness of the joint plate is assumed to be same as the maximum thickness of the links. This can be repeated at all the nodes, and the overlap length can be calculated. By knowing the overlap length, the width of the main link or the biggest link at a node (B_L), the thickness of the joint plate (t_1), the mass of the joint at each node can be calculated as given by Equation Equation 3.16.

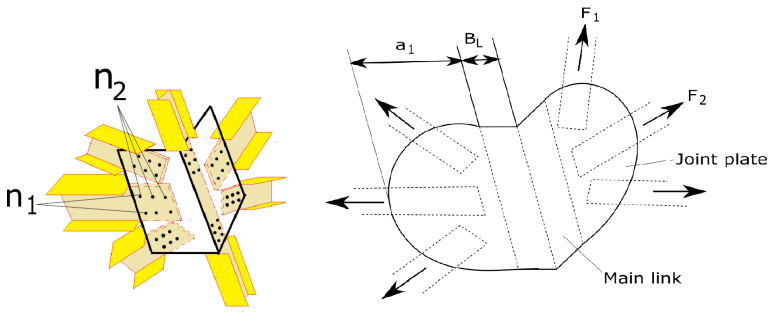

Figure 3.26: Approximation of the lattice joint

$$
\begin{aligned}
a_1 &= \frac{F_x}{B.\tau_{ut,adhesive}} \\
t_1 &= max(T_{L,1}, T_{L,2}...T_{L,n}) \\
Mass_{joint,adhesive} &= \sum_{n=1}^{nodes} 2.(\frac{\pi {a_1}^2}{2} + 2.a_1.B_L)t_1\rho_{mat}
\end{aligned}
\tag{3.16}
$$

4. To get the approximate joint mass using bolts, the bolt diameter(D_{bolt}) has to be fixed and the corresponding number of bolts (n_b) needed to take up the axial force with this bolt diameter can be calculated using Equation 3.17. The relations make sure that the bolt shear failure and the bearing failure in laminate is prevented.

$$\begin{aligned} N_1 &= \frac{F_x}{\frac{\pi}{4}{D_{bolt}}^2 \tau_{xy,bolt}} \\ N_2 &= \frac{F_x}{D_{bolt} T \sigma_{bear,lam}} \\ n_b &= \max(N_1, N_2) \end{aligned} \tag{3.17}$$

Here $\sigma_{bear,lam}$ is the bearing strength of the laminate.

Once the number of bolts is decided upon, it is important to know the arrangement in order to calculate the overlap length. Choose a pitch (p_{bolt}) between bolts of atleast $5D_{bolt}$ and calculate the number of bolts in width and length direction of the link to prevent shear out or net section failure in links. Subsequently the thickness of the joint plate to avoid net section failure is also calculated. The distance between the edge of the plate and the bolts was considered as half the pitch distance between the bolts. Equation 3.18 makes sure these failure modes are prevented and the thickness of the plate is calculated.

$$\begin{aligned} t_{plate} &= \frac{F_x}{n_1(2D_{bolt}2((n_2-1)p_{bolt} + p_{bolt}/2)\tau_{ut,plate})} \\ &\frac{F_x/n_1}{TD_{bolt}2((n_2-1)p_{bolt} + p_{bolt}/2)} < \tau_{ut} \\ &\frac{F_x/n_2}{(B - n_1 D_{bolt})T} < \tau_{ut} \end{aligned} \tag{3.18}$$

Here $\tau_{ut,plate}$ is the ultimate shear strength of the plate used and n_1 is the number of columns of bolts along the link X direction and n_2 is the number of rows of bolts transverse to the link direction.

If all the failure criteria pass, calculate the mass of bolted joint is calculated using the overlap length (a_1), the number of bolts, the thickness of the plate etc. as given in Equation 3.19.

$$\begin{aligned} a_1 &= p_{bolt}.D_{bolt}.n_1 \\ Mass_{joint,bolt} &= \sum_{n=1}^{nodes} 2.(\frac{\pi {a_1}^2}{2} + 2.a_1.B_L)t_{plate}.\rho_{mat} + n_b.Mass_{bolt} \\ Mass_{bolt} &= \frac{\pi}{4}{D^2}_{bolt}t_1 + 2.\frac{\pi}{4}.(2{D^2}_{bolt})D_{bolt} \end{aligned} \tag{3.19}$$

The data is saved, and this step can be repeated by considering a new bolt diameter and recalculated the plate thickness, the number of bolts, overlap length needed and the mass of the joint. By doing this iteratively, the joint design with the least mass can be identified.

5. Check if the adhesive joint has a mass advantage over the bolted joint and vice versa.

Table 3.4 shows the comparison in joint mass while using bolted joint and while using adhesive joint for the 2.1MW towers. The joint mass is influenced by a lot of factors like the forces appearing on the links, the thickness of the plate required to transfer this loads without undergoing material failure or the overlap area needed to transfer these load without adhesive failure, etc. It is seen that the adhesive joint has relatively lower mass for all the towers. Removal of the material to insert bolts will reduce the available area for load transfer causing failure in the laminate. To prevent all these failures, a large number of bolts must be used over a large surface area leading to the high joint overlap. The adhesive joint, on the other hand, doesn't involve removal of material from the links for joining and transfers the loads from links to joint via shear. This along with the fact that the joint plate is assumed to be made of GFRP in the case of the adhesive joint may be the reason for low mass of this joint. Hence, for the final joint design in lattice towers, the adhesive joint is considered.

Adhesive and bolted joint comparison for lattice towers						
Capacity (MW)	2.1	2.1	2.1	5	5	5
Height (m)	75	100	125	100	125	150
$Mass_{joint,bolt}$ (t)	47.3	70.0	32.4	78.0	80.9	140.9
$Mass_{joint,adhesive}$ (t)	14.9	22.8	28.8	38.6	58.3	89.1

Table 3.4: Adhesive and bolted joint comparison for lattice towers

6. Until now all joints have been assumed unique. But, for the ease of manufacturing, it is necessary to categorize the joints. Categorization of the joints in this study is done depending on the overlap length and thickness of the joint plate. Recalculate the total mass ($Mass_{joints}$) by grouping them based on the overlap length or thickness of the secondary plate needed.

3.4.6 Conclusion on lattice towers and flow chart

From the trade studies done in this chapter on lattice tower the following conclusions can be drawn:

1. I-section is the most feasible cross section, though box, O and C section have slightly lower masses, the joining is relatively simple with I-section. Hence the final design of lattice tower will be obtained using I cross sections for links.

2. Use the largest base leg distance possible that respects the blade tip deflection constraint.

3. Increasing the number of sections in lattice tower shows considerable mass advantage only for the 150m tall, 5MW tower. Hence, for tall hub height, the number of sections is increased from 4 to 6.

4. The ratio of the height of section 5/ section 1-4 shows the best mass when it is kept at 1:2. This ratio is assumed for towers with all hub heights.

5. LT-2 topology is better because of the web members present to prevent buckling. Hence this topology is adopted.

6. Adhesive joints will be considered for the final design of the towers.

3.4.7 Optimization framework and flowchart of the tool

1. Selection of starting point: The starting point is selected such that the tower frequency lies just below the 10% limit of the 3P frequency. To make this selection process easier all the links are assumed to have the same cross section. Thus the parameters are limited to 2 which are the link width and the thickness. They are varied using loops in the tool to search for a design that obeys the above-mentioned frequency requirement. This point is chosen as the initial point for the mass optimizer.

2. Mass optimizer: In general an optimizer in Matlab accepts an initial point from the user and searches for the closest minimum while ensuring that the point of convergence respects the constraint equations. The constraint equations are maintained negative. The initial point need not respect all the constraint equations as long as the design becomes feasible sometime during the process of optimization. A boundary must be defined for the parameters so that they do not wander away to unrealistic values. The list of constraints are:

$$\begin{gathered}\text{Tower top deflection} < 2.5\% \text{ of tower height} \\ \text{Material and buckling safety factor} > 1 \\ \text{Damage factor in fatigue} < 1 \\ 2 \times \text{link thickness} < 0.9 \times \text{Link width.}\end{gathered}$$

The last criterion is to prevent the thickness of the link increasing and becoming high enough to occupy the entire area of the cross section turning it into a block. The upper limit for the width and the thickness of all the links is 1m and 180mm respectively. The lower limit is 0.2m and 10mm respectively.

A structural optimization problem using a FEM is a black box type function where the derivative of the function to be minimized is unknown. Thus the partial derivatives of the mass function with respect to its parameters must be evaluated at every point during the procedure. This process is represented by "Region A" in Figure 3.27. This figure represents the optimization behavior of a 125m 2.1 MW GFRP tower. Many such regions are visible throughout the optimization procedure. This is done by successively incrementing each parameter at a point by a preset step value and evaluating the mass function at those points. The data from these points combined with the data from the current point will help determine the direction of greatest descent. The optimizer then takes a step in this direction and evaluates the mass and constraint values there. This point is represented as the "Prediction" in Figure 3.27. The optimizer continues to execute these steps of moving to a point, studying the partial derivatives, determining the direction and moving on to the next point until a design is attained that represents an optimized design. It is possible that this procedure fails and the optimizer is forced to correct itself to the nearest feasible point and move in a different direction. This behavior is seen in the region marked as "Self-correction". The optimizer has retraced

itself back to the nearest feasible point, and this is followed by a region similar to Region A.

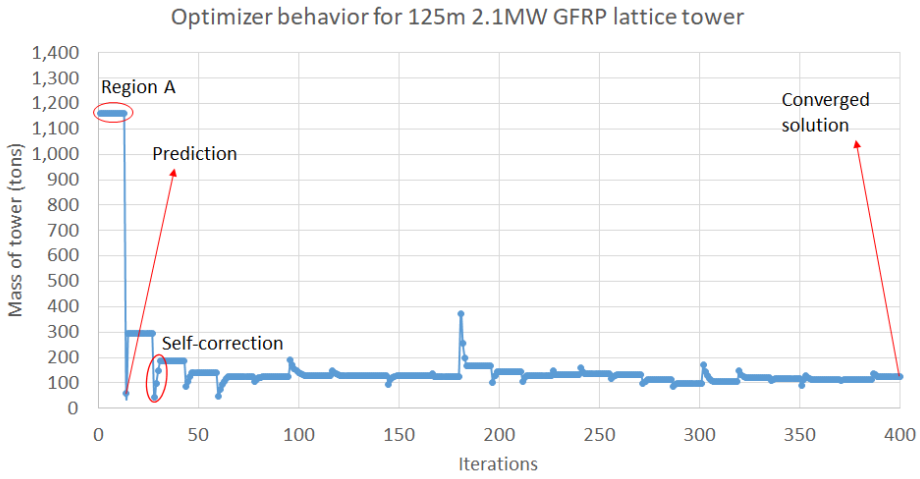

Figure 3.27: Optimization behavior

3. Convergence criteria: The optimizer will detect convergence if either the change in mass when the parameters are studied in the vicinity of the point is below a certain threshold or if any further modification to the parameters in the direction of reduction of mass causes failure of a constraint function. By definition of the mass function, it is a monotonically reducing function. Thus the first criteria cannot be expected in this study. This is because the link parameters can be made small enough such that the mass converges to 0. Thus at convergence one of the constraint function will be critical. Once the optimizer has converged, it is important to round off the link dimensions since the optimizer treats the parameters as floats. In this study, the link widths have been rounded off to the closest and greater second decimal. For the link thickness, it has been rounded off with a resolution of 0.5mm.

The methodology followed to develop the lattice tool has been concisely represented in Flowchart 3.28.

3.5 Chapter summary

This chapter outlined the methodology adopted to apply the load, perform static, frequency, buckling and fatigue analysis on a tubular and lattice geometry wind turbine tower. Further trade studies concerning various geometric parameters have been conducted for tubular as well as lattice towers. The various possible joining techniques and the methodology to obtain the approximate mass is discussed. The conclusions are drawn from the trade studies and the optimization framework & the flowchart to set up the design tool is presented.

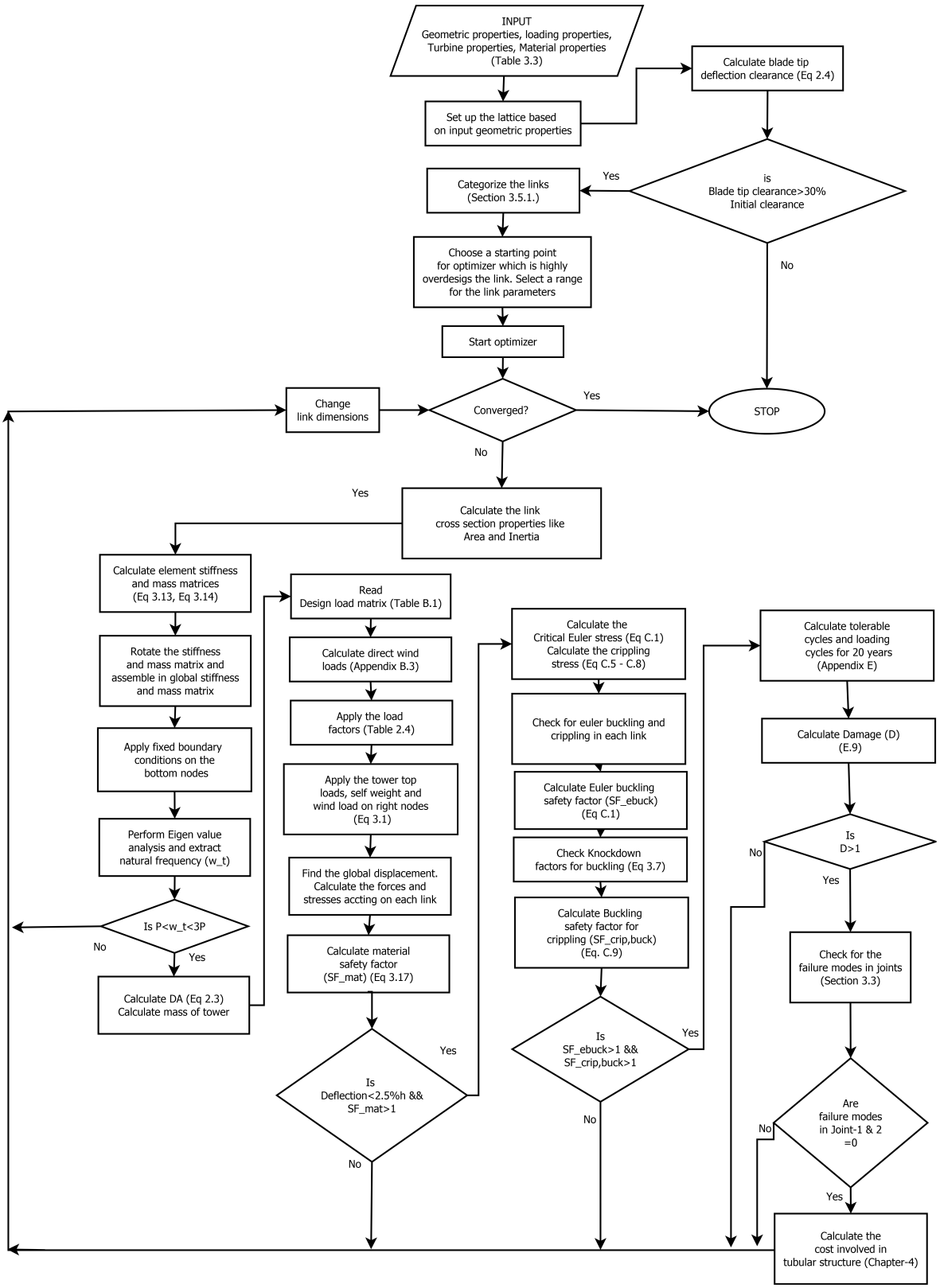

Figure 3.28: Flowchart for design of lattice tower

Chapter 4

Cost Modeling of the Tower

This chapter will discuss the cost contributors to the tower and the methodology adopted to calculate the total cost of the tower.

4.1 Cost contributors and methodology

It is discussed in literature survey, Section 2.4, throughout the composite structure's life, there are numerous cost contributors. Table 4.1 highlights the main cost contributors considered in this study and the method adopted to estimate them. Suzlon data refers to internal data gathered from Suzlon Energy Ltd. like the raw material cost or the labor rate/hour or the thumb rules regarding finishing time etc. Process Cost Analysis Database (PCAD) model is an extensive database containing a lot of manufacturing steps and their corresponding time equations. In this study, the PCAD model was setup for manufacturing steps and time involved in Vacuum Infusion (VI), Handlayup, and Automated Tape Placement (ATP). Since the cost model is an integral part of the design tool, running the PCAD model for every structural change is inefficient because it contains over 30 constituent equations. Hence, approximate parametric equations have been formulated to emulate the PCAD model for part sizes of interest for the thesis work.

4.1.1 Manufacturing costs

Raw material cost: These costs are provided by Suzlon Energy Ltd. Table A.3 gives the raw material costs considered in this study. A scrap rate of 15% is assumed over the raw material for every production process except pultrusion.

$$Cost_{raw} = Mass_{tower} * 1.15 * €/Kg \tag{4.1}$$

Aiding material cost and other auxiliary costs: These costs will aid in the manufacturing of the composite structure. These usually include the bagging material in case of hand layup or

	Cost contributor	Cost included	Method
Manufacturing	Raw material cost	Yes	Suzlon data
	Aiding materials and other costs	Yes	Suzlon data
	Labor cost for production	Yes	Parametric equations based on PCAD model
	Labor cost for finishing and inspection cost	Yes	Suzlon data
,	Certification cost	No	
Installation	Transportation cost	Yes	Refered from literature
	Crane and lifting cost	Yes	Referred from literature
	Foundation cost	Yes	Referred from literature
Maintenance and inspection	Maintenance and inspection	No	
Replacement	Replacementcost	No	

Table 4.1: Cost analysis

vacuum infusion. Mold cost also is a part of the aiding cost. These costs are given in Table A.3. In the case of vacuum infusion or hand lay-up, the approximate costs followed by Suzlon are given in Equation 4.2 can be applied to calculate the aiding material cost.

$$\begin{aligned} Cost_{mold} &= \frac{Mass_{tower}}{1000} * \text{Mold cost} \\ Cost_{bagging} &= 2n_{section} * \text{Vacuum bagging cost} \\ Cost_{aid} &= Cost_{mold} + Cost_{bagging} \end{aligned} \tag{4.2}$$

Labor cost for production: As mentioned in the literature survey, PCAD model developed by Gutowski consists of about 300 different steps involved in fabrication process including assembly and inspection [29]. Some of the possible manufacturing methods preferred for the production of the tubular and lattice tower are given in table 4.2

Tubular tower	Lattice tower
Hand layup	Pultrusion
Vacuum infusion	
Automated tape placement	
Filament winding	

Table 4.2: Possible production method for the tubular and lattice structure

Steps and the corresponding cost equations of all the methods except filament winding have been gathered from the PCAD database. The number of steps in the above process varies from approximately 40 in the case of hand lay-up and vacuum infusion to 15 in the case of pultrusion. For simplicity and ease of computation, the final total time has been converted to the parametric equation in terms of the area, perimeter, the number of plies and the curvature

of the part. Instead of recalculation of all 40 steps a single equation can be used that gives the same time in the region we are interested.

For handlayup and vacuum infusion, it was observed that the behavior of the total time was dependent on area, perimeter and the number of plies in the part and follows Equation 4.3. The corresponding constants for these 3 manufacturing techniques are given in Table 4.3.

$$Labor_{time} = \underbrace{K_1}_{K_1=K_3+n_{ply}K_4} *(A_{surf} - 100) + \underbrace{K_1}_{K_1=K_5+n_{ply}K_6} *(P_{surf} - 100) + \underbrace{C}_{C=K_7 n_{ply}+C_1} \quad (4.3)$$

A_{surf} - Surface area of the tubular structure
P_{surf} - Perimeter of the tubular structure surface
n_{ply} - Number of plies in tubular structure.

	K_3	K_4	K_5	K_6	K_7	C_1
Vacuum Infusion	39.95	1.65	10.03	0.00	171.49	5343.10
Handlayup	32.26	1.65	13.16	1.36	310.00	5313.00
ATP	38.01	7.11	5.88	0.00	712.24	4672.80

Table 4.3: Constants for time equations

In case of Pultrusion, which is used for the production of lattice links the total time was dependent on the length of the pultruded element and the area of the cross section and is given by Equation 4.4.

$$Labor_{time,pul} = \frac{(0.1 - A_L)}{0.1}(8.307 * L_T + 550.05) + \left(\frac{A_L}{0.1}\right)(16.362 * L_T + 804.7) \quad (4.4)$$

L_T is the total length of the links in a particular link category described in Section 3.4.1. Pultrusion is a machine intensive process. Hence machine time/cost also contributes to the overall cost. Hence, machine time is assumed to be 90% of the labor time.

The % error between the predicted time and the PCAD manufacturing time for a laminate with 100 plies and manufactured using vacuum infusion is given in Figure 4.3. The predicted time closely emulates the time predicted by the PCAD model. It is seen that in the probable region where the tower sections might lie the % error is less than 4%.

The cost for the 2.1MW Glass Fiber Reinforced Plastic (GFRP) towers manufactured using Vacuum Infusion, Hand-layup, ATP and Filament winding is shown in Figure 4.2. The output time/cost for the ATP, Vacuum infusion, and Handlayup was calculated using parametric equations given by Equation 4.3. For the Filament winding process, the thumb rules $Cost_{filament} = 9.5.Mass_{tower}$ has been used. It is seen that the Vacuum infusion and Handlayup have almost identical costs, with Vacuum infusion having a slight advantage over Handlayup. Due to the expertise of Suzlon Energy Ltd. in Vacuum infusion, this is used as the manufacturing method for tubular towers in the final design of the towers.

The PCAD model was developed in 1990 as a part of COSTADE project which attempted to model the cost of aircraft components [35]. The materials used in the wind industry are often of a lower grade compared to aerospace industries as well as the scale of structures is

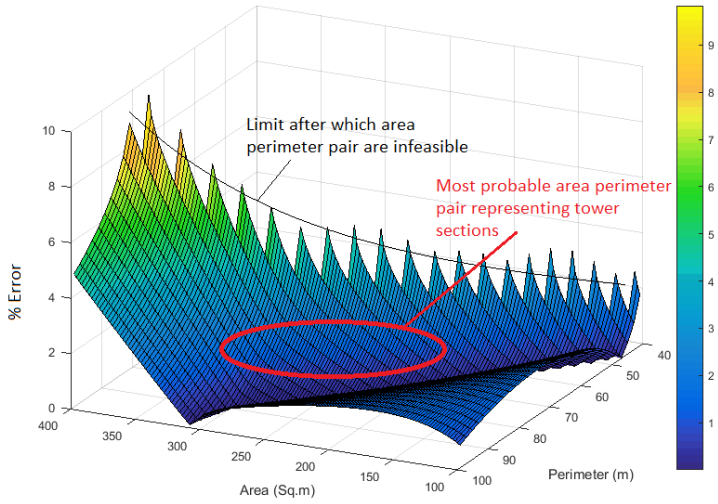

Figure 4.1: Comparison of predicted and PCAD model time

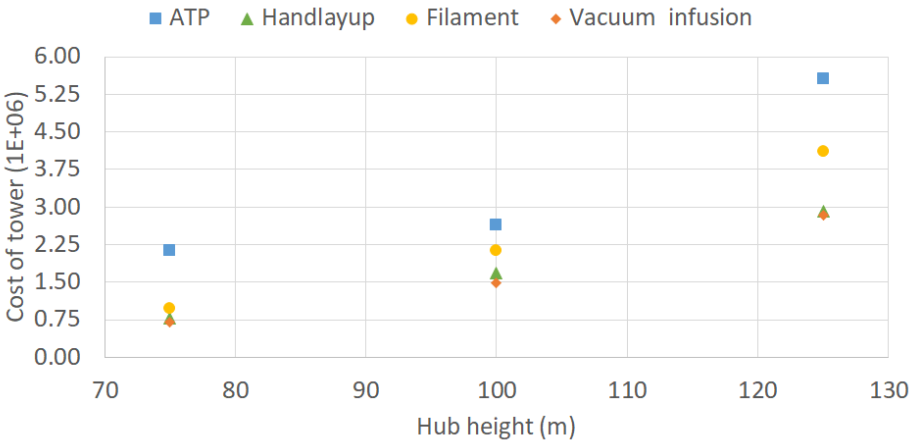

Figure 4.2: Cost of 2.1MW turbine capacity towers using various manufacturing methods

different. Thus, it is necessary to adjust the parametric time equations to better correlate with the processes at Suzlon. These equations have to be adapted to fit Suzlon's manufacturing characteristics. At Suzlon, vacuum infusion is used to manufacture blades. The total time involved in the manufacturing of 54m and 47 m long blade and its components like girder and blade root were considered to obtain the data and the correlation between the PCAD time and the actual time taken by Suzlon ($time_{suzlon}$) is given in Equation 4.5. The correlation factor was found to be a function of the area of the part and the number of plies used in it

$$\left(0.23 + \frac{1}{A_{surf}} + \frac{0.5}{n_{ply}}\right) Labor_{time} \cong Labor_{time,Suzlon} \tag{4.5}$$

Labor cost for finishing: Finishing includes activities like trimming, laminate check, repair, painting by roller and then a second layer of spray & final finishing followed by process control.

According to Suzlon the % labor cost for a finishing of a composite part is up to 40% of the overall labor cost involved in the production. The breakup of this cost and the different activities involved in finishing is given in Figure 4.3. For the study, the same thumb rule is applied. The finishing time is calculated based on the total process time.

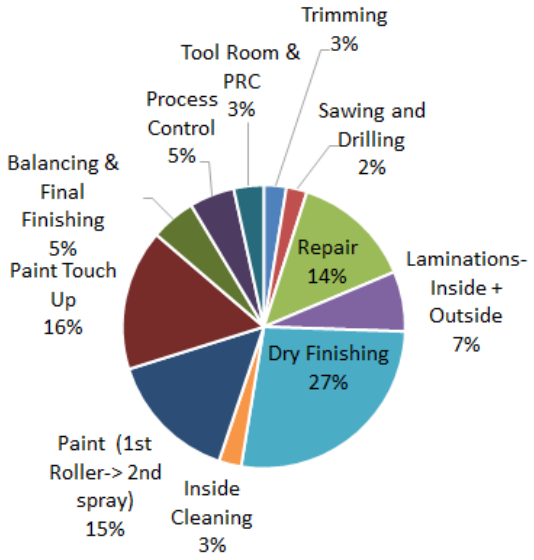

Figure 4.3: Cost breakup of finishing cycle (Courtesy: Suzlon Energy Ltd.

The total labor costs involved in the manufacturing of tubular components will be given by Equation 4.6.

$$Cost_{labor} = \sum_{1}^{n_{sections}} Labor_{time}.\frac{Labor_{rate}/hour}{60} + \frac{2}{3}Labor_{time}.\frac{Labor_{rate}/hour}{60} \tag{4.6}$$

Here $Labor_{time}$ is dependent on the manufacturing method choosen. For pultrusion the labor cost and machine cost will be given by Equation 4.7.

$$\begin{aligned} Cost_{labor} &= \sum_{1}^{5} Labor_{time,pul}.\frac{Labor_{rate}/hour}{60} + \frac{2}{3}Labor_{time,pul}.\frac{Labor_{rate}/hour}{60} \\ Cost_{machime} &= 0.9\frac{Cost_{labor}}{Labor_{rate}/hour}.Machine_{rate}/hour \end{aligned} \tag{4.7}$$

4.1.2 Installation costs

Installation cost can be broken down as transportation cost, crane and lifting cost and foundation cost.

Transportation: Engstrom [2] has considered a transportation cost of 0.53€/tonne.km. The same cost has been considered in this study. For lattice structure, half the rate is considered due to the ease of transportation of the links. For a 300km transport, adhering to the road limitation of 4.5m the relation between the mass of the tower and cost is shown in Figure

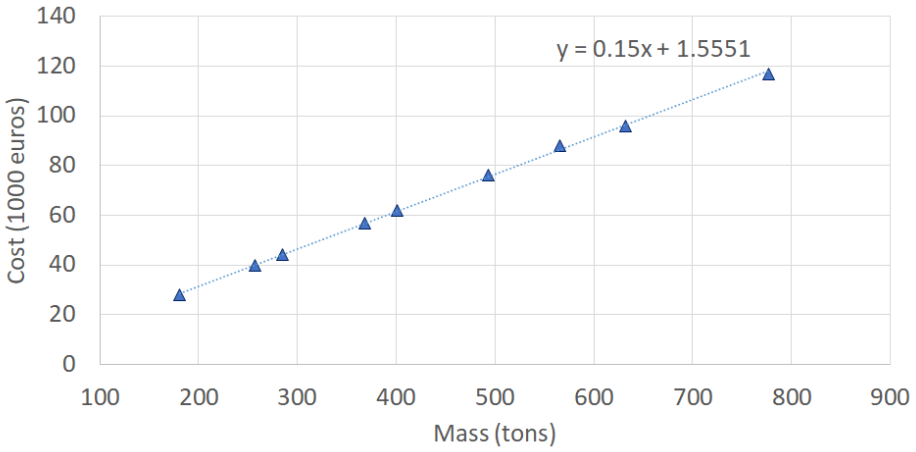

Figure 4.4: Transportation cost vs. mass

4.4. The parametric relation between the mass of the tower ($Mass_{tower}$) and cost is given by Equation 4.8.

$$Cost_{transport} = (0.15.\frac{Mass_{tower}}{1000} + 1.55).1000 \tag{4.8}$$

Crane and lifting: As discussed in the literature, for smaller capacity and smaller height tower, cranes can be effectively used for lifting and installation. For turbines with capacity above 5MW and height above 125m lifting tower should be used. Engstrom [2] uses a 120t max capacity crane for upto 150m tall & 3MW turbine and 240t max capacity crane for upto 125m tall & 5MW turbine and lifting tower for installation beyond this height and capacity. The cost considered by Engstrom is dependent only on the height of the tower and inclusive of installation of nacelle-rotor assembly and shown in Figure 4.5. Fitting the curves through the data given by Engstrom, Equations 4.9 gives cost w.r.t hub height for the 120t and 240t capacity crane respectively.

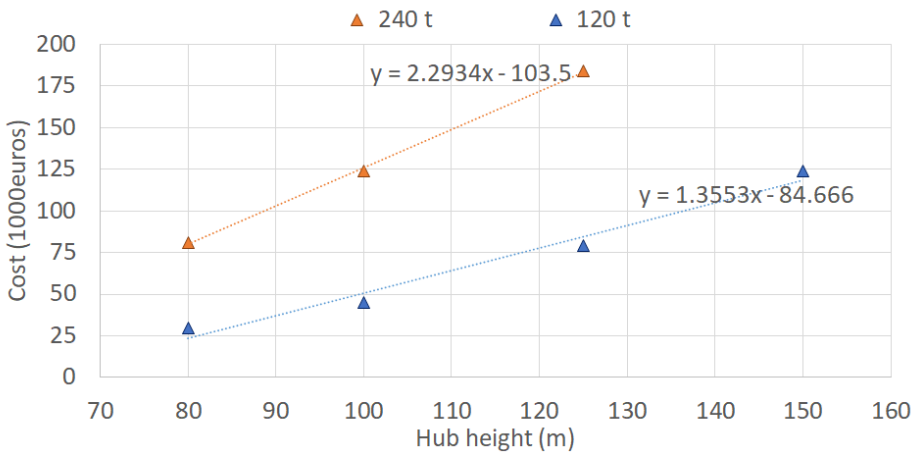

Figure 4.5: Crane cost vs. mass

$$\begin{aligned} Cost_{crane,240} &= (2.2934.h - 103.5).1000 \\ Cost_{crane,120} &= (1.355.3h - 84.66).1000 \\ Cost_{lifting-tower} &= 1302000 \end{aligned} \tag{4.9}$$

Foundation: Foundation design can either be governed by the overturning moment the foundation can resist or by the vertical loads the foundation can bear depending on the bearing strength of the soil. The overturning moment remains fairly constant for a specific hub height tower, irrespective of the tower geometry. Hence, Engstrom [2] has taken a constant cost of the foundation for a given hub height. On the other hand, the National Renewable Energy Ltd. (NREL) study has taken different foundation mass for the same hub height depending on the tower mass which shows that the mass of the tower indeed affects the mass of the foundation. With lower tower mass a smaller foundation will be required because of the reduced bearing forces on the foundation. The foundation mass and cost data collected from NREL [9] for the 100m tall tower using different material is plotted in Figure 4.6 and a linear equation as given in 4.10 is fit from the data to obtain the approximate foundation cost w.r.t. mass of the tower.

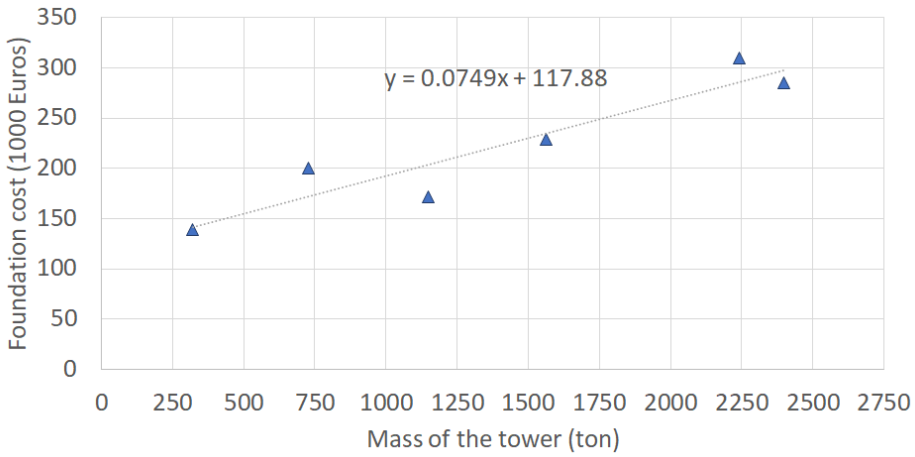

Figure 4.6: Foundation cost verses mass

$$Cost_{foundaton} = (0.0749.\frac{Mass_{tower}}{1000} + 117.88)1000 \tag{4.10}$$

4.1.3 Maintenance and inspection costs

Most commonly in literature, research has only been done on life cycle analysis of composite bridge structure. Due to the different scale of the composite tower used in wind turbine tower structures no cost will be included. Engstrom [2] suggests for a lattice tower, an additional maintenance of 3000€/year will be incurred for joint maintenance. Thus this additional maintenance cost will be considered.

4.1.4 Joint cost

For the bolted and the adhesive joint, the joint mass can be obtained by following the procedure given in Appendix D or following the methodology for lattice structures given in Section 3.4.5. The additional raw material cost in joints can be obtained by mass of the plate, excess material used in laminate near the joint and the bolt mass. No additional labor cost is considered in the case of joints.

4.2 Final cost of the composite towers

The final cost of the tubular tower will be given by Equation 4.11 and for lattice tower it will be given by Equation 4.12.

$$Cost_{tubular} = Cost_{raw} + Cost_{aid} + Cost_{labor} + Cost_{transport} + Cost_{crane} + Cost_{foundation} + Cost_{joint} \tag{4.11}$$

$$Cost_{lattice} = Cost_{raw} + Cost_{labor} + Cost_{machine} + Cost_{transport} + Cost_{crane} + Cost_{foundation} + Cost_{joint} + 3000 * N_{years} \tag{4.12}$$

4.3 Chapter summary

This chapter described the methodology used to setup the cost model for the project. The costs are either obtained from Suzlon inhouse knowledge or by literature survey. Parametric equations have been developed to calculate the labor costs and these equations are based on the PCAD model. For the installation costs, parametric equations that fit the data from the literature have been used. These equations help in setting up the cost model and in providing with the overall cost of the tubular and lattice composite towers.

Chapter 5

Results and Discussions

This chapter presents the final optimized dimensions of 2.1MW turbine capacity towers and 5MW turbine capacity towers using the Glass Fiber Reinforced Plastic (GFRP) and Carbon Fiber Reinforced Plastic (CFRP) material. The final estimated joint mass and cost for these towers are also discussed. Further, the static, buckling and fatigue analysis results of these towers are given. Finally, the total mass and cost data of these towers is presented followed by its comparison with steel towers.

The towers presented in this chapter are broadly classified into two categories based on their geometry, i.e., tubular and lattice tower. Each of this type of tower has been designed for three different heights and two different turbine capacities. For a 2.1MW capacity turbine, 75m, 100m, and 125m are the heights considered, and for 5MW turbine 100m, 125m, and 150m heights are considered. The difference in the starting hub heights is because of the different size of the rotors in a 2.1MW and 5MW turbine. The rotor radius considered in the case of 2.1 MW turbine is 54m and for 5 MW turbine it is 63m. The minimum hub height is usually taken as 1.4-1.5 times the rotor radius. The static analysis is performed for two load cases, operating condition (Extreme Turbulence Model (ETM)) and not operating condition (Extreme Wind Model (EWM)). The fatigue analysis is done for a service life of 20 years. The approximate joint mass and cost are calculated according to methodology outlined in Chapter 3, Section 3.3.6 and 3.4.5. The costs are estimated using the equations given in Chapter 4. The results for all of the above will be presented separately based on the material of the tower.

5.1 Tubular tower results

Based on the outcome of trade studies performed in Section 3.3.5, all the towers have variable thickness and linear taper. The base diameter is constrained at 9m for the ease of transportation for most of the towers. But, for the 150m tall tower design constraining the base diameter leads to a very heavy tower. Hence, the base diameter is limited by the blade clearance constraint. This constraint ensures that the tower diameter at the height of 87m from

the ground is kept at 6.5m. The nacelle constrains the top diameters, and in this study, it is assumed to be 3m and 4m for the 2.1MW and 5MW turbines respectively.

Adhesive joints have been used for assembling the tower sections, based on the trade study presented in Section 3.3.6. The sections are manufactured using vacuum infusion as it was seen to be the most economic manufacturing method based on trade study done in Section 4.1.1. The labor rate is chosen as 20 €/hour, and the material cost and aiding material cost is explained in Section 4.1.1. Other cost equations have been developed in Chapter 4 and have been used to calculate the final cost of the designs.

5.1.1 GFRP tubular towers

The details of static, buckling, fatigue, frequency, mass and cost analysis results of tubular GFRP towers for various hub heights are presented in Table 5.1.

		2.1MW			5 MW		
Height (h)	[m]	75	100	125	100	125	150
Base diameter (D_b)	[m]	6.00	8.10	8.90	7.60	8.60	9.70
Top diameter (D_t)	[m]	3	3	3	4	4	4
Base thickness (t_b)	[mm]	60.00	80.00	130.00	90.00	140.00	210.00
Top thickness (t_t)	[mm]	30.00	30.00	43.00	47.36	65.00	86.50
Frequency	[Hz]	0.31	0.31	0.29	0.25	0.24	0.23
DA	[-]	2.00	2.14	3.20	1.61	2.15	2.84
Operating load condition, ETM							
SF_{mat}	[-]	1.10	1.02	1.00	2.46	2.53	2.54
SF_{lbuck}	[-]	1.03	1.30	1.60	1.29	1.70	2.29
δ_{top}	[m]	2.00	2.14	3.30	2.40	3.19	3.89
Non-operating load condition, EWM							
SF_{mat}	[-]	1.19	1.17	1.70	2.00	2.77	3.67
SF_{lbuck}	[-]	1.04	1.40	2.50	1.31	2.11	3.26
δ_{top}	[m]	2.07	2.00	2.16	2.21	2.53	2.67
Fatigue analysis							
DF	[-]	0.17	0.02	0.09	0.54	0.58	0.70
Joint analysis							
$Mass_{joint}$	[t]	4.54	4.77	12.32	8.62	14.49	24.88
$Cost_{joint}$	[10^3€]	23.4	27.1	56.6	40.7	64.2	103.4
Total cost and mass of the tower							
$Mass_{tower}$	[t]	102.41	207.14	444.88	263.62	535.34	1014.62
$Cost_{tower}$	[10^6€]	0.65	1.26	2.64	1.62	3.11	6.81

Table 5.1: Dimensions of the 2.1MW and 5MW turbine capacity GFRP tubular towers

Though a maximum of up to 9m is allowed for the base diameter, the best design with the

least mass is obtained when the base diameter is less than this limit for hub heights up to 100m as seen from Table 5.1. A reduction in the thickness of the laminate is expected as the diameter of the base increases. But, the thickness saturates after a certain base diameter to prevent local buckling of laminate under compression. From this point increasing base diameter increases the mass and shows no advantage.

It is seen from the Table 5.1 that for the GFRP towers, the operating loads are the critical loads. As a combined effect of relatively pliant material and slender geometry, the structural stiffness is relatively low, and this causes the tower natural frequency to approach the rotor frequency (P). This leads to high dynamic amplification factor (DA). The minimum allowable natural frequency with 10% margin from P for the 2.1MW and 5MW towers is 0.27Hz and 0.22Hz respectively. It can be seen that the from the table the natural frequency of the towers approaches their lower limits with progressively increasing hub heights.

In most of the GFRP towers, the tower top deflection is the critical constraint again, owing to the low stiffness as discussed above. But, in the 2.1MW towers, the failures can also be expected in the material or in buckling due to the reduction in the laminate thickness during optimization.

The 5MW towers are subjected to considerably larger forces compared to the 2.1MW turbines as is expected. It implies higher stresses in the laminate during the normal operating conditions. This coupled with the dynamic amplification factor makes the fatigue loading of the laminate progressively more critical with increasing hub heights.

Both the mass and cost of the joint and tower progressively increase with hub heights and agrees with expectation. The mass of the tower represented by $Mass_{tower}$ includes the mass of the joints as well. The cost of the tower, represented by $Cost_{tower}$ includes all the contributing costs discussed in Chapter 4.

5.1.2 CFRP tubular towers

The details of static, buckling, fatigue, frequency, mass and cost analysis results of tubular CFRP towers for various hub heights are presented in Table 5.2.

Though the upper limit for the base diameter was constrained to 9m, none of the designs have reached this limit. This is because with increasing base diameter, the laminate thickness at the base tends to reduce and subsequently the buckling safety factor approaches 1. The laminate thickness cannot reduce beyond the values presented in Table 5.2 since the buckling is already critical in the presented designs.

The tower natural frequency is relatively high compared to GFRP designs owing to the high material stiffness of CFRP laminates. Thus the design has enough margin between the tower natural frequency and the rotor frequencies (P & 3P). Thus the dynamic amplification factors (DA) are relatively low compared to GFRP designs. As a consequence of this, the non-operating load conditions are now critical and govern the design of the towers.

Buckling is the most critical constraint due to the above-mentioned reasons. It must be noted that the buckling safety factors that are presented as 1 are in reality greater than one and their precision is lost while rounding off for presenting it in the document. The tower deflection is well below the limit of 2.5% of the hub height due to high structural stiffness.

		2.1 MW			5 MW		
Height (h)	[m]	75	100	125	100	125	150
Base diameter (D_b)	[m]	4.5	6.9	7.6	6.9	8.6	8.3
Top diameter (D_t)	[m]	3	3	3	4	4	4
Base thickness (t_b)	[mm]	60	60	70	70	80	100
Top thickness (t_t)	[mm]	40	26	28	40	38	48
Frequency	[Hz]	0.39	0.388	0.32	0.338	0.31	0.25
DA	[-]	1.34	1.33	1.7	1.46	1.36	1.77
Operating load condition, ETM							
SF_{mat}	[-]	2.22	1.46	1.21	2.38	2.34	2.34
SF_{lbuck}	[-]	1.49	1.49	1.18	1.02	1.22	1.18
δ_{top}	[m]	0.83	0.82	1.47	1.12	1.15	2.27
Non-operating load condition, EWM							
SF_{mat}	[-]	1.6	1.05	1.11	1.73	1.59	2.09
SF_{lbuck}	[-]	1.02	1	1	1	1	1
δ_{top}	[m]	1.23	1.26	1.81	1.15	1.4	2.47
Fatigue analysis							
DF	[-]	1.7E-06	2.0E-08	7.9E-09	1.4E-06	3.8E-08	4.0E-06
Joint analysis							
$Mass_{joint}$	[t]	6.47	5.53	7.17	9.04	10.83	19.72
$Cost_{joint}$	[1000€]	111.33	99.15	128.22	155.05	186.83	331.72
Total cost and mass of the tower							
$Mass_{tower}$	[t]	92.862	142.04	216.43	196.64	304.27	451
$Cost_{tower}$	[10^6€]	1.90	2.89	4.45	4.00	6.00	10.04

Table 5.2: Dimensions of the 2.1MW 5MW turbine capacity CFRP tubular towers

Since the non-operating load condition is the governing load, the laminate stresses in operating condition are relatively low compared to GFRP designs. This also reflected in the fatigue analysis where the predicted damage factor due to wind loading in the service life of 20 years is considerably low.

The joint is also designed with CFRP material to minimize the local variation in stiffness in the adhesive joints. Bolted joints are not recommended for CFRP towers due to the risk of corrosion, thus necessitating the use of novel materials. This might adversely affect the cost of the joint which is already expensive because of the CFRP material.

Both the mass and cost of the joint and tower progressively increase with hub heights and agrees the expectation. The mass of the tower represented by $Mass_{tower}$ includes the mass of the joints as well. The cost of the tower, represented by $Cost_{tower}$ includes all the contributing costs discussed in Chapter 4.

5.2 Lattice towers

The final dimensions of the GFRP and CFRP lattice towers for both 2.1MW and 5MW turbines with their respective hub heights have been presented in this section.

Based on the trade studies conducted in Chapter 3, the base leg distance of the tower (b_{leg}) has been chosen to be as large as possible without violating the blade tip clearance constraint. Thus the base leg distance is unique for each design presented. The number of sections in the tower ($n_{section}$) has been maintained at 4 for most designs with the 5MW, 150m GFRP tower where it was found during the trade studies that increasing $n_{section}$ to 6 has sufficient mass advantage.The general topology of the tower is fixed based on the conclusions from the Chapter 3.

The links are categorized into five broad categories (M-1, M-2, D-1, D-2 & W-1) based their location and has been schematically presented in Figure 3.16. The link dimensions are presented as breadth, thickness pairs (b_L, t_L). The link dimensions of the five categories were found by using the inbuilt Matlab optimizer *fmincon* using the Sequential Quadratic Programmer (SQP) algorithm which is a robust algorithm to find an optimum solution with boundaries and constraints. All the links use the I-section, and the upper limits for the width and thickness of the links were maintained at 1m and 180mm respectively.

The joining technique adopted is adhesive joint, since it showed the highest mass and cost advantage based on the trade studies done in Chapter 3. For the final total cost of the GFRP towers the labor rate is chosen as 20 €/hour, and the material cost and aiding material cost is explained in Section 4.1.1. The composite links are manufactured using pultrusion.

5.2.1 GFRP lattice towers

The details of static, buckling, fatigue, frequency, mass and cost analysis results of lattice GFRP towers for various hub heights are presented in Table 5.3.

The main links categories, M-1 and M-2, are the bulkiest. This is because they serve the purpose of resisting the external overturning moments and forces. The web members, W-1, are the least bulky of the five categories. This is because they serve the purpose of improving the buckling properties of the other two categories of links and thus do not take up much load. The Diagonal link categories, D-1, and D-2, have bulkiness intermediate to the main links and the web members. They are responsible for the torsional and bending stiffness of the tower. The link dimensions achieved from the mass optimization agree with this expected behavior.

The lattice tower is pre-dispositioned to be stiffer than the tubular tower in the bending mode, due to its wider base. This improves the first natural frequency of the tower and ensures good margin between the natural frequency and the P & 3P frequencies. This reduced the dynamic amplification of the tower. Thus non-operating load condition is the critical load case for these designs.

As is expected in lattice towers, the most critical mode of failure is the Euler buckling of the most slender links. In towers, up to a hub height of 100m, the optimizer was able to solve for a design that has both material failure and link buckling as probable modes of failure. This

		2.1MW			5MW		
Height (h)	[m]	75	100	125	100	125	150
bel	[m]	10	15	18	12	15	20
h2/h1	[-]	33.33	33.33	33.33 3	33.33	33.33	33.33
$n_{section}$	[-]	4	4	4	4	4	6
(b_L,t_L) [m,mm]	M-1	(0.4,100)	(0.55,75)	(1.00,70)	(0.6,115)	(0.61,180)	(0.85,180)
	M-2	(0.77,15)	(0.5,35)	(1.00,25)	(1,21)	(0.61,45)	(0.6,75)
	D-1	(0.30,15)	(0.38,11)	(0.70,10)	(0.55,12.5)	(0.39,30)	(0.38,40)
	D-2	(0.5,12.5)	(0.70,11)	(0.75,15.5)	(0.87,15)	(0.93,12.5)	(0.65,15)
	W-1	(0.25,10)	(0.30,15)	(0.5,10)	(0.5,15)	(0.48,12.5)	(0.4,20)
Frequency	[Hz]	0.406	0.336	0.33	0.325	0.301	0.30
DA	[-]	1.37	1.42	1.41	1.41	1.40 1.33	1.34
Operating load condition, ETM							
SF_{mat}	[-]	1.74	1.68	2.95	1.88	1.42	2.48
SF_{ebuck}	[-]	1.38	1.37	1.65	2.50	1.33	1.35
δ_{top}	[m]	0.95	1.44	1.37	1.34	1.45	1.37
Non-operating load condition, EWM							
SF_{mat}	[-]	1	1.09	1.78	1.46	1.73	2.31
SF_{ebuck}	[-]	1.01	1	1	1.08	1.02	1.03
δ_{top}	[m]	1.02	1.7	1.925	2.47	3.03	2.31
Fatigue analysis							
DF	[-]	0.56	0.82	0.014	0.79	0.41	0.99
Joint analysis							
$Mass_{joint}$	[t]	26.0	22.8	28.8	38.6	45.3	89.1
$Cost_{joint}$	[1000€]	158.0	147.0	161.0	204.0	231.0	379.0
Total cost and mass of the tower							
$Mass_{tower}$	[t]	111.44	163.3	304.22	260.6	387.01	666.1
$Cost_{tower}$	[10^6€]	0.85	1.11	1.84	1.59	2.19	3.51

Table 5.3: Dimensions of the 2.1MW 5MW turbine capacity GFRP lattice towers

indicates very lean design. The deflection is not critical anymore owing to the high structural stiffness of the tower.

In lattice towers, the links at the base experience the largest stress amplitudes and these are highly critical in fatigue. The stress states in the links are highly sensitive to the link dimensions and drastically change when the link dimensions are modified. Thus it is convoluted even for a robust optimizer such as the SQP algorithm and gives rise to the highly nonlinear behavior of the mass function. Thus the fatigue damage factor (DF) does not show a definitive trend, but the optimizer manages to maintain it below 1.

The mass and the cost of the joint of the designs are much higher compared to the tubular tower because they are commensurately numerous. There are over 170 nodes, and this neces-

sitates 170 joints. The mass and cost of the tower increase with tower height and this is in agreement with the expected behavior.

5.2.2 CFRP lattice towers

The details of static, buckling, fatigue, frequency, mass and cost analysis results of lattice CFRP towers for various hub heights are presented in Table 5.3.

		2.1MW			5MW		
Height (h)	[m]	75	100	125	100	125	150
bel	[m]	10	15	18	12	15	20
h2/h1	[-]	33.33	33.33	33.33 3	33.33	33.33	33.33
$n_{section}$	[-]	4	4	4	4	4	4
(b_L,t_L) [m,mm]	M-1	(0.31,47)	(0.70,17)	(0.71,23)	(0.41,75)	(0.72,41)	(0.77,55)
	M-2	(0.60,21)	(0.85,16)	(0.53,28)	(0.84,14)	(0.87,12)	(0.97,14)
	D-1	(0.20,10)	(0.27,10)	(0.32,12)	(0.37,10)	(0.37,10)	(0.64,13)
	D-2	(0.40,10)	(0.62,10)	(0.74,10)	(0.58,10)	(0.79,10)	(1.00,14)
	W-1	(0.20,10)	(0.32,10)	(0.36,10)	(0.29,10)	(0.44,10)	(0.57,10)
Frequency	[Hz]	0.45	0.36	0.32	0.37	0.3136	0.324
DA	[-]	1.54	1.28	1.78	1.64	1.37	1.41
Operating load condition, ETM							
SF_{mat}	[-]	1.55	1.84	1.4	1.38	1.02	1.44
SF_{lbuck}	[-]	1.12	1.43	1.13	1.34	1.67	2.47
δ_{top}	[m]	0.82	1.08	1.92	1.19	1.44	1.38
Non-operating load condition, EWM							
SF_{mat}	[-]	1.02	1.06	1.03	1.05	1.09	1.24
SF_{lbuck}	[-]	1.02	1.06	1.01	1.01	1.06	1.01
δ_{top}	[m]	0.76	1.44	2.016	1.39	2.83	3.21
Fatigue analysis							
DF	[-]	0.88	0.98	0.49	0.72	0.11	0.016
Joint analysis							
$Mass_{joint}$	[t]	31.34	35.39	38.61	40.71	53.38	66
$Cost_{joint}$	[1000€]	592.00	659.98	713.00	749.19	961.41	1172.00
Total cost and mass of the tower							
$Mass_{tower}$	[t]	75.41	108.47	147.61	138.25	194.38	331.8
$Cost_{tower}$	[10^6€]	1.68	2.32	3.18	3.05	4.02	7.68

Table 5.4: Dimensions of the 2.1MW 5MW turbine capacity CFRP lattice towers

The link dimensions of the CFRP design show a similar trend as seen with the GFRP design. The bulkiness of the link is highest in the main links (M-1 & M-2) and is least in the web links (W-1) and the diagonal links show an intermediate degree of bulkiness.

Owing to the high structural stiffness of the lattice design the natural frequency is well within its limit, and thus the non-operating conditions offer the critical loads on the tower. This is also reflected in the buckling and material safety factors which are close to 1. However, the tower top deflections are well within their limits owing to the high structural stiffness of the lattice design.

Similar to the GFRP designs, the base members of the main link category are highly loaded and experience the most intense fatigue loading among all the links during operating conditions. Thus they show a relatively large prediction for fatigue damage in the 20-year service life compared to the tubular designs.

Similar to the GFRP designs, the number of joints in a lattice tower are numerous and due to this the additional mass and cost for joining the links are equally high. The mass and cost of the tower show a trend similar to GFRP designs, and this is agreement with the expectations.

5.3 Tower cost distribution

The cost distribution of the tubular tower made of GFRP and CFRP composite is given in Figure 5.1. Though the individual towers may show variation from the presented generalized distribution, overall the trend remains similar. The variation might be particularly high for the crane and lifting cost because depending on the hub height different capacity cranes or lifting towers will be used.

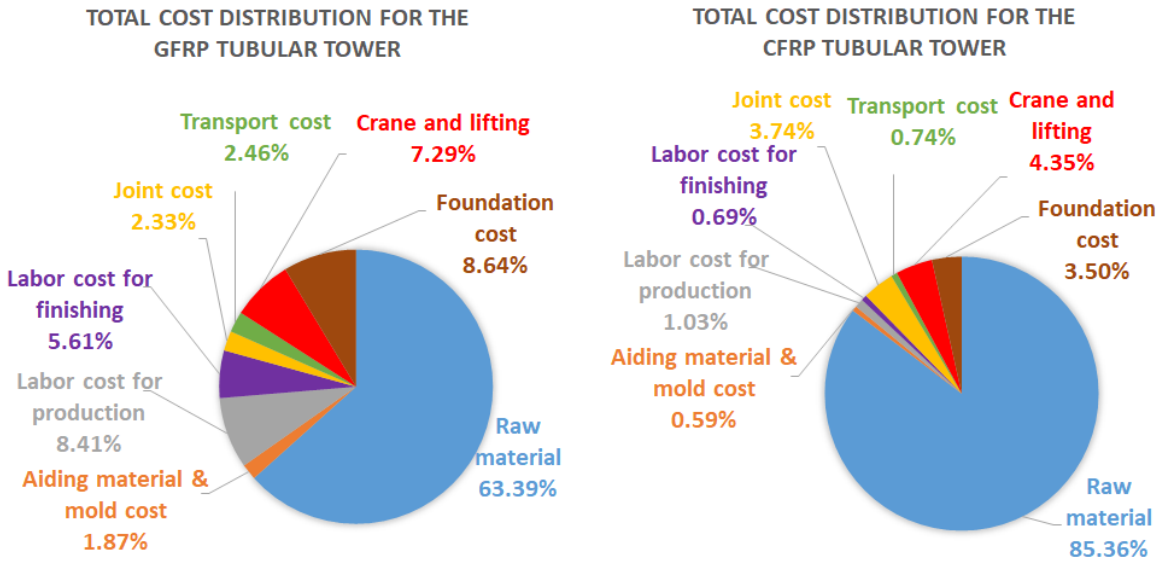

Figure 5.1: Total cost distribution in a tubular tower

The raw material cost has the greatest influence on the overall cost. This is justified due to the high material cost of the GFRP material. The other major contribution is the labor cost due to the labor intensive Vacuum infusion process adopted for manufacturing. The effect of the mass of the tower on the crane and lifting cost has not been considered in this study. The sensitivity of the mass of the tower on foundation cost is low. The joint cost and transportation cost doesn't have much contribution to the overall cost.

For the CFRP tubular towers, the material cost is the biggest contributing factor because CFRP is roughly 4-5 times costlier than GFRP composite. The trend in other cost contributors is similar to that seen in GFRP. The contribution of the labor cost has reduced because the volume of the CFRP material to be handled by the laborers is much lower compared to the volume of GFRP materials. The joint cost contribution has increased due to the use of the CFRP material.

The cost distribution of the lattice tower made of GFRP and CFRP composite is given in Figure 5.2.

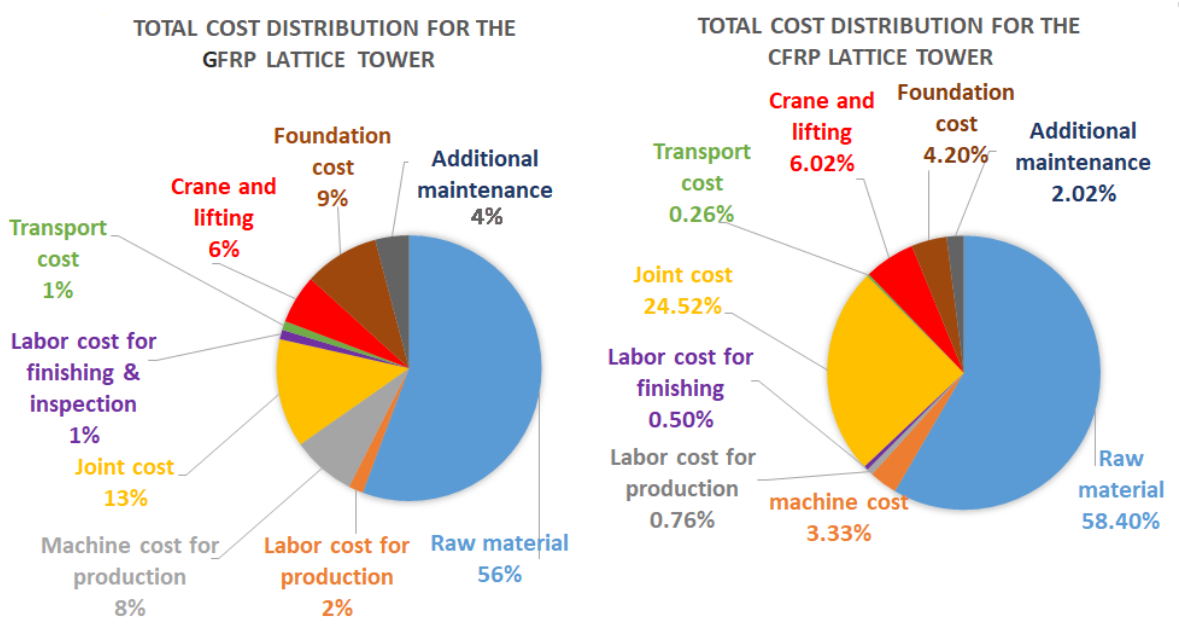

Figure 5.2: Total cost distribution in lattice tower

In general, the cost of the lattice towers is contributed to by five major factors. The highest contribution is from the raw materials and is in agreement with the expectations. In GFRP designs, the material cost of tower and joint is relatively low compared to the same in CFRP designs. As opposed to the tubular design, lattice design costs show joints as a major contributor owing to a large number of joints. Since the links used in the lattice towers are pultruded, there is an additional machine cost in the case of the lattice design. This can be expensive because of the high machine rates. As opposed to tubular towers the transportation of the lattice links is simpler and consequently cheaper.

5.4 Comparision with steel design

To compare the designs developed for composite wind turbine towers with existing steel towers with bolted joints, data from Engstrom [2] is used. Engstrom refers to the 5MW NREL turbine and a 3MW turbine in his work. The steel tower cost data includes manufacturing, transportation, cranes and installation and foundation costs. The 3MW turbine has a configuration and mass similar to the 2.1MW turbine of Suzlon. Hence, the steel tower data has

not been modified and is directly adopted for comparison. The tubular and lattice designs are compared in Table 5.5 and 5.6 respectively.

Tubular tower mass and cost comparison							
Capacity	[MW]	2.1	2.1	2.1	5	5	5
Height	[m]	75	100	125	100	125	150
$Mass_{steel}$	[t]	168.22	257	368	401	566	777
$Mass_{GFRP}$	[t]	102.41	207.14	444.88	263.62	535.34	1014.62
$Mass_{CFRP}$	[t]	92.862	142.04	216.43	196.64	304.27	451
$Cost_{steel}$	[1E6€]	0.58	0.96	1.35	1.56	2.15	2.74
$Cost_{GFRP}$	[1E6€]	0.65	1.26	2.64	1.62	3.11	6.81
$Cost_{CFRP}$	[1E6€]	1.90	2.89	4.45	4.00	6.00	10.04

Table 5.5: Tubular tower mass and cost comparison with steel towers

Comparing the tubular composite towers with steel towers, it can be seen that CFRP towers are much lighter than their contemporary steel counterparts. GFRP towers also offer a definitive mass advantage but only for the towers up to hub height of 100m. But, for higher hub heights due to the slender geometry and relatively low material stiffness of GFRP towers, the designs get bulkier than steel design.

In spite of the lighter designs of the CFRP towers, they are 3-4 times more expensive than steel designs. Since the wind industry is more cost driven, there is no advantage of using CFRP designs over steel in case of tubular towers. The GFRP design does not show any definitive cost advantage either, but for hub heights up to 100m, the cost of the GFRP tower is at most 30% costlier than the Steel counterparts. An example of this trend is the GFRP design for 5MW 100m tower which is roughly 4% costlier than the steel design. This is attributed to the high degree of mass advantage (roughly 35%) possible in the GFRP design compared to Steel. Although the motivation for this work was to investigate the feasibility of composite material as an alternative to steel in tall towers, it is not recommended based on the outcomes of the study and the contemporary understanding of the designs of the towers. For smaller hub heights composites could be used to produce designs for the towers that are equivalent in cost to the steel designs, but they could offer other advantages like ease of manufacturing and resistance to environmental degradation.

Lattice tower mass and cost comparison							
Capacity	[MW]	2.1	2.1	2.1	5	5	5
Height	[m]	75	100	125	100	125	150
$Mass_{steel}$	[t]	168	247	307	388.00	482.00	569.50
$Mass_{GFRP}$	[t]	111.44	163.3	304.22	260.6	387.01	666.1
$Mass_{CFRP}$	[t]	75.41	108.47	147.61	138.25	194.38	331.8
$Cost_{steel}$	[1E6€]	0.59	0.87	1.10	1.36	1.69	1.99
$Cost_{GFRP}$	[1E6€]	0.85	1.11	1.84	1.59	2.19	3.51
$Cost_{CFRP}$	[1E+06€]	1.68	2.32	3.18	3.05	4.02	7.68

Table 5.6: Lattice tower cost and mass comparison between Steel and GFRP, CFRP towers

Similar to the tubular designs, the composite lattice designs are also lighter than their steel counterparts. But this advantage is not seen for the 150m GFRP lattice tower. As the height increases the buckling of links become progressively more critical and to compensate for this, the links must be made bulkier which increases the mass of the tower.

Similar to the CFRP tubular tower designs, the cost of the CFRP lattice towers are also roughly 3-4 times higher than the cost of the Steel counterparts. The cost difference between the CFRP and steel design drastically increases as the hub height increases thus CFRP is not recommended as an alternative to steel. This difference in cost is not so drastic for GFRP designs, owing to the cheaper material used. But, it still is more expensive than the existing Steel designs.

One of the most prominent short comings of the lattice design is the lack of an elegant joining technique. Using pultruded composite lattice links for load bearing structures such as a high capacity turbine tower is in itself an uncommon practice, and few examples exist as a proof of concept. The result of this study is based on joining techniques and manufacturing methods that are well established and tested. With the existing technology pultrusion of links with the dimensions recommended in this study will prove to be a challenge. This implies that a lattice turbine tower cannot feasibly be designed using composite materials unless, in the future, the raw material cost can be reduced and its properties improved, and a more elegant and cheaper joining technique can be adopted.

5.5 Chapter summary

This chapter presented the results of tubular and lattice towers made up of GFRP and CFRP material and for various hub height. The critical loading conditions were identified. The tower cost distribution was discussed, and the highest cost contributors were identified. In the final section, the mass and cost of the composite towers were compared with equivalent steel towers, and it was found that composite had a mass advantage only for smaller hub height towers. The cost of the CFRP towers were 3-4 times that of steel towers. The GFRP towers did not show any cost advantages either. But, for smaller hub heights composites showed some promising results as the towers were only 4% costlier compared to steel.

Chapter 6

Conclusions and Recommendations

In this chapter, the work done in the thesis is summarized and concluded and the research questions framed to guide the work is then be answered.

The problem statement from Suzlon was to investigate the feasibility of composites as an alternative material to steel for wind turbine towers. Composites were attractive as they could potentially solve the various issues in manufacturing, transportation, and mass. To investigate the feasibility of composites, initially, a literature survey was conducted that provided insight into aspects like the various designs, modeling techniques, joining techniques, loads, failure modes and cost contributors in a wind turbine tower. This helped setup a tool that helps in the structural analysis of the design that also predicts the cost and its contributors. This tool played the central role in the trade studies and optimization phase that followed. Tubular and lattice designs for various hub heights (75m, 100m, 125m and 150m) and turbine capacities (2.1MW and 5MW) were drawn up, and these were then compared to their steel counterparts. Based on the study no conclusive advantage is found in using composites as an alternative to steel but areas of future research and development are identified to enable Suzlon to further investigate into the shortcomings. The designs that do show some promise were for shorter hub heights and did not address the initial issues with tall towers and thus do not hold merit.

Keeping in view the work of the thesis, the research questions can now be addressed that have helped in guiding the thesis to its conclusion.

What is the defining geometrical parameters for the tubular and lattice tower?

In a tubular tower, it is seen that the defining geometrical parameters are limited and are usually the base radius, thickness of the tower base, the thickness variation along the height.

In the case of a lattice tower, the main parameters chosen for the work of this thesis are the base leg distance, number of sections in the tower, the top width of the tower, the topology, the link dimensions and the link profile. In this study, two topologies were chosen. The first topology can be used for turbine capacities of up to 1MW and up to a hub height of 60m. This topology does not contain any web members and becomes susceptible to buckling at large heights. The second topology is recommended for higher capacities and taller hub

heights. This topology incorporates web members and thus has better buckling resistance at larger height.

What type of composite material should be chosen?

Both the Carbon Fiber Reinforced Plastic (CFRP) and Glass Fiber Reinforced Plastic (GFRP) designs were pursued. It is found that designs with GFRP were cheaper whereas the ones with the CFRP material were lighter. Since wind industry is highly cost driven, it can be concluded that GFRP is the recommended material for the composite tower design.

What are the most critical loading conditions acting on a wind turbine tower throughout its service life?

Static analysis was performed considering two load cases. One for operating condition and the other for the non-operating condition of the turbine. Fatigue analysis was performed for a service life of 20 years assuming a weibull distribution in the wind velocity spectrum. In all the tower designs except for the GFRP tubular tower designs, it was found that the non-operating load case is the most critical loading condition. This is because the wind loads appearing in this condition are extremely high although it has a recurrence rate of once in 50 years. For the GFRP tubular towers, the operating loading condition was the most critical because these loads get multiplied by the dynamic amplification factor (DA). Due to the low tower frequencies which are closer to the rotor frequency, the tubular GFRP towers have high DA and thus the exception.

What are the most critical constraints when designing the wind turbine tower?

The geometric constraints identified for the composite wind turbine tower are clearance between the blade and tower and the upper limit for the base diameter. The frequency constraint ensured that the tower frequency strictly avoids the rotor frequency (P) and the blade passing frequency (3P) by 10% margin.

The structural constraints imposed are the material and buckling safety factors, the tower top deflection and the fatigue damage caused by the wind loading. The tower top deflection was found to be critical for GFRP tubular towers because of the low stiffness due to combined effect of slender geometry and material. The local buckling of the laminate was found to be critical for CFRP tubular towers due to the low thickness at the base of the tower. In the case of lattice towers, the criticality was shared by buckling of the links and material failure. Tower top deflection was not critical owing to the wide base.

Which is the best joining technique to join tubular tower sections and lattice tower links made up of composites?

There is no joining technique developed by the industry specifically for joining composite tubular tower sections or lattice tower links. In this study, the most popular joining techniques are studied which are bolted joints and adhesive joints. Bolted joints were found to be heavier and costlier in general. Because of the material removal during drilling for bolted joints, the link dimensions are influenced by the number of bolts in the joint. Thus the tower design and joint design should be done iteratively until a solution is achieved. This is out of the scope of the thesis and can be pursued in the future. Hence, adhesive joints are recommended for both tubular and lattice designs, and approximate joint mass and cost using adhesive joining methods have been calculated.

What are the major cost contributors for a wind turbine tower?

The major cost contributors included in this study is the raw material cost, labor cost for production and finishing, aiding material cost in case of tubular towers, machine cost in case of lattice towers, joint cost, transportation cost, crane & installation cost and foundation cost. An additional 60000€is added in the case of lattice towers for the maintenance of tower joints over a lifetime of 20 years.

The raw material contributes highest to the overall cost of a tubular tower, but this contribution was found to be much higher in the case of CFRP towers (85%) compared to GFRP towers (63%) due to the high cost of the raw material. Labor cost is another major contributor due to the high labor intensive nature of vacuum infusion process. Other major contributors include the crane hiring and lifting costs and the foundation cost due to the high mass of the towers sections. The joint mass does not contribute as much to the overall cost as the contributors mentioned above. This is due to a relatively low number of joints present in tubular towers as compared to lattice towers.

A similar distribution of cost contribution is observed in lattice towers, but unlike tubular towers, the joint mass is the second major contributor due to a large number of joints. Here there is an added cost contributor attributed to the machine cost for pultruding the links.

What are the geometric parameters of a tubular structure and a lattice structure that can be modified to get the best mass and cost in a wind turbine tower?

For a tubular tower, the base diameter and thickness are the chosen parameters that can be modified to find the best design iteratively. Other geometric parameters such as the thickness variation along the height and the taper of the tower were fixed based on the trade studies. Linear variation in the thickness of tower and a linear taper was chosen because they were found to produce a lighter and simpler design among their alternatives.

For a lattice tower, the link dimensions are the chosen parameters that can be modified to find the best design. Each tower has been presented with a custom set of link dimensions, where the links have been categorized into five categories based on their location in the tower. Other geometric parameters like the topology and the link cross-section shape were fixed after a series of trade studies. All the links have an I-section for easier joining and show better mass and buckling behavior compared to their alternatives. The base leg distance was kept as large as possible while respecting the blade clearance constraint. Except for 150m tall tower where the number of sections in the tower was increased to 6 to prevent buckling, all other designs have four sections.

What is the best method to obtain the most optimized design w.r.t. mass and cost?

For the tubular towers, there were two parameters to be modified which are the base diameter and the laminate thickness at the base. Hence, a brute force approach was adopted where the Matlab tool analyses each design inside a given range for the parameters and searches for the best design. The base diameter was varied in steps of 0.1m, and the base thickness was varied in steps of 10mm.

For the lattice towers, the link dimensions were defined by the link width and the thickness of the I-section. Considering five categories for links, ten distinct parameters were modified using the inbuilt function optimizer called fmincon in Matlab. This optimizer uses the Sequential Quadratic Programmer (SQP) algorithm which is the most robust among the range of algorithms available in Matlab.

Does composite hold a potential promise over steel as an alternative material for wind tower?

In this study, CFRP and GFRP material systems were studied. CFRP tubular towers show a mass advantage of up to 52% for lower hub heights (<=100m), and this decreases with height. Due to the high material cost, CFRP towers are at least 3-4 times costlier than steel towers. A similar observation was made with CFRP lattice tower where in spite of the mass advantage of even up to 60%, the design was still three times costlier.

For the GFRP material system, considerable mass advantage was found for the tubular towers with lower hub height (<=100m), but this advantage diminishes as the height is increased. The study proved that only for hub heights below 100m, do composite materials show any promise for cost advantage. The 5MW-100m hub height GFRP tubular tower showed the highest mass advantage (35%) and was the closest in cost to the steel design with the GFRP tower being 4% costlier. GFRP lattice towers show a similar trend with up to 35% mass advantage for smaller hub heights, but this advantage diminishes with height. The GFRP lattice towers evaluated in this study were at least 27% costlier than steel towers.

With the above summary of results it is clear that the only region where composites do show any promises of mass and cost feasibility is for smaller hub heights (<=100m) and on tubular towers. The major existing difficulties with steel towers are for heights in the range of 125-150m. Recommending composites for towers where steel is already in use is counter productive and will be an attempt at solving a non-problem.

Based on the results of the various trade studies and optimized designs presented to support the work of the thesis, it can be concluded that composites do not hold a definitive promise as an alternative material for wind turbine towers over steel. As a general trend in the wind industry, the towers will be taller and will be expected to hold larger and more powerful turbines in the future. The mass advantage promised by composite towers are not enough for composites to be deemed a viable alternative that can thrive in a competitive market for renewable energy.

6.1 Recommendations

Based on the results and outcomes of the study the following recommendations are made:

1. The joining techniques considered in this study may be overestimated and even inappropriate for the joining of composite components. Further detailed design and consideration of joining techniques using T-bolts could lead to a better design. For the lattice structure novel joining techniques can be adopted and this may lead to a decrease in cost since 13-25% of the cost in lattice tower is attributed to joint cost.

2. The joints between the foundation and the tower as well as the joint between the tower and the nacelle has not been considered in this study. This can increase the mass of the tower due to increase in local thickness near the joints.

3. CFRP tubular towers fail mainly due to buckling. The structural properties of the tower may be improved by incorporating a sandwich structure.

4. In this study static analysis has been carried out, use of dynamic analysis and constraining the tower top accelaration rather than deflection may lead to a more relaxed constraint. Thus offering some additional mass advantage atleast in the GFRP tubular towers.

5. Future research can focus more on the manufacturing feasibility of thick laminates and large links used in tubular structures and lattice structures respectively since they may pose manufacturing complexities.

References

[1] US EIA et al. International energy outlook. *US Energy Information Administration, Washington, DC*, 2016.

[2] Staffan Engström, Tomas Lyrner, Manouchehr Hassanzadeh, Thomas Stalin, and John Johansson. Tall towers for large wind turbines. *Report from Vindforsk project*, 342:50, 2010.

[3] Sungjin Lim, Changduk Kong, and Huynbum Park. A study on optimal design of filament winding composite tower for 2 mw class horizontal axis wind turbine systems. *International Journal of Composite Materials*, 3(1):15–23, 2013.

[4] Taek Hee Han, Young Hyun Park, Deokhee Won, and Joo-Ha Lee. Design feasibility of double-skinned composite tubular wind turbine tower. *Wind and Structures*, 21(6):727–753, 2015.

[5] Erich Hau and Horst Von Renouard. *Wind turbines: fundamentals, technologies, application, economics*, volume 2. Springer Berlin, 2006.

[6] Dimos J Polyzois, Ioannis G Raftoyiannis, and Nibong Ungkurapinan. Static and dynamic characteristics of multi-cell jointed gfrp wind turbine towers. *Composite structures*, 90(1):34–42, 2009.

[7] Dayton A Griffin. Windpact turbine design scaling studies technical area 1-composite blades for 80-to 120-meter rotor. *National Renewable Energy Laboratory, Colorado, USA, Tech. Rep. NREL/SR-500-29492*, 2001.

[8] International Electrotechnical Commission et al. Iec 61400-1: Wind turbines part 1: Design requirements. *International Electrotechnical Commission*, 2005.

[9] Michael W LaNier. Lwst phase i project conceptual design study: Evaluation of design and construction approaches for economical hybrid steel/concrete wind turbine towers; june 28, 2002–july 31, 2004. 2005.

[10] Katherine Dykes, B Resor, A Platt, Y Guo, A Ning, R King, T Parsons, D Petch, and P Veers. Effect of tip-speed constraints on the optimized design of a wind turbine. Technical report, National Renewable Energy Laboratory (NREL), Golden, CO., 2014.

[11] GL Wind Guideline. Guideline for the certification of wind turbines. *Hamburg: Germanischer Lloyd Wind Energie Gmb H*, 2010.

[12] Yin Zhou and Ahsan Kareem. Definition of wind profiles in asce 7. *Journal of structural Engineering*, 128(8):1082–1086, 2002.

[13] Xiong Liu, Cheng Lu, Gangqiang Li, Ajit Godbole, and Yan Chen. Effects of aerodynamic damping on the tower load of offshore horizontal axis wind turbines. *Applied Energy*, 2017.

[14] M arc Seidel, Gunnar Foss, and OWEC Tower AS. Impact of different substructures on turbine loading and dynamic behaviour for the downvind project in 45m water depth. 2006.

[15] Laszlo Arany, S Bhattacharya, John HG Macdonald, and S John Hogan. Closed form solution of eigen frequency of monopile supported offshore wind turbines in deeper waters incorporating stiffness of substructure and ssi. *Soil Dynamics and Earthquake Engineering*, 83:18–32, 2016.

[16] John Corbett Nicholson. Design of wind turbine tower and foundation systems: optimization approach. 2011.

[17] Jason Jonkman, Sandy Butterfield, Walter Musial, and George Scott. Definition of a 5-mw reference wind turbine for offshore system development. *National Renewable Energy Laboratory, Golden, CO, Technical Report No. NREL/TP-500-38060*, 2009.

[18] Graham Harcourt Powell. *Modeling for structural analysis: behavior and basics*. Computers and Structures, 2010.

[19] Stephen W Tsai. Strength theories of filamentary structure. *Fundamental aspects of fiber reinforced plastic composites*, 1968.

[20] Rodney Hill. *The mathematical theory of plasticity*, volume 11. Oxford university press, 1998.

[21] Stephen W Tsai and Edward M Wu. A general theory of strength for anisotropic materials. *Journal of composite materials*, 5(1):58–80, 1971.

[22] Christos Kassapoglou. *Design and analysis of composite structures: with applications to aerospace structures*. John Wiley & Sons, 2013.

[23] Autar K Kaw. *Mechanics of composite materials*. CRC press, 2005.

[24] David Bushnell. Buckling of shells-pitfall for designers. *AIAA journal*, 19(9):1183–1226, 1981.

[25] Michael P Nemeth and Martin M Mikulas Jr. Simple formulas and results for buckling-resistance and stiffness design of compression-loaded laminated-composite cylinders. 2009.

[26] Paul Seide. A donnell type theory for asymmetrical bending and buckling of thin conical shells. *Journal of Applied Mechanics*, 24(4):547–552, 1957.

[27] AI Manevich and EF Prokopalo. Stability of orthotropic thin-walled cylindrical shells under torsion. part 1. theory. *Strength of Materials*, 40(3):292–301, 2008.

[28] Yadong Zhou, Qingguo Fei, and Jiayue Tao. Profile design of loaded pins in composite single lap joints: From circular to non-circular. *Results in Physics*, 6:471–480, 2016.

[29] Timothy Gutowski, David Hoult, Greg Dillon, Ein-Teck Neoh, Stuart Muter, Eric Kim, and Mawuli Tse. Development of a theoretical cost model for advanced composite fabrication. *Composites Manufacturing*, 5(4):231–239, 1994.

[30] Timothy George Peter Gutowski. *Advanced composites manufacturing*. John Wiley & Sons, 1997.

[31] Brent Kawahara, Hector Estrada, and Luke S Lee. Life-cycle cost comparison for steel reinforced concrete and fiber reinforced polymer bridge decks. In *Fiber Reinforced Polymer (FRP) Composites for Infrastructure Applications*, pages 237–273. Springer, 2012.

[32] Deepak Richard, Taehoon Hong, Makarand Hastak, Amir Mirmiran, and Ossama Salem. Life-cycle performance model for composites in construction. *Composites Part B: Engineering*, 38(2):236–246, 2007.

[33] GS Levenson, Stephen M Barro, et al. *Cost-estimating relationships for aircraft airframes*. Rand Corporation, 1966.

[34] Donald J LeBlanc, A Kokawa, T Bettner, F Timson, and J Lorenzara. Advanced composites cost estimating manual (accem). Technical report, AFFDL-TR-76-87, Northrop Corporation, Hawthorne, California, 1976.

[35] Jin-Woo Choi, Don Kelly, and John Raju. A knowledge-based engineering tool to estimate cost and weight of composite aerospace structures at the conceptual stage of the design process. *Aircraft Engineering and Aerospace Technology*, 79(5):459–468, 2007.

[36] Halvard E Nystrom, Steve E Watkins, Antonio Nanni, and Susan Murray. Financial viability of fiber-reinforced polymer (frp) bridges. *Journal of Management in Engineering*, 19(1):2–8, 2003.

[37] Dolf Gielen. Renewable energy technologies: Cost analysis series. Technical report, International Renewable Energy Agency, 2012.

[38] DET NORSKE VERITAS AS. Buckling strength of shells. 2013.

[39] Andrew Christopher Way. A study on the design and material costs of tall wind turbine towers in south africa. Technical report, Stellenbosch University, 2014.

[40] Haiyan Long, Geir Moe, and Tim Fischer. Lattice towers for bottom-fixed offshore wind turbines in the ultimate limit state: variation of some geometric parameters. *Journal of Offshore Mechanics and Arctic Engineering*, 134(2):021202, 2012.

[41] B Gencturk, A Attar, and C Tort. Optimal design of lattice wind turbine towers. In *15th World Conference on Earthquake Engineering*, pages 24–28, 2012.

[42] Joseph E Shigley, Charles R Mischke, Milan Montreal New Delhi San Juan, and Singapore Sydney Tokyo Toronto. Machine design. 1996.

Appendix A

Turbine, Material and Cost properties

This appendix contains the material, soil, turbine and cost properties used in this study.

A.1 Material properties

The material properties of Fiber Reinforced Plastic (FRP)-composite plies used in the study is presented in this section. The data was obtained from Suzlon Energy Ltd. Table A.1 presents the material properties for single ply made up of Glass Fiber Reinforced Plastic (GFRP) composite material and Carbon Fiber Reinforced Plastic (CFRP) composite material. Both the FRPs use Epoxy.

		CFRP UD ply	GFRP UD ply	GFRP biaxial ply
t_{ply}	[mm]	1.884	0.781	0.576
ρ_{mat}	[kg/m3]	1590	2006	1969
E_x	Mpa	132000	52000	13100
E_y	Mpa	8850	13900	13850
G_{xy}	Mpa	4500	4900	12300
σ_x	Mpa	545	370	50
σ_y	Mpa	25	25	50
τ_{xy}	Mpa	25	25	25

Table A.1: Material properties of the FRP-ply (Courtesy: Suzlon Energy Ltd.)

The soil and foundation properties considered for studying the effect of the foundation stiffness on the natural frequency of the tower is given in Table A.2. The foundation stiffness and mass element of the foundation is given by Equation A.1.

Property	Unit	Value
μ_{soil}	[-]	0.35
G_{soil}	[Mpa]	20.68
ρ_{soil}	$[Kg/m^3]$	1921
$\rho_{concrete}$	$[Kg/m^3]$	2400

Table A.2: Soil properties [9]

Material	Unit	Cost
GFRP raw material	€/Kg	3.5
CFRP raw material	€/Kg	16
Machine rate	€/hour	100
Labor rate	€/hour	20
Mold cost	€/ton	100
Vacuum bagging material cost	€/part	300
Bolt cost (Steel bolts)	€/kg	6
Adhesive material cost	€/part	1500

Table A.3: Cost data (Courtesy: Suzlon Energy Ltd.)

$$
\begin{aligned}
Mass_{foundation} &= (b_f.w_f.h_f).\rho_{concrete} \\
K_{11,s} = \frac{4.7 G_{soil} b_f}{2(1-\mu_{soil})}; M_{11,s} &= Mass_{foundation} + 0.095 \frac{32(1-\mu_{soil})\rho_{soil} {b^3}_f/\pi^{3/2}}{(7-8\mu_{soil})} \\
K22_s = \frac{4 G_{soil} {b^3}_f}{8(1-\upsilon_{soil})} M_{22,s} &= Mass_{foundation} + 0.24 \frac{8\rho {b^3}_f/(3\pi)^{3/4}}{3(1-\mu_{soil})} \\
K_{e,soil} = \begin{bmatrix} K_{11,s} & 0 \\ 0 & K_{22,s} \end{bmatrix}; M_{e,soil} &= \begin{bmatrix} M_{11,s} & 0 \\ 0 & M_{22,s} \end{bmatrix}
\end{aligned} \tag{A.1}
$$

A.2 Cost properties

The cost data used in the cost modeling of this study is given in Table A.3.

A.3 Turbine properties

		2.1MW turbine	NREL 5MW turbine
Rated power	[MW]	2.1	5
IEC class	[-]	III A	I B
Cut in wind speed	[m/s]	4	3 m/s
Rated wind speed	[m/s]	14	11.4 m/s
Cut out wind speed	[m/s]	25	25 m/s
Rotor diameter	[m]	111	126 m
Rated rotor speed	[rpm]	14.5	12
Rotor frequency (1P)	[Hz]	0.24.1	0.2
Maximum blade deflection(L_b)	[m]	6	7
Tower top mass	[tons]	180	350

Table A.4: Turbine properties of Suzlon 2.1MW turbine and 5MW NREL turbine [17], (Courtesy: Suzlon Energy Ltd.)

Appendix B

Load Cases

This appendix contains min/max force table provided by Dykes et.al. [10], the critical wind loading cases during operation and non-operating condition for a 2.1MW capacity Suzlon turbine and a 5MW NREL turbine. The detail steps to calculate direct wind load according to American Society of Civil Engineers (ASCE)-7 standards is outlined. Also, turbine properties like the rotor diameter, rpm range, tower top mass, etc. are provided in this section.

B.1 Tower top design loads for 2.1MW and 5MW turbine

It was discussed in Section 3.3 that Extreme Turbulence Model (ETM) load case is considered during operating condition and Extreme Wind Model (EWM) load case during non-operating load condition. The tower top wind loads for these loading condition for a 5MW and 2.1MW turbine is given in Table B.1

		2.1MW 90m		5MW 90m	
		ETM	EWM 1	ETM	EWM50
$F_{x,top}$	[KN]	754.5	956.7	1437.8	369.3
$F_{y,top}$	[KN]	18.6	-790.0	-1914.3	-1265.0
$F_{z,top}$	[KN]	-1877.6	-1321.8	-4707.5	-3179.0
F_{top}	[KN]	754.7	1240.7	1437.9	1317.8
$M_{x,top}$	[KN.m]	-2646.1	1940.5	6179.0	4186.6
$M_{y,top}$	[KN.m]	381.9	-7132.3	2308.5	-4964.3
$M_{z,top}$	[KN.m]	2400.0	4974.0	1410.8	9315.9
M_{top}	[KN.m]	2673.5	7391.6	6596.1	4215.9
V_{hub}	[m/s]	12	39.3	14.2	70

Table B.1: Tower top loads for EWM and ETM load cases for a 2.1MW and 5MW turbine [10], (Courtesy: Suzlon Energy Ltd.)

B.2 Direct wind loads

The steps to calculate the direct wind load as given by ASCE and are as follows.

1. Calculate the basic wind speed (V_b) and the wind directionality factor (K_d)from ASCE-7, Section 6.5.4. The equation for basic wind speed is given in Equation B.1 and calculated from the wind velocity at the hub height and the wind shear factor (β) for the loading case considered. The directionality factor takes into account that the probability the maximum wind may not impact the structural component or system in its weakest orientation. This is done to avoid being over-conservative in wind load calculation. This is 0.95 for tubular structures and 0.85 for lattice structures.

$$V(z) = V_b\left(\frac{z}{10}\right)^{\beta}$$
$$V_b = V_{hub}\left(\frac{10}{h}\right)^{\beta} \tag{B.1}$$

V_b - Basic wind speed at height 10 m from ground $[m.s^{-}1]$
h - Hub height of the tower $[m]$
β - Wind shear factor usually taken as 0.2
z - Arbitrary height in m from the ground $[m]$

2. Calculate the importance factor (Im), Section 6.5.5. It is assumed in this study that the wind turbine tower come under occupancy category II since it is located away from any human congregate. The importance factor for structures under this category is 1.

3. Determine the exposure category for the structure and terrain coefficient K2 according to ASCE-7, section 6.5.6. In this study it is assumed this category is D, the tower is located on a flat and unobstructed area. For this category, the constants are defined in Table B.2 and the terrain coefficient ($K2$) is given by Equation B.2.

Coefficient	Value
γ	4
μ	1.5
Lh	100000
H	1
K11	$1.55\frac{H}{\mu.Lh}$
K22	1
K33	$e^{-\gamma\frac{z}{Lh}}$

Table B.2: Coefficient for a terrain category D [12]

Coefficient		Value
$\alpha 1$		11.5
Zg	[m]	213.36
c		0.15
b		0.8
α		1/9
ε		1/8
e1	[m]	198.12
β_d	Damping factor	0.02

Table B.3: Topographic coefficient for category D [12]

$$K2 = (1 + K11.K22.K33)^2 = 1 \tag{B.2}$$

4. Determine the topographic factor K3 according to ASCE section 6.5.7. The constants for a site under category D is given by Table B.3 and the factor is given by Equation B.3.

$$K3 = \begin{cases} \left[2.01\left(\frac{4.57}{zg}\right)^{\frac{2}{\alpha 1}}\right] & if\ z < 4.572 \\ \left[2.01\left(\frac{z}{zg}\right)^{\frac{2}{\alpha 1}}\right] & if\ z \geq 4.572 \end{cases} \tag{B.3}$$

5. Calculate the wind velocity pressure (Q) as a function of height (z) using Equation B.4.

$$Q(z) = 0.613.V_b^2.K2.K3.Kd; \tag{B.4}$$

6. Calculate gust factor G for a rigid or flexible structure according to ASCE-7, section 6.5.8. Since in this study, the tower design is a soft- stiff design with $\omega_t < 1$, the gust factor for a flexible structure is calculated in Table B.4.

Intensity of turbulence	Iz	$c.\frac{10}{z}$
Integral length scale of turbulence	Lz	$e1.\frac{10}{z}$
Peak factor of resonance	Gq	3.4
	Gv	3.4
	Gr	$\sqrt{2\ln(3600\omega_t)}, +\frac{0.577}{\sqrt{2\ln(3600\omega_t)}}$
Background response	q	$\sqrt{\frac{1}{1+0.63\left(\frac{B+h}{Lz}\right)^{0.63}}}$
Mean hourly wind speed	$\overline{V}_z$	$b\left(\frac{z}{10}\right)^{\alpha}V_b$
	N1	$\frac{\omega_t Lz}{\overline{V}_z}$
Resonance response factor	RL	$\frac{1}{\eta} - \frac{1}{2\eta^2}(1 - e^{-2\eta})$
	Rh	RL, setting $\eta = 4.6\frac{\omega_t h}{\overline{V}_z}$
	Rb	RL, setting $\eta = 4.6\frac{d(z)}{\overline{V}_z}$
	Rl	RL, setting $\eta = 15.4\frac{d(z)}{\overline{V}_z}$
	Rn	$\frac{7.47\omega_1}{(1+10.3\omega_1)^{5/3}}$
	R	$\sqrt{\frac{1}{\beta}Rn.Rh.Rb.(0.53 + 0.47Rl)}$
Gust factor for flexible structure	G_{flex}	$0.925\left(\frac{1+1.7Iz\sqrt{Gq^2q^2+Gr^2R^2}}{1+1.7Gv.Iz}\right)$

Table B.4: Gust factor for flexible structures [12]

7. Determine the direct wind load F as given in ASCE-7 and given by Equation B.4.

$$F_z(z) = Q(z).G.C_f.A(z) \tag{B.5}$$

$A(z)$ - Width of the tower at that height z
G - Gust factor
C_f - Force coefficient

$Q(z)$ - Velocity pressure

ϵ - Solidity ratio, Projected area of links in lattice tower/area of the section normal to wind

C_f - Force coefficient, 0.7 for tubular structures, $4\epsilon^2 - 5.9\epsilon + 4$ for lattice structures

Appendix C

Buckling failure

This Appendix presents the various calculations relevant to buckling failure modes in a tubular and lattice structure.

C.1 Buckling in tubular section

Euler buckling: For Euler buckling of orthotropic shells with simply supported or clamped boundary condition the critical buckling stress is given by C.1. This equation takes into consideration the shear stress as well. In this study, the simply supported boundary condition is assumed, so the factor C_b is chosen as 1.

$$\begin{aligned} \sigma_{cr,ebuck} &= \sigma_{cr,euler}\left[1+\frac{2}{3}\left(\frac{\pi R_o}{L}\right)^2\frac{E_x}{G_{xy}}\right]^{-1} \\ \sigma_{cr,euler} &= \frac{C_b.\pi^2.E_x.I}{AL^2} \\ SF_{ebuck} &= \frac{\sigma_c}{\sigma_{cr,euler}} \end{aligned} \tag{C.1}$$

C_b - Factor determined by boundary condition, 4 for fixed-fixed and 1 for simply supported beams
E_x - Modulus in longitudinal direction
G_{xy} - Modulus in shear
I,A,R - Geometric properties of the tubular section averaged over the section length which is 25 m in this study

Buckling under axial and bending loading: Nemeth et.al. [25] have given simplified equations for the buckling of the orthotropic shells under axial loading, given by Equation C.2. To prevent buckling the applied stress should be lesser than the critical buckling stress. No post

buckling study has been carried out in this study. Hence, the tubular tower design is assumed to have failed once the critical buckling stress in any section is reached.

$$\sigma_{cr,lbuck'} = \frac{1}{2}\sqrt{\frac{2G_{xy}\sqrt{E_x E_y}}{3(1-\sqrt{\mu_{xy}\mu_{yx}}}}.Er_b\frac{t}{R_o} \tag{C.2}$$

$G_{xy}, E_x, E_y, \mu_{xy}, \mu_{yx}$ - Material properties
t, R_o - tubular section dimensions
Er_b - Error value due to assumption that number of half waves in circumferential direction is a continuous function

Under pure bending the buckling occurs when the peak stress along the circumference reaches buckling stress under pure axial compression. To verify this, an orthotropic cylinder with Glass Fiber Reinforced Plastic (GFRP) material properties was modeled in Ansys and buckling analysis was carried out under axial compression loading and under bending moment and presented in Table C.1. The critical buckling moment obtained was converted to an equivalent axial load using Equation C.3.

$$M_{cr} = N_{cr}.\pi.R_O^2 \tag{C.3}$$

Here N_{cr} is the critical buckling force/length and M_{cr} is the critical buckling moment. In Table

R_o	t	L	Material	Critical moment (N.m) M_{cr}	corresponding critical force (N) N_{cr}	Critical axial force (N) N_{cr}	Error (%)
5	0.1	10	GFRP	1.57E+09	6.28E+08	6.42E+08	2.09
2	0.1	20	GFRP	6.54E+08	6.54E+08	6.77E+08	3.3

Table C.1: Critical buckling load under axial compression and bending for two GFRP cylinders

C.1 both the analysis showed the same critical buckling load, which confirms the statement by Seide & Weingarten [26] that buckling occurs when the peak stress in the structure at any point reaches the critical buckling stress irrespective of the type of loading.

Buckling under torsional and shear loading: The analytical equations to calculate the critical buckling stress in a tubular structure under torsion as given by Manevich et.al. [27] and given in Equation C.4 and Equation C.5.

$$\begin{aligned} \eta &= \frac{E_x}{E_y} \\ \rho_o &= \frac{1}{\sqrt{12(1-\upsilon_x y \upsilon_y x}}\frac{t}{R} \\ \varepsilon_o &= \left(\frac{\pi R_o}{L}\right)\sqrt{\pi_o} \\ \rho_1 &= \frac{\rho_o}{\sqrt{\eta}} \\ \varepsilon &= \frac{\varepsilon_o}{\sqrt[4]{\eta}} \end{aligned} \tag{C.4}$$

$$
\begin{aligned}
F_0 &= m(m+2)(3m^2+6m+4) \\
F_1 &= 5m^4+20m^3+40m^2+40+16 \\
F_2 &= \frac{m^2(m+2)(7m^3+21m^2+20m+6)}{\sqrt[4]{F_o}} \\
F_3 &= \frac{m^2(2m^4+(m+2)F_1{F_o}^{-0.5}(m^3+9m^2+12m+6)}{\sqrt[4]{{F_o}^3}} \\
\varphi_2 &= \frac{(\mu_{xy}+\mu_{yx}+2)F_2}{\sqrt{\eta}(1+\eta_{xy})+\frac{1}{\sqrt{\eta}}(1+\eta_{xy})} - \frac{1}{2}\left(\frac{1}{\sqrt{\eta}}+\sqrt{\eta}\right)F_3 \\
\varphi_1 &= \frac{1}{m{F_o}^{5/8}}(F_o+m^4+\varphi_2\sqrt[4]{\eta}\varepsilon_o) \\
\tau_{cr,lbuck'} &= \frac{\rho_1^{\frac{5}{4}}}{2}\sqrt{\frac{\pi R_o}{L}}\min(\varphi_1)E_x
\end{aligned}
\tag{C.5}
$$

Where $\tau_{cr,lbuck'}$ is the critical buckling shear stress and m is the number of half waves. For buckling under shear force, it is assumed that buckling occurs when the peak stress at any location in the cylinder reaches the critical buckling stress as given by Equation C.4. This statement is further verified by taking a cylindrical structure and applying a torsional moment and then a shear force and observing the critical buckling stress in both cases. The results are given in Table C.2. It is seen that the critical shear stress during buckling due to shear force is higher than the critical shear stress during buckling due to torsional moment. But, in this study, the same critical stress as given by applying torsional moment is considered as the critical buckling stress.

R_o	t	L	Material	Critical shear stress when torsion is applied	critical shear stress when shear force is applied	Error (%)
2.5	0.2	20	GFRP	2.09E+08	2.42E+08	13.59
5	0.05	20	GFRP	2.22E+07	2.71E+07	18.62

Table C.2: Critical shear stress under axial torsion and shear force for two GFRP cylinders

C.2 Buckling in Lattice links

It is discussed in the literature survey that links can undergo Euler buckling as well as local buckling like crippling in its web or flanges. The critical buckling loads for these type of failures is given in the following subsections.

Euler buckling: The critical stress for euler buckling ($\sigma_{cr,ebuck}$)is given by Equation C.1. In the case of lattice structures the boundary condition of the links is considered to be simply supported. This is a conservative assumption. In reality the boundary condition will be intermediate to fixed fixed and a simply supported.

Crippling in a lattice structure links: The crippling strength of flanges and web in a beam can be found using semi empirical relationship by Kassapoglou [22]. In a beam, flanges have one free edge and the web has no free edges leading to distinct failure loads given by Equation

C.6 and Equation C.8 respectively. But these relationships are developed for a laminate with atleast 25% of cross plies and angle plies each. For other laminates the buckling equation for an infinitely long flange can be used as given in Equation C.7 and C.9 respectively.

$$\frac{\sigma_{cr,crip}}{\sigma_{ut,x,C}} = \frac{2.151}{\left(\frac{b_{flange}}{t_{flange}}\right)^{0.717}} \quad for\ b_{flange} \geq 2.91 t_{flange} \tag{C.6}$$

$$N_{cr,crit} = \frac{G_{xy}.t_{flange}^3}{b_{flange}^2} \tag{C.7}$$

$$\frac{\sigma_{cr,crip}}{\sigma_{ut,x,C}} = \frac{11}{\left(\frac{b_{flange}}{t_{flange}}\right)^{1.124}} \quad for\ b_{flange} \geq 11.07 t_{flange} \tag{C.8}$$

$$\begin{aligned} N_{cr,crit} &= \frac{2\pi^2}{b_{flange}^2}\left[\sqrt{D_{11}D_{22}} + (D_{12} + 2D_{66})\right] \\ D_{11} &= \frac{E_x.t_{flange}^3}{12(1-\mu_{xy}.\mu_{yx})} \\ D_{22} &= \frac{E_y.t_{flange}^3}{12(1-\mu_{xy}.\mu_{yx})} \\ D_{12} &= \mu_{yx}.D_{11} \\ D_{66} &= \frac{G_{xy}.t_{flange}^3}{6} \end{aligned} \tag{C.9}$$

b_{flange}, t_{flange} - Breadth and thickness of the flange
$\sigma_{ut,x,C}$ - Axial strength in compression
$E_x, E_y, G_{xy}, \mu_{xy}, \mu_{yx}$ - Material properties of the laminate

Appendix D

Joint failure

This chapter deals with the failure modes included in the design of the joints and the design procedure for the tubular tower, joint-1.

D.1 Bolted flange joint

The details of the bolted flange joint are shown in Figure D.1. There are two critical regions in this joint. Region 1 is where the maximum tensile force occurs due to dead loads and the moments caused by wind loads. Region 2 is where the maximum shear force occurs due to the torsion appearing on the tower due to turbine load and the shear force due to direct wind load. To prevent bearing failure in region 2, it is necessary for the plies in the flange to have at least 50% +-45 degree plies.

The assumptions made are:

1. Only the tension side is critical as the critical failure in compression side has already been taken care of by first ply failure.
2. The joint itself is modeled as a combination of linear springs, the properties of which are taken from Shigley et al. [42].
3. The joint remains in linear range and separation of composite inside the cone region has not occurred even at the highest load.
4. The number of bolts along circumference is limited by the thumb rule of $5D_{bolt}$ spacing.

The bolt properties considered are given in Table D.1.

The expected failure modes in the joint structure have been already tabulated in Table 3.2 and the details of these failure modes are given below.

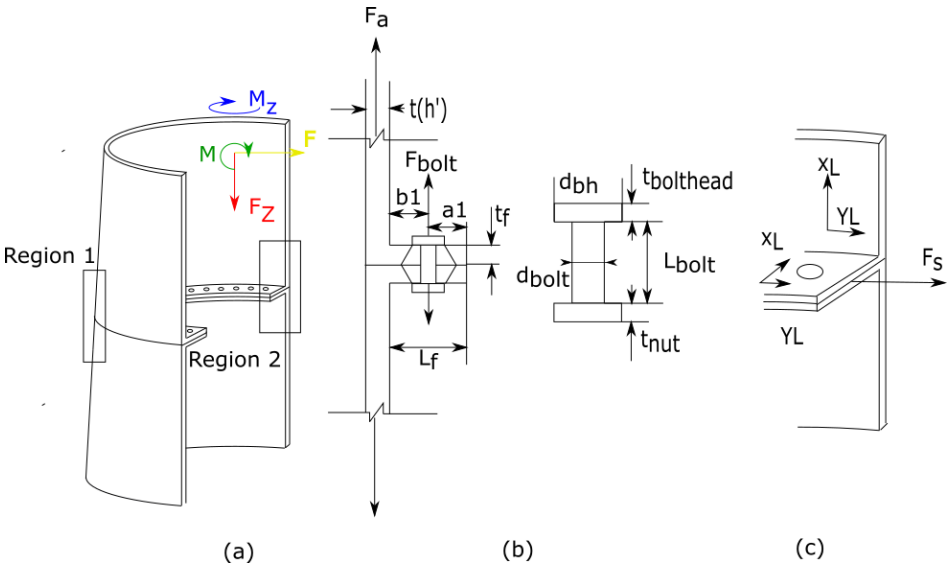

Figure D.1: (a) Bolted flange joint (b) Region 1 (b) Region 2

Material property of bolt		Value
Bolt Modulus (E_{bolt})	[Pa]	200E+09
Bolt possoin's ratio (μ_{bolt})	[-]	0.27
Shear strength of the bolt ($\tau_{ut,bolt}$)	[Pa]	296E+06
Tensile strength of the bolt ($\sigma_{ut,bolt}$)	[Pa]	513E+06
Bolt preload (σ_p)	[Pa]	560E+06
Bearing strength of the flange, GFRP ($\sigma_{bear,flange}$)	[Pa]	100E+06
Bearing strength of the flange, CFRP ($\sigma_{bear,flange}$)	[Pa]	150E+06
Bolt preload (σ_p)	[Pa]	560E+06

Table D.1: Steel bolt material properties (Courtesy: Suzlon Energy Ltd)

1. Joint separation in region 1

$$
\begin{aligned}
F_a &= \sigma t(h') \\
F_p &= \frac{\sigma_p}{\pi/4.D_{bolt}^2} \\
\left(\frac{\pi D(h')}{n_b} F_a\right) \frac{a_1 + b_1}{b_1} &< F_p \left(\frac{K_f + K_b}{K_f}\right) \\
K_f &= \frac{\pi E_f}{4t_f \left(\frac{1}{D_{bh}(D_{bh}+2t_f \cos(\alpha_{cone})-{D_{bolt}}^2}\right) + \frac{(1+\mu_{xy,f}) \ln 2}{t_f}} \\
K_{bolt} &= \frac{1}{\frac{1}{K_{bs}} + \frac{1}{K_{bh}} + \frac{1}{K_{nut}}} = \frac{\pi E_{bolt}}{\frac{4L_{bolt}}{D_{bolt}} + (1+\mu_{bolt}) \ln 2 \left(\frac{1}{t_{nut}} + \frac{1}{t_{bolthead}}\right)}
\end{aligned}
\tag{D.1}
$$

$\sigma = \sigma_b - \sigma_c$ - Total tensile stress on the laminate due to bending and compressive stress.

D_{bolt},D_{bh} - Bolt diameter and Bolt head diameter
t_f - Thickness of the flange
$D_{bh} = 2.D_{bolt}$
$t_{bolthead} = t_{nut} = 0.5t_f$
α_{cone} - Shigley's stress cone angle, 45°
E_f, $\mu_{xy,f}$ - Flange modulus and possoins ratio
F_p - Bolt preload, $\sigma_p.\pi/4.D_{bolt}^2$
E_{bolt},μ_{bolt} - Bolt modulus and possoins ratio
n_b - Number of bolts around the circumference, 80 in this study

2. Shear failure in bolts in region 2

$$\frac{\left[\frac{2M_z}{D(h')n_b} + \frac{F}{n_b}\right]}{\pi\left(\frac{D_{bolt}}{2}\right)^2} < \tau_{ut,bolt} \tag{D.2}$$

3. Bearing failure in laminate in region 2

$$\frac{\left[\frac{2M_z}{d(h')n_b} + \frac{F}{n_b}\right]}{t_f D_{bolt}} < \sigma_{bear,flange} \tag{D.3}$$

4. Bolt shear out in region 1

$$\frac{\left(\frac{F}{n_b}\right)}{L_f t_f} < \sigma_{bear,flange} \tag{D.4}$$

5. Bolt pull through in region 1.

$$\frac{2\frac{\pi D(h')}{n_b}F_a}{2\pi(D_{bh})t_f} < \tau_{ut,flange} \tag{D.5}$$

The design steps to obtain the final dimensions of the joint is given in the flowchart D.2. The number of bolts is restricted to 80 in all sections; the design procedure is then carried out to calculate the minimum D_{bolt} needed to make sure that the joint doesn't fail. The thickness of the flange is equal to $4.t(h')$ because of the additional 50% +-45 plies added for bolted joints.

D.2 Bolted vertical lap joint

The flange joint is adapted from steel tower design and may not be the appropriate joining method for composite materials due to the high prying stresses leading to joint separation. Hence, a vertical bolted lap joint is also considered. The joint plate is made up of metal and in this study considered to be made of steel with the material properties given in Table D.2. Again due to the high bearing stress appearing on the laminate, +-45 degree plies have to be added locally to provide adequate strength to the laminate to prevent bolt shear out. In this study, this additional thickness is considered to be the same as the original thickness. Hence near the joint, the thickness of the tubular section will be $(2t(h'))$. The laminate will

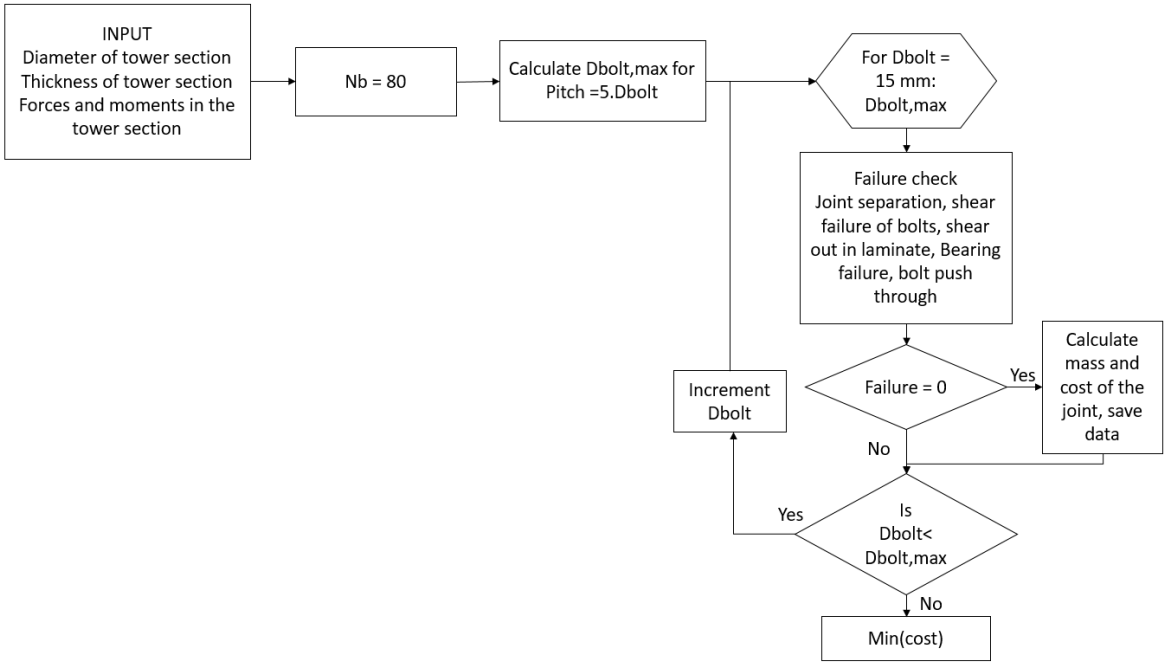

Figure D.2: Flow chart of the design procedure for bolted flange joint

50% +-45 degree plies and 50% UD plies. The bearing strength of this laminate is 100 Mpa for Glass Fiber Reinforced Plastic (GFRP) laminate and 150 Mpa Carbon Fiber Reinforced Plastic (CFRP) laminate. These values are adopted from GL guidelines [11]. For the bolts, properties provided by Suzlon is referred and these are given in Table D.1.

Material property of steel plate		Value
Modulus of the plate (E_{plate})	[pa]	200e9
Poisson's ratio of the plate (μ_{plate})	[-]	0.27
Shear strength of the plate ($\tau_{ut,plate}$)	[pa]	513e6
Tensile strength of the plate ($\sigma_{ut,plate}$)	[pa]	900e6

Table D.2: Material properties of the steel (Courtesy: Suzlon Energy Ltc.)

The terminology of the joint is shown in Figure D.3. In region 1, the axial force per unit length and the shear force per unit length is given by Equation D.6.

$$\begin{aligned} \mathrm{F}_a &= \sigma \frac{\pi D(h') 2t(h')}{n_b} \frac{1}{n_{row}} \\ F_s &= \frac{2M_z}{d(h')n_b} \frac{1}{n_{row}} \\ \mathrm{F}_{total} &= \sqrt{{F_s}^2 + {\mathrm{F}_a}^2} \end{aligned} \tag{D.6}$$

$\sigma = \sigma_b - \sigma_c$ - Maximum tensile force on the joint
n_b - Number of bolts, 80 in this study
n_{row} - Number of rows of bolts/2, 3 in this study

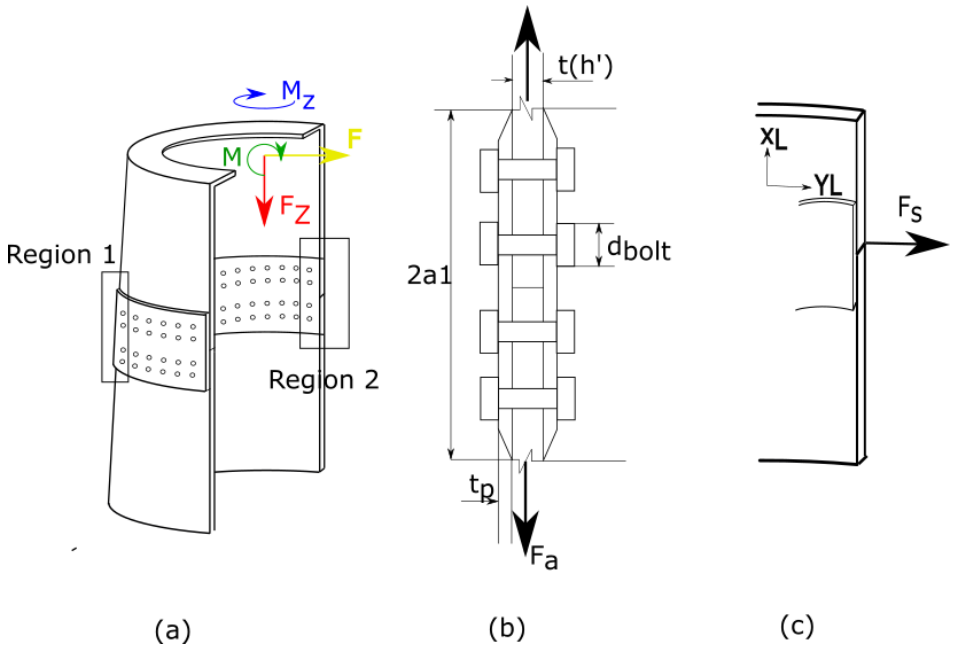

Figure D.3: (a) Bolted vertical lap joint (b) Region 1 (b) Region 2

1. Shear failure in bolts in region 1

$$\frac{\mathrm{F}_{total}}{n_{row}\pi\left(\frac{D_{bolt}}{2}\right)^2} < \tau_{ut,bolt} \tag{D.7}$$

2. Shear out in laminate and plate in region 1

$$\begin{aligned} \frac{\mathrm{F}_a}{2\left(\frac{n_{row}}{1+n_{row}}\right)a_1 2t(h')} &< \tau_{ut,lam} \\ \frac{\mathrm{F}_a}{4\left(\frac{n_{row}}{1+n_{row}}\right)a_1 t_p} &< \tau_{ut,plate} \end{aligned} \tag{D.8}$$

3. Bearing failure in laminate and plate in region 1

$$\begin{aligned} \sigma_{x,b} &= \frac{F_a}{D_{bolt}2t(h')} \\ \sigma_{y,b} &= \frac{F_s}{D_{bolt}2t(h')} \\ tsaihill(\sigma_{x,b},&\sigma_{y,b}) < 1 \end{aligned} \tag{D.9}$$

The bearing strength $()\sigma_{bear}$ while checking for Tsai-Hill failure criteria is consider 100Mpa for GFRP laminate and 150Mpa for CFRP laminate.

$$\frac{\mathrm{F}_{total}}{2D_{bolt}t_p n_{row}} < \sigma_{ut,plate} \tag{D.10}$$

4. Net section failure in laminate and plate in region 1

$$\begin{aligned} \frac{\left(\frac{F_{total}}{n_{row}}\right)}{(\pi d(h') - n_b D_{bolt})2t(h')} &< \sigma_{x,ut} \\ \frac{\left(\frac{F_{total}}{n_{row}}\right)}{(\pi d(h') - n_b D_{bolt})2t_p} &< \sigma_{ut,plate} \end{aligned} \tag{D.11}$$

5. Bearing failure in laminate and plate in region 2

$$\begin{aligned} \frac{\left(\frac{M_z}{n_b}\frac{1}{n_{row}} + \frac{F}{n_b}\frac{1}{n_{row}}\right)}{D_{bolt}2t(h')} &< \sigma_{bear} \\ \frac{\left(\frac{M_z}{n_b}\frac{1}{n_{row}} + \frac{F}{n_b}\frac{1}{n_{row}}\right)}{2D_{bolt}t_p} &< \sigma_{ut,plate} \end{aligned} \tag{D.12}$$

The design steps to obtain the final dimensions of the joint is given in The Figure D.4. The number of bolts (N_b) is set to 80 in all sections and the number of rows of bolt (n_{row}) is set at 3, the design procedure is then carried out to calculate the minimum D_{bolt}, thickness of the plate (t_p) and the overlap length $a1$ needed to make sure that the joint doesn't undergo failure.

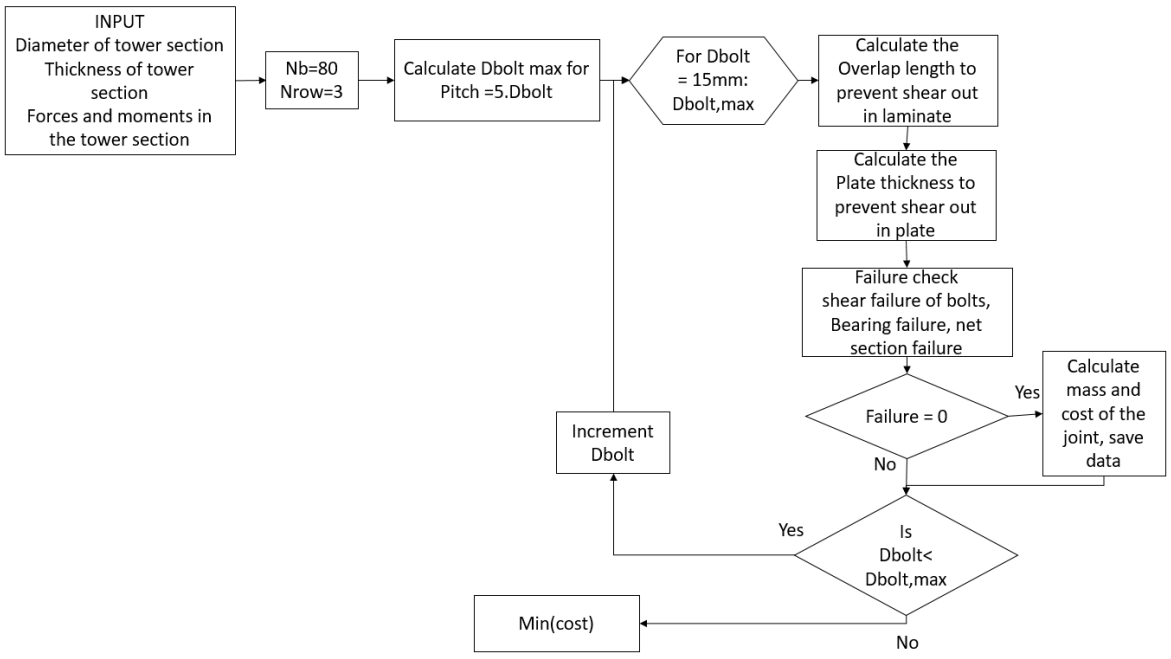

Figure D.4: Flow chart of the design procedure for vertical bolted joints

D.3 Adhesive vertical lap joint

The adhesive joint has a similar design to the vertical bolted joint. The details of the adhesive joint design are shown in Figure D.5.

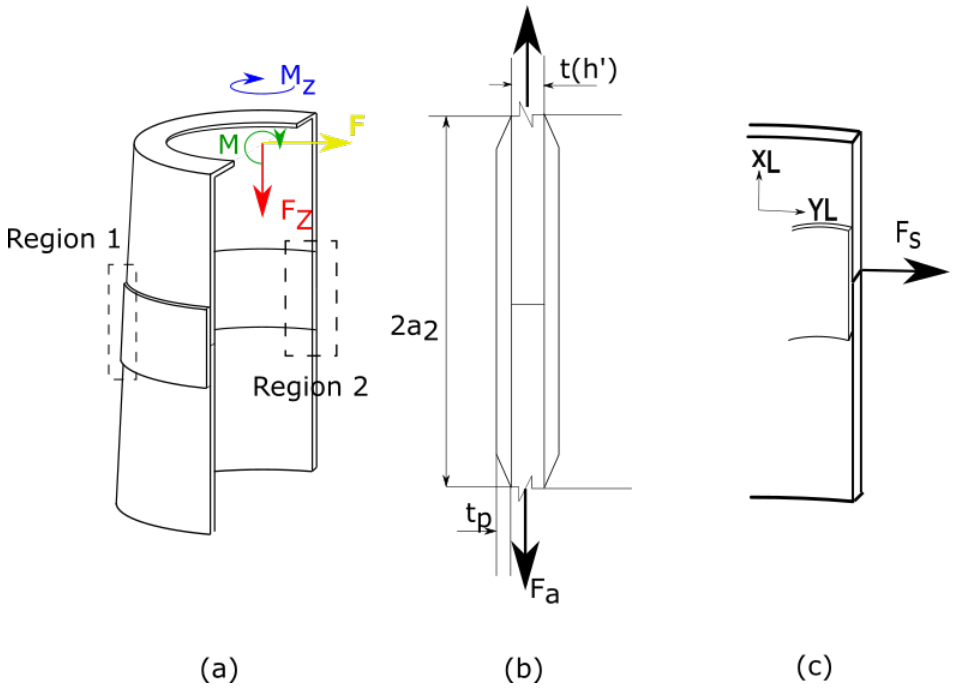

Figure D.5: (a) Adhesive lap joint (b) Region 1 (b) Region 2

The prominent failure modes in an adhesive joint is the failure in adhesive or the failure in the joint plate. The joint plate is assumed to be made of same material and layup as the tower laminate. The region where the maximum axial stress and shear stress occurs is in two different location. The following failure modes are checked for in the final design of the joint.

1. Adhesive failure

$$\sqrt{\left(\sigma(h')\frac{t(h')}{2a_2}\right)^2+\left(\frac{2M_z}{D(h')(\pi D(h'))}\frac{1}{2a_2}\right)^2} < \tau_{ut,adhesive} \tag{D.13}$$

   $\tau_{ut,adhesive}$ is the ultimate shear strength of the adhesive. In this study a value of 3.14 Mpa is chosen after refering to Germanischer Lloyd (GL) guidelines. This value includes a material factor and a stress concentration of 3.

2. Material failure in plate at region 1

$$\begin{aligned} t_p &= \frac{t(h')}{2} \\ \sigma_{x,plate} &= \sigma\frac{t(h')}{(t_p+t_p)} \\ \tau_{plate} &= \frac{2M_z}{d(h')(\pi d(h'))(t_p+t_p)} \\ tsaihill(\sigma_{x,plate},&\tau_{plate}) < 1 \end{aligned} \tag{D.14}$$

3. Shear failure in plate in region 2

$$\left(\frac{2M_z}{d(h')\pi d(h')(t_p+t_p)}+\frac{F}{\pi d(h')(t_p+t_p)}\right) < \tau_{ut,plate} \tag{D.15}$$

The details to reach the final joint design using adhesive in a tubular tower is given in Figure D.6. Initially the thickness of the plate is assumed to be half that of laminate thickness. These design steps needs to be carried out iteratively in order to determine the overlap length of the joint as well as the thickness of the secondary plate.

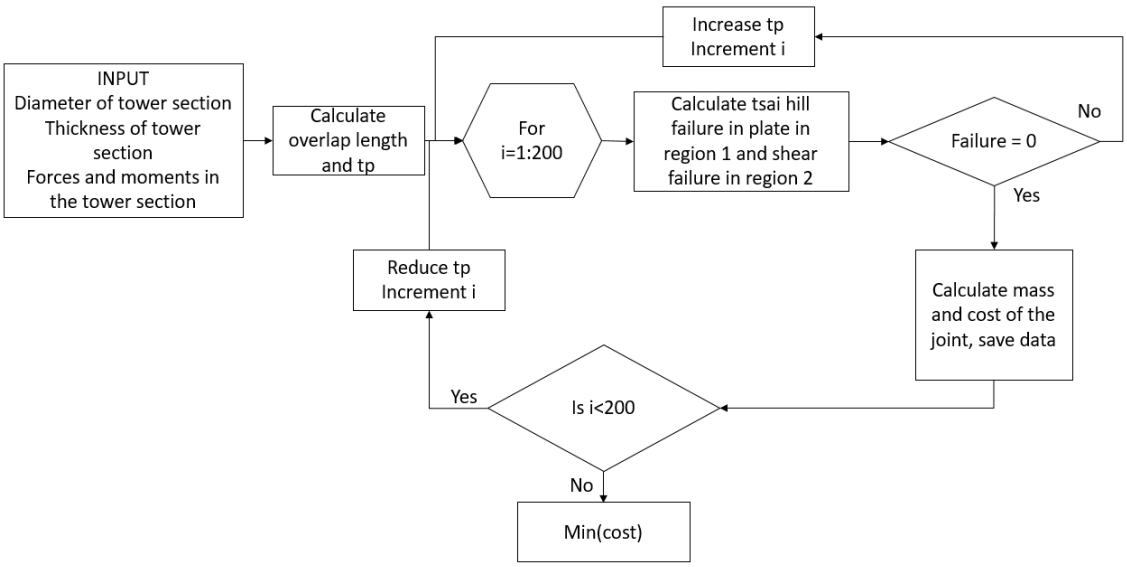

Figure D.6: Flowchart of the design procedure for adhesive vertical lap joint

Appendix E

Fatigue

The fatigue calculations have been briefly described in literature study Section 2.2.3. This appendix elaborates on this topic. Only the thrust and dead loads are considered as these are the major loads. The tower top moments and the direct wind load on the tower are neglected. The dynamic amplification factor is taken into consideration and used to amplify the loads depending on the rpm of the rotor. The following steps are performed to calculate the fatigue damage factor.

1. Input the tower dimensions and turbine properties, wind velocity and turbine parameters like height, cut in/cut off velocity (V_{cutoff},V_{cutin}) of the wind, rotor diameter, rated power, turbine class, etc.

2. Discritize the velocity between cut in and cut off velocity

$$\begin{aligned} dV &= \frac{V_{cutoff} - V_{cutin}}{n_v} \\ V_i &= V_{cutin} + i.dV \end{aligned} \tag{E.1}$$

3. Calculate the axial induction factor (a_{ind}), Coefficient of power (C_P), power(Pow) vs velocity graph.

$$\begin{aligned} a_{ind} &= 0.33 \\ C_P &= 4a_{ind}(1 - a_{ind})^2 \\ Pow &= \frac{1}{2}\rho_{air} C_P {R^2}_{rotor} \pi {V_i}^3 \\ &\text{while } Pow > Rated\_Pow \\ a_{ind} &= 0.33 - 0.0001 \\ &\text{calculate new } C_P \text{ and } Pow \end{aligned} \tag{E.2}$$

4. Calculate the coefficient of thrust (C_T) on the turbine at a given velocity, thrust (F_{top}) and turbulence standard deviation on the velocity ($\sigma_{v,i}$) .

$$\begin{aligned} C_T &= 4a_{ind}(1 - a_{ind}) \\ F_{top,i} &= \frac{1}{2}\rho_{air} C_T R^2{}_{rotor} \pi V_i{}^2 \\ \sigma_{v,i} &= I_{ref}\,(0.75V_i + 5.6) \end{aligned} \tag{E.3}$$

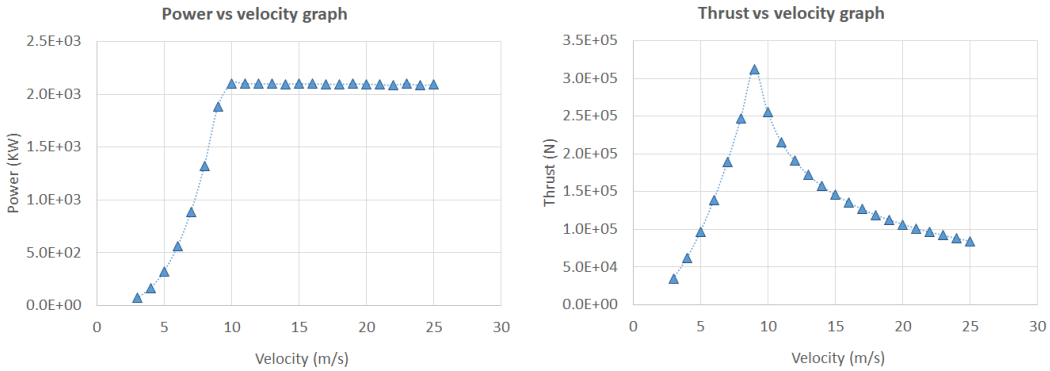

Figure E.1: Power curve and thrust of a 2.1 MW turbine

5. Calculate the standard deviation in thrust by multiplying the standard deviation in velocity with the slope of Thrust vs velocity graph.

$$\begin{aligned} \frac{dF_{top,i}}{dV} &= \frac{F_{top,i+1} - F_{top,i}}{V_{i+1} - V_i} \\ if\ \frac{dF_{top,i+1}}{dV} &< \frac{dF_{top,i}}{dV} \\ \frac{dF_{top,i+1}}{dV} &= \max\left(\frac{dF_{top}}{dV}\right) \end{aligned} \tag{E.4}$$

6. Calculate the max and min thrust at each velocity on the tower top.

$$\begin{aligned} \sigma_{T,i} &= \sigma_{V,i}.\frac{dF_{top,i}}{dV} \\ F_{top,i,\max} &= F_{top,i} + 3\sigma_{T,i} \\ F_{top,i,\min} &= F_{top,i} - 3\sigma_{T,i} \end{aligned} \tag{E.5}$$

7. Calculate the min and max base stress at each velocity and the corresponding stress amplitude ($\sigma_{amplitude}$) and mean stress (σ_{mean}). For the lattice tower, this max and min thrust is applied on the tower top along with dead loads, to get the stress amplitude and the mean stress in each link.

8. Calculate the rpm of the tower corresponding to each velocity using tip speed ratio of the turbine and rotor radius.

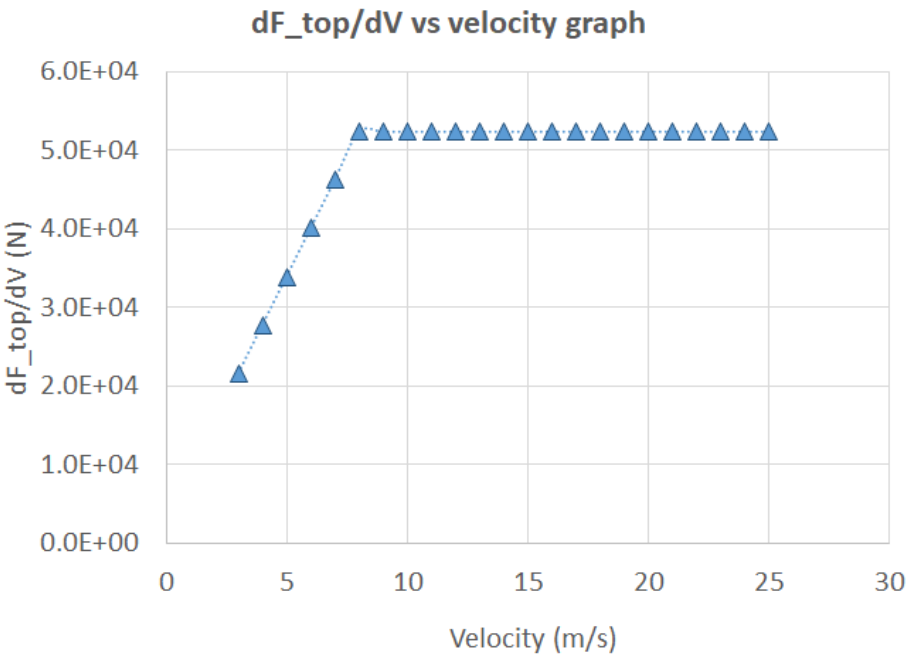

Figure E.2: Slope of Thrust vs velocity graph according to equations

9. Calculate the wind load distribution in hours using Weibull cumulative probability distribution.

$$N_{hours,V_i} = N_{year}.8760\left(\left(1-e^{\left(-e^{2\ln 2\left(\frac{V_i+dV/2}{1.1284V_{mean}}\right)}\right)}\right)-\left(1-e^{\left(-e^{2\ln 2\left(\frac{V_i-dV/2}{1.1284V_{mean}}\right)}\right)}\right)\right) \tag{E.6}$$

Here N_{year} is the number of years of service life, which is 20 in this study

10. Calculate the total loading cycles over the tower's service life with the help of rpm of the rotor.

$$N_{/hour} = 3600.\frac{RPM(i)}{60}$$
$$N_{V_i} = N_{hours,V_i}.N_{/hour} \tag{E.7}$$

Here $N_{/hour}$ is the number of loading cycles per hour.

11. Calculate the tolerable number of cycles (N_{cr}) at each velocity, using the Equation E.8 given by Germanischer Lloyd (GL) guidelines. The number of tolerable load cycles N_{cr,V_i} for each velocity is given by Equation E.8.

$$N_{cr,V_i} = \left[\frac{\sigma_{u,t}+|\sigma_{u,c}|-|2\gamma_m\sigma_{mean}-\sigma_{u,t}+|\sigma_{u,c}||}{2\gamma_m\sigma_{amplitude}}\right]^m \tag{E.8}$$

$\sigma_{u,t}$,$\sigma_{u,c}$ - Ultimate strength in tension/compression
γ_m - Material safety factor

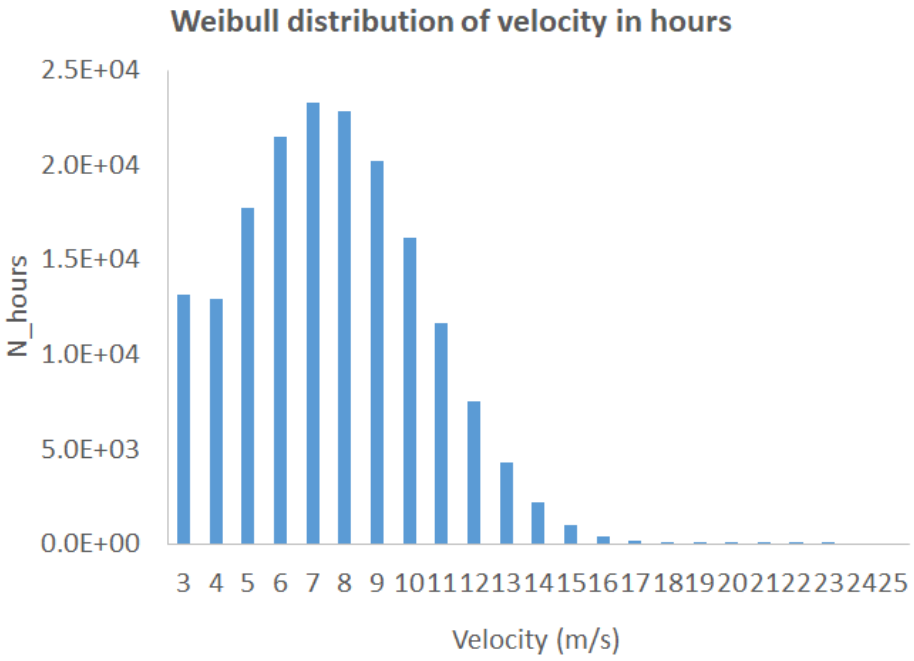

Figure E.3: Weibull distribution of the loading hours in 20 years

σ_{mean} - Mean stress
$\sigma_{amplitude}$ - Stress amplitude
m - Slope parameter for SN curve depending on material
m - 10 for Glass Fiber Reinforced Plastic (GFRP) and 14 for Carbon Fiber Reinforced Plastic (CFRP) composite

12. calculate the damage factor (DF) as given in Equation E.9.

$$DF = \Sigma \frac{N_{V_i}}{N_{cr,V_i}} \leq 1 \tag{E.9}$$

DF - Damage factor
N_{V_i} - Number of loading cycles at a windspeed
N_{cr,V_i} - Number of allowable cycles at that stress

Appendix F

Verification

This appendix presents the verification of the tubular structure and lattice structure tool.

F.1 Verification of the tubular tool

Table F.1 gives the verification between the tubular design code and the Ansys FEM model for two of the tubular tower design using Glass Fiber Reinforced Plastic (GFRP) material. In the Ansys FEM model, Shell 181 elements have been used for the modeling. In the matlab tool, analytical equations have been used to find the deflection and the stresses. The natural frequency has been found using 2D beam elements. The error in the natural frequency predicted by the methodology used in this study and a similar tower designed in Ansys has less than 1% difference. Table F.2 shows the verification of static results for two tubular tower

D_t	D_b	t	h	$Mass_{top}$	Material	Turbine type	Frequency Matlab	Frequency Ansys	Error Ansys-Matlab
(m)	(m)	(m)	(m)	(tons)		(MW)	(Hz)	(Hz)	(%)
3	7	0.1	90	180	GF	2.1	0.384	0.382	-0.63
3	7	0.1	120	350	GF	5	0.184	0.185	0.28

Table F.1: Frequency verification for tubular towers

configuration. In Matlab, the deflection and stresses were found out using Euler beam theory. In Ansys, the same towers are modeled using shell elements, and the results are presented in Table F.2 and continued in Table F.3. The error between the results predicted by Matlab code and Ansys model is less than 5%. The difference may be due to the element type used in the Ansys modeling.

D_t	D_b	t	h	Mass$_{top}$	Material	Turbine type	F_{top}	M_{top}	Matlab δ_{top}	ANSYS δ_{top}	Error
(m)	(m)	(m)	(m)	(ton)		(MW)	(MN)	(MN.m)	(m)	(m)	(%)
3	7	0.1	90	180	GF	2.1	1.24	7.39	1.09	1.09	0.37
3	7	0.1	120	350	GF	5	1.32	4.22	2.48	2.55	2.66

Table F.2: Verification of stress and deflection in tubular tower using Ansys

Matlab axial stress compression side	ANSYS axial stress compression side	Error	Matlab axial stress tension side	ANSYS axial stress tension side	Error	Matlab shear strain	ANSYS shear strain	Error
(MPa)	(MPa)	(%)	(MPa)	(MPa)	(%)	[–]	[–]	(%)
35.97	35.70	-0.76	32.21	31.90	-0.97	583.23	574.63	-1.50
49.01	47.80	-2.52	42.69	41.00	-4.11	619.47	609.48	-1.64

Table F.3: Verification of stress and deflection in tubular tower using Ansys (continued)

F.2 Verification of the lattice code

In this study, the FEM approach to design the lattice tower has been setup using Matlab. The code has been verified with Ansys to make sure that both the FEM models have a good correlation. Ansys FEM codes are well validated and reliable. Hence, comparing the Matlab results with Ansys results will increase the reliability of the Matlab FEM code used in this study. Beam4 is used to model the links of the lattice tower in Ansys. The comparison of the frequencies predicted by Matlab code and Ansys for a 2.1MW, 125m tower is given in Table F.4. The deflection and the maximum/minimum tensile stress when the turbine top loads, dead loads, and wind loads are applied together is compared with the Ansys results and given in Table F.4. The difference between the two FEM codes is less than 1% which indicates the Matlab FEM code is reliable and the FEM operations used in the code are accurate.

	Ansys	Matlab	% error
Frequency (Hz)	0.3308	0.3315	0.21
$\delta_{top,X}$ (m)	1.716	1.716	0
$\delta_{top,Y}$ (m)	0.9386	.0.9451	0.69
$\delta_{top,Z}$ (m)	0.07939	0.0793	0
σ_{max} (MPa)	72.7	72.9	0.27
σ_{min} (Mpa)	-64.7	-65.0	0.61

Table F.4: Frequency and static results comparison for a 125m tall 2.1MW lattice tower between Matlab and Ansys

Appendix G

Example Problem

In this appendix, the properties, loads and stress distribution along the tower is presented for a 100m 2.1MW tubular Glass Fiber Reinforced Plastic (GFRP) tower. The sensitivity study with respect to base diameter and thickness is provided. The appendix also contains the likely critical links in different constraints in a lattice tower structure. This appendix can be referred while using the tower design tool and if any intermediate values have to be cross verified.

G.1 5MW, 100m GFRP tubular tower details and sensitivity graph

The dimensions of the tubular tower have been discussed in Table 5.1. Figure G.1 presents the mass and moment of area distribution along the height. The shear force diagram and the bending moment diagram under the combination of applied loads are given in Figure G.1 . The tower base experiences the max shear as well as the moment. The shear stress and compressive stress acting on each tower section along the height is given in Figure G.1. It is seen that maximum compressive stress occurs at tower base and maximum shear stress occurs at the tower top. This is because of the smaller area at the tower top. The tower deflection and the material safety factor distribution is given in Figure G.1.

The local buckling factor in each section of the tower is given in Table G.1.

		Section-1	Section-2	Section-3	Section-4
Operating load case	SF_{lbuck}	1.3779	1.2913	1.3215	1.8543
Non-operating load case	SF_{lbuck}	1.3177	1.5207	2.0196	4.3295

Table G.1: Local buckling safety factor in each section

The joint mass, cost, overlap length and thickness of the secondary plate for joint-1 is given in Table G.2 .

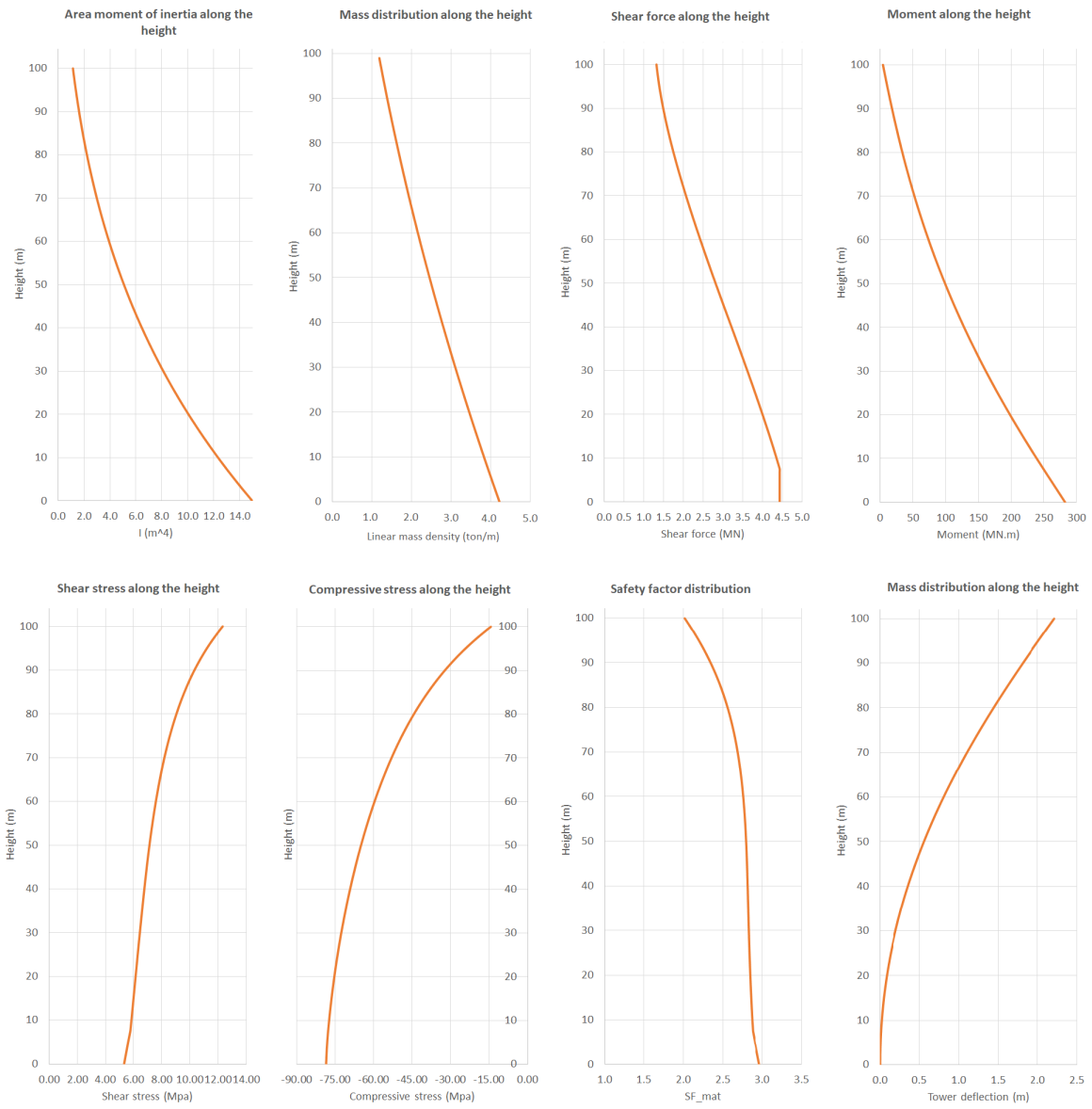

Figure G.1: Properties, forces, stress and deflection along the height of the tower

	Units	Section-1 & 2	Section-2 & 3	Section-3 & 4
Mass	[t]	1.39	1.26	1.04
Cost	[€]	6377.70	5922.90	5122.70
Overlap	[m]	0.84	0.74	0.51
Thickness of plate	[mm]	10	10	20

Table G.2: Joint-1 design details for 5MW 100m GFRP tubular tower

The joint mass, cost, overlap width of the secondary plate for joint-2 is given in Table G.3 . The cost distribution of the tower is given in Table G.4 .

	Units	Section-1	Section-2	Section-3	Section- 4
Mass	[t]	1.26	1.20	1.16	1.31
Cost	[€]	5914.60	5684.50	5572.90	6090.00
width	[m]	0.16	0.16	0.16	0.19
Thickness of plate	[mm]	80	70	60	50

Table G.3: Joint-2 design details for 5MW 100m GFRP tubular tower

Cost contributor	€
Raw material	1026471
Aiding material & mold cost	30302
Labor cost for production	132521
Labor cost for finishing	88348
Joint cost	40700
Transport cost	39808
Crane and lifting	125840
Foundation cost	136965
Total	1620955

Table G.4: Cost distribution of 5MW 100m GFRP tubular tower

The sensitivity of base diameter and thickness when 1 mm change is done to the respective parameters are given in Figure G.2. This can help in understanding the system and in predicting the most critical of the constraints. Here, 1 represents operating load case and 2 represents non-operating load case.

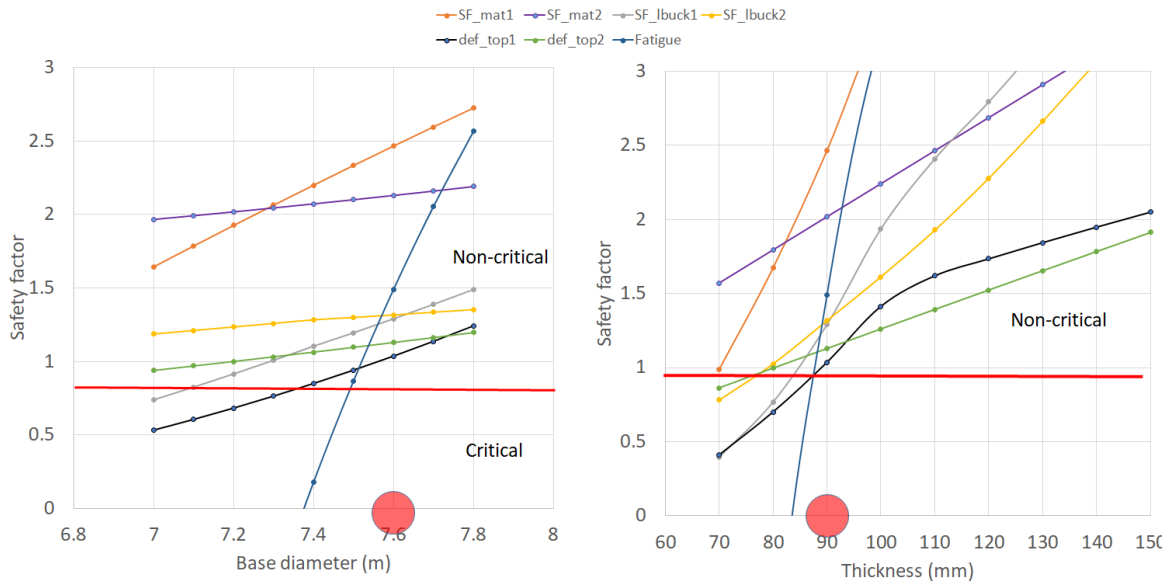

Figure G.2: Sensitivity study near optimum solution for the 5 MW, 100m tower

G.2 Lattice tower critical links

In a lattice tower, the general location of the critical links and their modes of failure are presented in Figure G.3.

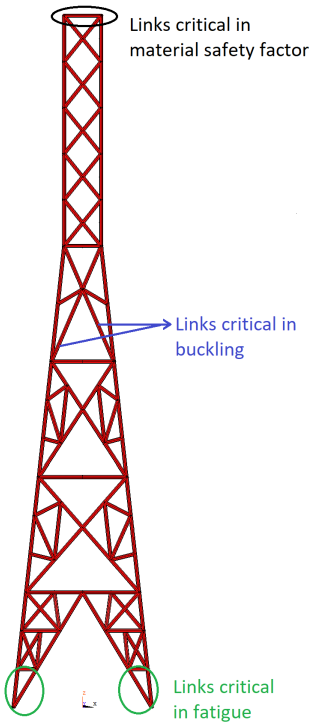

Figure G.3: Critical links in a 2.1MW 125m CFRP lattice structure

Due to a highly nonlinear relationship between the link parameters and the properties like mass and safety factors, there may be cases when the failures might occur in a different location or a different class of links. This must be studied separately for each design. The links presented in Figure G.3 represent one out of the 12 designs presented. They are specifically for the 125m 2.1MW CFRP Lattice tower.

As a conclusion, the main link members are highly loaded in tension/compression as they resist major portion of the externally applied moment and forces. They often show failure in material safety factor. But, the point of load introduction often tends to be the most critical in material safety factor.

The diagonal elements serve the purpose of resisting the torsional moments and bending moments applied on the tower top. Thus they are expected to fail in Euler buckling owing to their large aspect ratio compared to links in other categories.

The web members are the least loaded links as they serve the purpose of improving the buckling properties of other links. The links at the base are subjected to the combined effect of forces and moments and experience the highest fatigue loading owing to their position in the tower.